이학박사 학위논문

Study for intracellular targeting based on peptides for regulation of stem cell differentiation

줄기세포의 분화제어를 위한 펩타이드 기반 세포 내 표적화 연구

2014 년 8 월

서울대학교 대학원

치의과학과 치의재생생명공학 전공

서 진 숙

Study for intracellular targeting based on peptides for regulation of stem cell differentiation

줄기세포의 분화제어를 위한 펩타이드 기반 세포 내 표적화 연구

지도교수 박 윤 정

이 논문을 이학박사 학위논문으로 제출함

2014년 4월

서울대학교 대학원

치의과학과 치의재생생명공학 전공

서 진 숙

서진숙의 박사학위논문을 인준함

2014년 6월

위 원 장	박 승 범 (인)
부 위 원 장	박 윤 정 (인)
위 원	박 종 철 (인)
위 원	박 상 현 (인)
위 원	이 진 (인)

SUMMARY

One role of peptides in biological pathways is that of receptor antagonists or inhibitors of protein-protein interactions. Recently, peptide-based drugs have received increased attention due to the adverse side effects conferred by several protein-based drugs and the difficulty in screening for small molecules that act as antagonists of protein-protein interactions that form the molecular basis of human diseases. Peptides reportedly have the advantage of high target affinity, specificity and potency; relatively low cost; easy synthesis and storage; low toxicity; and reduced antigenicity. In the field of regenerative medicine, peptides may be applied to bioactive molecules, such as drugs and drug carriers; however, a vehicle must be included to load the molecules to promote tissue regeneration. Mesenchymal stem cells (MSCs) are an attractive vehicle for cellular therapies due to their variety of cell-intrinsic and environmentally responsive properties. To promote differentiation in target cells or tissues, appropriate strategies were required to regulate the commitment of stem cells, such as physical stress, chemical treatment or gene delivery.

Gene therapy, including microRNA (miRNA), is an efficient method for treating several diseases because miRNAs can bind specific targets. However, the primary limiting factor in the use of miRNAs is their reduced penetration into cells. A gene delivery vehicle is needed to efficiently deliver the gene product to the target cells. Recently, several cell-penetrating peptides (CPPs) have been investigated as a means to overcome the limited penetration of oligonucleotides, such as miRNAs. The authors described a peptide/miRNA complex containing the arginine-rich CPP, called low-molecular weight protamine (LMWP), from natural protamine. Additionally, miRNA-29b, which was used as a drug, is a key regulator of development of the osteoblast phenotype by targeting anti-osteogenic factors and modulating bone extracellular matrix proteins. We solved the difficult problem of transfection into human mesenchymal stem cells (hMSCs) by generating a complex with LMWP. Next, we determined that the LMWP/miRNA-29b complex could induce osteoblast differentiation and mineralization. Our results are significant in that they support the highly efficient application of miRNAs as therapeutic drugs and revalidate the efficacy of miRNA-29b in the bone regeneration field.

Protein-peptide interactions are involved in wide range of cellular process. In general, protein-peptide interactions play pivotal roles in controlling cellular signaling networks, protein subcellular localization, protein degradation, and post-translational modification. During osteoblastic differentiation, BMP-specific Smads, e.g., Smad1, can be irreversibly removed by an ubiquitin-dependent proteasome-mediated degradation system via protein-protein interactions between Smurf1, a HECT-class ubiquitin ligase, and the Smads. In the current study, a cell-penetrating Smurf1 binding peptide was designed and demonstrated to inhibit the interaction between Smurf1 and Smad1/5/8 due to its stronger affinity to Smurf1 compared to Smad1. Additionally, to use the peptide as a diagnostic tool, the peptide was modified by attaching a fluorescent donor and fluorescent adopter. When the target Smurf1 combines the complementary sequences of the peptide probe, the resulting conformational change occurs the distance between the fluorescent donor and adopter, resulting in fluorescence recovery. Simultaneously, restored Smads enter the nucleus, thereby increasing the expression of osteoinductive genes in concert with other transcription factors. The identification of a human-derived cell-permeable bioactive peptide may be applied as a drug-

delivery system or a procedure for stem cell engineering to promote tissue regeneration. We propose to name these peptides that use fluorescence resonance energy transfer (FRET) and employ a switchable on/off detection system 'peptide probe'. We envision that the peptide probe may be integrated with targeting, imaging and tracking therapeutic drugs to develop multifunctional nanoparticles that can be used to noninvasively image, diagnose and treat bone defects and Smurf1 over-expressed chronic inflammation disease.

Taken together, these data suggest that peptide-based drug delivery vectors and bioactive molecules, which are used in several medical fields for disease diagnosis and therapy, can be used as a tool to regulate stem cell differentiation.

Keywords: Cell penetrating peptide, Target binding domain, Drug delivery system, Diagnostic probe, microRNA, Bone tissue regeneration

Student Number: 2006-23511

CONTENTS

LIST OF ABBREVIATION

SPSS : solid phage peptide synthesis

ECM : extracelluar matrix

CPP : cell penetrating peptide

PTD : protein transduction domain

FACS : fluorescence assisted cell sorting

HMSCs : human mesenchymal stem cells

MiRNA : micro ribonucleic acid

Anti-miRNA : antisense-micro ribonucleic acid

Control-miRNA : control-micro ribonucleic acid

LMWP : low molecular weight protamine

FITC : fluorescein isothiocyanate

TAMRA : Tetramethyl-6-Carboxyrhodamine

BHQ1 : Black hole quencher 1

MTT : 3-(4,5-dimethylthiazol-2-ly)-2,5-diphenyltetrazolium bromide

FBS : fetal bovine serum

DPBS : dulbecco`s phosphate buffered saline

PBS : phosphate buffered saline

MALDI - TOF : matrix assisted laser desorption ionization – time of flight

DMSO : dimethyl sulfoxide

F-moc : fluoren-9-ylmethoxycarbonyl

DMF : N,N-dimethyl formamide

NMP : N-methylpirrolidone

DIPEA : diisopropylethylamine

HBTU : 2-(1H-Benzotriazol-1-yl)-1, 1, 3, 3-tetramethyluronium hexafluorophosphate

TFA : trifluoroacetic acid

EDT : 1,2-ethanedithiol

TIS : triisopropylsilane

HPLC : high pressure liquid chromatography

TEM : transmitting electron micrograph

SDS : sodium dodecyl polyacrylamide

DTT : dithiothreitol

TBST : tris buffered saline with Tween 20

SPR : surface plasmon resonance

CM5 chip : carboxyl methyl dextran chip

NHS : N-hydroxysuccinimide

EDC : N-ethyl-N`-(3-dimethylaminopropyl)-carbodiimide hydrochloride

K_a : association rate constant

K_d : dissociation rate constant

K_A : equilibrium association rate constant

K_D : equilibrium dissociation rate constant

DNA : deoxyribonucleic acid

DMEM : Dulbecco`s modified eagle medium

GAPDH : glyceraldehyde 3-phosphate dehydrogenase

ALP : alkaline phosphatase

HDAC4 : Histone deacetylase 4

CTNNBIP1 : Catenin-β interacting protein 1

DUSP2 : Dual specificity phosphatase 2

COL1A1 : Collagen type 1 alpha 1

COL5A3 : Collagen type 5 alpha 3

OCN : Osteocalcin

RUNX2 : Runt-related transcription factor 2

TAZ : Transcriptional coactivator with PDZ-binding motif

TNFα : Tumor necrosis factor alpha

PPI : protein-protein interaction

PCR : polymerase chain reaction

UPS : ubiquitin-proteasome system

LMP1 : LIM mineralization protein 1

CHAPTER Ⅰ

Review of the literature

1. PEPTIDES AS BIOACTIVE MATERIALS

Proteins are involved in nearly every aspect of cellular life, including cell shape, subcellular organization, waste cleanup, product manufacturing, and routine maintenance. Proteins also receive extracellular signals and mobilize an intracellular response. Cells secrete various proteins that are incorporated into the extracellular matrix. Proteins are essential macromolecules for cells and are as diverse as the functions they serve. Proteins can be large or small (typically larger than peptides), primarily hydrophilic or primarily hydrophobic, exist alone or as part of a multi-unit structure, and change shape frequently or remain virtually immobile. All of these differences arise from the functional groups of the specific amino acids that compose each protein. Properly folded proteins have distinct surface characteristics that determine which other molecules they interact with [1]. When proteins bind to other molecules, protein conformation can change in subtle or dramatic ways. This diversity in protein structure and function has driven many studies investigating protein-protein interactions (PPIs) [2]. Knowledge of PPIs may help to reveal cellular characteristics controlled by selective protein regulation.

However, the use of proteins, such as antibodies and cytokines, to regulate cellular signaling is associated with many disadvantages, such as poor bioavailability, the neutralization of antibody production, rebound symptoms, limited long-term efficiency, low stability, and a risk of severe, sometimes lethal side effects resulting from the antigen–antibody reaction [3]. These types of therapy are also expensive and are not always covered by insurance. Conversely, therapeutic peptides may represent effective treatments that can address the aforementioned issues raised by the use of proteins. These peptides are small molecules of less than 50 amino acid residues and can be produced by fully synthetic chemical methods instead of biological purification.

The use of peptides in modern science has grown exponentially in recent years. Additionally, peptides are considered as small molecules for the treatment of many human diseases [3, 4]. However, the application of peptides in a biological system confers several disadvantages: rapid degradation by proteases, hepatic clearance, and low membrane permeability due to the hydrophilic characteristics of partial motifs. However, there are many advantages of using peptides as bioactive molecules in therapeutic fields. Peptides are primarily interesting because they bind

with exquisite specificity to their in vivo targets, resulting in high functional potencies and relatively few off-target side effects. This high degree of selectivity in their interactions is the product of millions of years of evolutionary selection for complementary shapes and sizes from among a number of arrays of structural and functional diversity. Thus, peptides have been selected to interact specifically with biological targets, evolving into potent endogenous hormones, growth factors, enzymes, signaling molecules, and immunologic and defense molecules.

To transition from the use of peptides as bioactive molecules on a cellular level to a systemic level in humans, pharmaceutical industries are introducing peptides into their products [5]. Furthermore, peptides are also used in the development of drug delivery systems and diagnostic kits [6]. Finally, new biomaterials representing a broad range of applications are currently prepared from peptides [7]. The introduction of these biomolecules into multiple fields of research has primarily been fuelled by the development and optimization of the solid-phase synthetic strategy, which was first described by Merrifield [8]. In brief, solid-phase peptide synthesis (SPPS) is based on a supported protecting group, a polymeric support that facilitates the stepwise elongation of this resin through sequential steps

of coupling and deprotection of protected groups on amino acids, thus allowing the use of sufficient reagent concentrations. Following the synthetic process, a chemical treatment is typically applied to remove the F-mock-based protective groups and detach the peptide from the resin [9]. The establishment of the synthetic protocol using SPPS promotes peptide availability, development, and medical application of peptides.

The most important aspect of peptide-based therapeutic molecule design is the determination of a specific peptide sequence that binds to a target protein with high affinity. To preserve the original function, it is critical to identify the appropriate peptide for the region and to refine the peptide to promote stable binding. When the binding surface is known, a peptide can be designed in two principal ways (computable and experimental discovery). Automated peptide binding search techniques from known protein databases have generally been used as bioinformatics tools [10]. A previous study has reported peptide design methods based on a bioinformatics approach that successfully identified the peptide binding sites using a de novo molecular design computational tool [11]. In addition to structure-based software programs, two predominant experimental approaches have

been used to investigate recognition specificity of some motifs, namely SPOT synthesis and phage display; both methods have high-throughput potential and can reveal domain interaction networks with information regarding protein-peptide interactions.

Array technologies, especially protein arrays, are a more recent advancement in PPI research due to critical factors such as proper folding stability and functionality. In contrast, peptides are easier to handle while retaining partial features of protein function. Most peptide arrays described to date were produced using the SPOT synthesis concept because SPOT synthesis is a simple but extremely robust method for the highly parallel synthesis of peptides on membrane surfaces [12]. SPOT technology simplified the chemical synthesis of peptide arrays to the intended deposition of reagents on a planar material. Multiple synthesis techniques facilitate the potential synthesis and screening of up to 10,000 peptides on membrane surfaces. Moreover, chemical synthesis facilitates the incorporation of methylated [13], phosphorylated or acetylated amino acids [14]; the use of unnatural building blocks [15]; the preparation of branched and cyclic structures [16]; and the ability to label compounds with imaging molecules or short biological tags, such as biotin

[17]. Although the preparative SPOT synthesis mode has been primarily used in cell-based screening assays [18], it has also been used to promote quality control of spot-synthesized peptides. The analytical mode, which is another SPOT synthesis mode, enables the synthesis of approximately 6,000 cellulose membrane-bound peptides by producing spots with diameters of ~1 mm. It was not possible to down-size the spot diameter below 1 mm due to the capillary effect of cellulose membranes. In both cases, membranes with dimensions of 18.3 x 28.5 cm were used as a special platform with the fully automatic synthesizer, allowing for four coupling steps per day. Several interesting screening methodologies can be performed with SPOT synthesis to create peptides with original activities, such as epitope mapping [19], replacement analysis [20], combinatorial peptide libraries [21], and random peptide libraries [22].

Phage display is a powerful biological library comprising up to 1,200 peptides of random sequences displayed on a bacteriophage. Since its discovery in 1985 [24], many researchers have used phage display to determine the recognition specificity of several domains [23]. The concept is simple; a phage population is engineered to express random-sequence peptides, proteins or antibodies on its

surface. From this population, a selection step is performed to identify phages that bind the desired target. To create this display, randomized cDNA sequences are inserted into the phage genome such that they will be expressed as a fusion protein with one of the phage coat proteins [25]. Proteins and peptides with a wide range of sizes and properties have been successfully displayed by filamentous phages [26]. Phage display has several advantages over conventional random screening methods used in drug discovery, including cost effectiveness, simplicity, and speed. The primary strength of this technique is the ability to generate the considerably diverse array of exogenous peptides and proteins displayed on the phage surface using rapid molecular biology methods as opposed to individually using genetically engineered peptides or protein variants. Phage products can be rapidly screened for binding to a target protein, and the final resident can ultimately be identified using DNA sequencing [27, 28]. Once identified through phage display, selected sequences can be structurally analyzed to provide a more detailed understanding of the ligand–target interaction [29]. This additional information is useful when proceeding to subsequent stages of drug discovery and pipeline development.

As outlined above, synthetic peptides inherently confer specific properties and are chemically manufactured to produce the natural structure. The following advantages are derived from the use of synthetic peptides as therapeutic drugs or delivery vehicles: i) peptides can be modified accordingly with carbohydrates, lipids or phosphate groups to improve stability and/or binding affinity; modified with unnatural amino acids or cyclized to increase metabolic stability against enzymes such as proteases; or modified with various chemical reactive groups to produce a targeting molecule that can be optically imaged to promote drug transport and to facilitate the tracking of changes in pharmacokinetics; ii) well-established analytical techniques, such as analytical chromatography and mass spectrometry techniques, are available to rapidly and thoroughly validate the peptide batches; iii) peptides can be easily produced in a scaled-up experimental environment; iv) peptides can be stored in a freeze-dried state, thus limiting the problems of long-term storage, transport and distribution; v) unlike phages or adenoviruses dedicated to drug transport, peptides do not involve infectious material; vi) the sequence can be reduced to the binding domain only, thus eliminating risks of undesired effects conferred by side sequences.

Peptides for drug delivery

Although a phospholipid outer membrane is essential for cell survival and function, it presents a major challenge for the intracellular delivery of cargo. An even more difficult task is the delivery of cargo across the blood-brain barrier (BBB), a dynamic interface that prevents the translocation of most drugs from the vasculature into the brain parenchyma [30]. The efficient delivery of impermeable molecules often requires the administration of high quantities of drugs to obtain the expected intracellular biological effect. Therefore, improving the process of translocation across these membranes may successfully reduce costs by decreasing the required therapeutic drug quantity and preventing side effects on other tissues [31]. Carriers for drug delivery into cells must satisfy several major requisites as follows: i) efficient transportation into diverse and challenging cell lines, such as primary cultured cells; ii) lack of toxicity; iii) ability to reach the target site; iv) activity at low doses; and v) rapid endosomal release. Over the past few decades, several pharmaceutical carriers, such as nanospheres, polymers, nanocapsules, liposomes, micelles, and dendrimers, have been widely used to deliver diagnostic and therapeutic agents into cells. Because the delivery of these nanovectors is

generally based on their passive accumulation in the pathological tissues, they cannot efficiently deliver their diagnostic and therapeutic cargo to specific cells or to particular intracellular components [32]. In recent years, small peptides, including relatively short cationic and/or amphipathic peptides, received attention as cellular delivery vectors due to their intrinsic ability to enter cells and mediate the uptake of a wide range of macromolecular cargo [33]. Cell penetrating peptides (CPPs) are synthetic peptides of less than 30 amino acids long and are a component of the most promising strategy to overcome extracellular and intracellular limitations to the administration of various biomolecules, including plasmid DNAs, small RNAs, proteins, impermeable peptides, and inorganic molecules. CPPs can be an associated with cargo molecules in two different ways; the first requires chemical linkage with the cargo, and the second involves the formation of stable, non-covalent complexes [33]. Using the first strategy, it is possible to quantitatively analyze tags, such as fluorophores, and to investigate the tagging site. The second strategy is primarily used to deliver drugs used in high concentrations. CPPs can be divided into the three following groups based on their origin or sequence characteristics: cationic, anionic and amphipathic CPPs. Cationic CPPs

often consist of arginine, lysine and histidine residues. These CPPs have been suggested to depend on the highly basic guanidine moiety of arginine. Indeed, guanidine functional groups can form divalent hydrogen bonds with various functional groups associated with cellular molecules, such as phosphates, carboxylates and sulfates, thereby enhancing the affinity of arginine-rich CPPs for cell surfaces [34]. The neutralization of the positive charges on arginine residues by these counter ions is likely beneficial to the translocation of arginine-rich CPPs through lipid bilayers [35]. Cationic CPPs have been referred to as 'Trojan horse' delivery vehicles because they can enter cells without eliciting a cellular response [36]. Nevertheless, cationic CPPs can induce a wide range of side effects, including effects on membrane integrity and cell viability, which may be more subtle than cell death. Well-known cationic CPPs include R8 [37], Tat [38], and LMWP [39]. Secondly, anionic peptides contain hydrophobic amino acids and have a low net charge. To date, only a few hydrophobic CPPs have been discovered, including the signal sequences from Kaposi fibroblast growth factor (AAVALLPAVLLALLAP) and integrin β3 (VTVLALGALAGVGVG) [40]. Hydrophobic amino acids are also integral to amphipathic CPPs [41] and to other longer chimeric CPPs containing

additional cationic residues that enhance the delivery capacity [42]. Finally, amphipathic CPPs, which are subdivided into primary amphipathic CPPs (e.g., Pep-1 and pVEC), secondary amphipathic α-helical CPPs (e.g., hCT18–32), β-sheet amphipathic CPPs (e.g., VT5), and Proline-rich amphipathic CPPs (e.g., Bac7) [31]. These peptides contain hydrophobic and hydrophilic blocks that mediate peptide translocation across the cell membrane [43].

Many studies have focused on the use of CPPs to deliver theragnostic drugs, resulting in the generation of agents with improved permeability [44]. Recently, research studies aimed to deliver agents across the BBB [45], target radiolabeled antibodies to intracellular sites [46], and visualize viral infection in real time [47] have generated powerful tools for the development of novel molecular imaging agents. Furthermore, CPPs are useful for translocating therapeutic drugs and activating the restoration of damaged cells. Abundant small molecule chemotherapeutics, such as cyclosporine A [48], Taxol [49], and methotrexate [50], have demonstrated improved activity when conjugated to a CPP. Remarkably, even though a CPP-drug conjugate demonstrates less activity in a purified biochemical system, highly efficient cellular uptake can overcome this shortcoming. Although a

CPP-methotrexate conjugate experiences a 20-fold loss in potency compared to the drug alone, it has been demonstrated to confer highly efficient cytotoxicity to a methotrexate-resistant cell line [50]. This study demonstrated that CPP conjugates can effectively increase the intracellular concentrations of anti-cancer drugs even in drug-resistant cells, and this effect can counteract conjugation-induced decreases in drug activity.

One of the most common mechanisms of multidrug resistance is the over-expression of drug efflux pumps by tumor cells [51]. These pumps often induce resistance to a range of chemotherapeutic agents, severely limiting treatment options [52]. Upon cellular uptake using CPP-drug conjugates, the high intracellular glutathione concentration has been shown to cause disulfide cleavage, releasing Taxol from the conjugate and thereby preventing the CPP from interfering with drug activity [49]. The conjugates were more active than Taxol alone, both in vitro and in vivo. Thus, this approach may be generalizable to other drugs for which resistance has been encountered.

Non-targeted drug distribution can cause undesired effects at sites other than those intended. Moreover, many drugs partially degrade before they reach the

desired site, leading to a reduction in their therapeutic effects. Advances in chemical, biological and engineering techniques have stimulated the generation of many specific targeting systems that have successfully directed attached drugs to desired disease sites. To date, numerous peptide ligands have been discovered for various types of receptor proteins and cell types, such as integrin receptors [53], thrombin receptors [54], cardiomyocytes [55], pancreatic β cells [56], and tumor cells [57, 58].

Moreover, peptides targeting various healthy organs have generated data regarding the tissue-specific molecular diversity of the vasculature. Some molecules expressed by normal vasculature are down-regulated in the tumors of the target organ. A previous study described two peptides sharing a GFE motif (GFE-1; CGFERVRQCPERC and GFE-2; CGFELETC) that were selectively directed to the alveolar capillaries of normal murine lung vasculature but not lung tumors [59]. The target receptor for the lung-homing peptide (GFE-1) was isolated from a murine lung lysate using an affinity column with immobilized GFE-1 peptide and identified as a metalloprotease membrane dipeptidase (MDP) [60]. Tumor blood vessels contain structural and morphological differences from normal vasculature.

Compared to normal vessels, tumor blood vessels are leaky and convoluted [61, 62]. Many of the specific molecular markers in tumor vessels are absolutely associated with angiogenesis. The RGD [53] and NGR [63] peptides represent first-generation homing peptides. The tumor homing abilities of these two peptides are apparently independent of the tumor type, indicating that the receptors for these peptides are up-regulated during angiogenesis. The F3 peptide also homes to angiogenic blood vessels. Cell surface-expressed nucleolin was identified as the receptor for the F3 peptide on tumor cells, representing a novel marker for angiogenic vasculature in tumors [64]. The LyP-1 peptide was discovered to home to the tumor-associated lymphatic vessels and tumor cells in hypoxic tumor regions but not to the tumor blood vessels. In addition, LyP-1 moved only to a tumor sub-compartment, indicating that tumor lymphatics express tumor type-specific molecules [65]. The LyP-1 receptor is mitochondrial protein p32, which is expressed on lipid membranes [66]. The p32 shows aberrant cell surface expression in tumor cells, tumor lymphatics, and a subset of myeloid cells, which contributes to the specificity of LyP-1 homing to tumors. Because $(KLAKLAK)_2$, an apoptosis-inducing peptide and antimicrobial peptide, has cytotoxicity activity on

its own, it is unique among the tumor homing peptides. Its internalization causes mitochondrial swelling and mitochondrial membrane disruption, leading to apoptosis [67]. RGD-$(KLAKLAK)_2$ and NGR-$(KLAKLAK)_2$ were shown to be particularly toxic to angiogenic endothelial cells, leading to reduced tumor growth, metastases, and prolonged proliferation [68].

Peptides for therapeutic application

The application of nanotechnology to biomedical imaging is highly active and interesting [69]. The impact of nanotechnology on this field helps to improve the efficacy of conventional imaging moieties and supports the development of new imaging methods [70]. Numerous challenging developments and clinical applications of novel nano-scaled molecules and techniques have been developed with the help of bio-, imaging-, nano-technology fusions [71]. The various applications of these fusion technologies on biomedical imaging, such as diagnostic kits, cell tracking, isolated tissue analysis, and real-time live imaging, can be used to facilitate real-time live imaging using nanoprobes to detect molecular changes of the microenvironments in living systems. The innovative design of nanoprobes for live imaging is valuable for multiple applications, and these probes can be simply modified or improved to support various purposes for both imaging and therapy, referred to as 'theragnosis'. Moreover, target specificity can be provided by the simple conjugation of active targeting moieties, such as antibodies and peptides [72]. Among various target molecules, such as proteins, many can transduce specific signals based on protein-protein interactions that

influence many biological mechanisms. Therefore, this sequence-specific recognition and binding has been applied to design peptide-based probes conjugated to contrast agents or molecular probes [6, 73].

Two different designs of general peptide probes are available for optical imaging depending on the type of quencher used. The first design depends upon a self-quenching mechanism in which the dye/donor and quencher/acceptor are the same or similar fluorophores [74]. This idea is similar to the concept of contact quenching (static quenching). This probe offers advantages including a relatively simple synthesis process, although they generally confer less efficient fluorescent quenching. An NIR fluorescent probe, consisting of multiple Cy5.5 bound to a long circulating graft copolymer containing a poly-lysine backbone and a methoxy polyethylene glycol graft, has previously been reported [75]. The presence of multiple Cy5.5 on the graft copolymer results in self-quenching due to the strong binding affinities between the fluorophores. The second design is based upon fluorescence resonance energy transfer (FRET) and a self-quenching mechanism, in which a different type of quencher is used to suppress the fluorophore's fluorescent signal [76]. This design is advantageous with respect to its high

quenching efficiency, which can improve both the sensitivity and specificity of optical imaging. The basic structure of peptide probes used to image targeted proteins is very simple. The probe consists of a fluorophore and quencher that are covalently linked to the opposite terminus of a short peptide that is the substrate of specific target site [77]. In the native condition, the emitted light from the fluorophore is quenched into the acceptor by FRET. Once the target protein binds the peptide probe, the extent of fluorescence is considerably enhanced by increasing the physical distance between the fluorophore and the quencher due to a conformational change induced by the binding proteins. These peptide probes may be selected by modifying known native peptides within proteins, utilizing peptide libraries such as phage display, or by computationally modeling the peptide in the binding pocket of a target protein [78]. Peptide-based probes are required to properly target rapid binding kinetics and cell permeability and have a short circulation time [77].

Recently, the development of biomaterials for tissue engineering applications has focused on the design of bioactive peptide-modified biomaterials that can

interact with surrounding tissues via biomolecule recognition. The bioactive peptides for tissue regeneration are applied to scaffolding materials to increase their bone regeneration activity [79]. In regenerative therapy, the use of peptides may have advantages over the use of entire proteins with regard to lowering susceptibility to degradation, overcoming possible immunogenicity, and tumor-generable side effects. Biomaterials can improve bioactivity by chemically or physically immobilizing cell-binding peptides on their surfaces by activating cell signaling pathways. These bioactive peptides have historically been derived from proteins bound to the extracellular matrix (ECM) that can bind hydroxyapatite (HA) and induce bio-mineralization.

Osteopontin (OPN), one of the primary non-collagenous proteins found in hard tissues, can bind collagen and create minerals; it regulates bone formation by forming a complex with collagen in hard tissue. A previous study demonstrated that an OPN-derived collagen-binding motif (CBM, GLRSKSKKFRRPDIQYPDATDEDITSHM) could strongly bind collagen through non-covalent binding (as opposed to chemical conjugation) and displayed apatite-forming behavior in pre-osteoblasts and animal models [80]. The binding sequence

SVVYGLR was recently identified adjacent to the RGD sequence in osteopontin following thrombin cleavage at Arg 168, suggesting its involvement in osteo-immune signaling cross-talk [81]. The SVVYGLR peptide significantly increased the adhesion and proliferation of several human mesenchymal stem cells, including bone marrow-derived mesenchymal stem cells. These findings imply that the small synthetic peptide SVVYGLR may represent a potentially useful bioactive material in bone tissue engineering. Bonesialoprotein (BSP) is the major non-collagenous protein in bone and has been shown to be primarily localized near mature osteoblasts and osteoblasts and is incorporated into newly synthesized bone matrix. Furthermore, BSP has been shown to have a degree of specificity in osteoblast-like cell attachment. One recently identified regenerative peptide that interacts with transmembrane proteoglycans, FHRRIKA, can bind heparin [82]. The fusion of two different peptide sequences, RGD and FHRRIKA, was shown to potentially result in enhanced osteoblast adhesion, spreading, and mineralization. These results demonstrate that the utilization of peptide sequences that incorporate both the ECM of cells and heparin-adhesive motifs can increase the degree of cell surface interactions and influence the long-term sustainability of mineral formation in vitro.

KRSR is a sequence present in the five following bone-related adhesive proteins: fibronectin, vitronectin, BSP, thrombospondin, and OPN [83]. KRSR was immobilized onto calcium phosphate-based blocks via aminosilane chemistry with a maleimide cross-linker molecule. Osteoblast adhesion was found to be similar on unfunctionalized nano-crystalline HA compared to conventional HA functionalized with KRSR [84].

HA was originally used to fill bone defects and to accelerate osteointegration in sites created by tooth extraction [85]. HA can be made osteoinductive by the attachment, incorporation, or adsorption of biological factors, such as growth factors, DNA, proteins, and peptides. However, the efficacy of incorporated biological factors is limited by processing conditions, such as pH or temperature [86]. Although HA is a component in human body, the surface of hydroxyapatite-based materials is not easily modified to form functional amino, hydroxyl, or carboxyl groups, such as those found on polymers and metals. Peptides designed to adsorb are a logical alternative. Poly-acidic motifs are a common domain in proteins that interact with inorganic ions and mineral surfaces [87]. The acidic domains directly mediate the binding of proteins to HA. A previous study reported

the selection and characterization of HA-binding peptides using phage display. The strongest binding domain (CMLPHHGAC) and a weak-binding domain (CNPGFAQAC) from the library showed disparate binding. The two peptides (HABPI, CMLPHHGAC and HABP2, CNPGFAQAC) were investigated to determine their binding affinities and structural properties with respect to calcium phosphate mineralization. Scanning electron microscopy (SEM) revealed that the strong-binding peptide (HABP1) yielded significantly larger mineral particles compared to those formed in the presence of a weak-binding peptide (HABP2) or in the negative control. These results indicate that sequence, structure, and molecular stability strongly influence the mineralization activity of the peptides.

The design of a self-assembled peptide was used to create three-dimensional scaffolds for tissue engineering applications [88]. Scaffold materials have modified surfaces that display bioactivity through the chemical or physical immobilization of growth factors and cellular adhesion related-proteins [79] and have been shown to enhance other intracellular functions. The self-assembly of natural or synthetic molecules produces nanoscale macromolecular structures and nanofibers, such as ECM.

Self-assembled nanostructures consisting of BMP receptor-binding peptides and hydrophobic alkyl chains were synthesized with the goal of developing three-dimensional scaffolding materials for osteoblastic differentiation [88]. Furthermore, the self-scaffold generated by the RAD16-I peptide was used to culture cells due to its nanostructural and biomechanical properties and its commercial availability as PuraMatrixTM (3DM Inc., MA, USA) [89]. Its amino acid sequence is RADARADARADARADA. When applied to bone defects in mice calvaria, RAD16-I promoted bone regeneration by inducing the expression of bone-related genes, such as alkaline phosphatase, Runx2, and Osterix, in the cells [90]. These examples indicate that nanoscale fibers produced by the self-assembly of amphipathic peptides have great potential for use in the fields of biomaterials and tissue engineering.

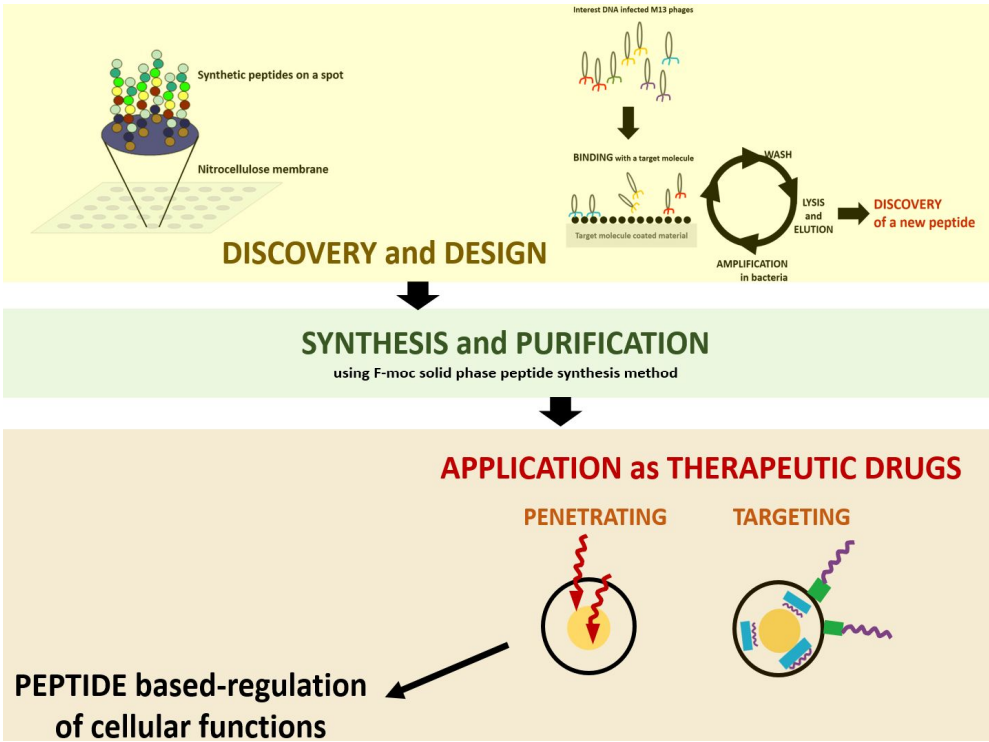

Figure 1.1. The synthetic peptides as therapeutic drugs: from design to application

2. THE AIM OF THIS THESIS

In the thesis, two chapter, Chapter Ⅱ and Ⅲ were described experimental applications using peptides as bioactive molecules. The object of chapter Ⅱ was to describe that peptide-based drug delivery to transport the bioactive small RNA, miRNA-29b. The peptide as a carrier was investigated the overcoming effects of uptake efficiency, cytotoxicity and bioactivity in compared to a conventional gene delivery system. Also, chapterⅢ was aimed to use peptide as imaging and therapeutic molecule for diagnosis and indirect regeneration. The peptide as a biosensor was considered accuracy that can bind the intracellular target and simultaneous inducing bioactivity though protein-peptide interaction.

3. REFERENCES

[1] Singhal G, Jaehne EJ, Corrigan F, Baune BT. Cellular and molecular mechanisms of immunomodulation in the brain through environmental enrichment. Front Cell Neurosci. 2014;8:97.

[2] Lage K. Protein-protein interactions and genetic diseases: The Interactome. Biochim Biophys Acta. 2014.

[3] Mahmoudi M, Meng J, Xue X, Liang XJ, Rahman M, Pfeiffer C, et al. Interaction of stable colloidal nanoparticles with cellular membranes. Biotechnol Adv. 2014;32:679-92.

[4] Lee LC, Maurice DH, Baillie GS. Targeting protein-protein interactions within the cyclic AMP signaling system as a therapeutic strategy for cardiovascular disease. Future Med Chem. 2013;5:451-64.

[5] Gonzalez-Aramundiz JV, Lozano MV, Sousa-Herves A, Fernandez-Megia E, Csaba N. Polypeptides and polyaminoacids in drug delivery. Expert Opin Drug Deliv. 2012;9:183-201.

[6] Lee S, Xie J, Chen X. Peptide-based probes for targeted molecular imaging. Biochemistry. 2010;49:1364-76.

[7] Gagner JE, Kim W, Chaikof EL. Designing protein-based biomaterials for medical applications. Acta Biomater. 2014;10:1542-57.

[8] Merrifield RB. SOLID-PHASE PEPTIDE SYNTHESES. Endeavour. 1965;24:3-7.

[9] Alsina J, Albericio F. Solid-phase synthesis of C-terminal modified peptides. Biopolymers. 2003;71:454-77.

[10] Moreau V, Fleury C, Piquer D, Nguyen C, Novali N, Villard S, et al. PEPOP: computational design of immunogenic peptides. BMC Bioinformatics. 2008;9:71.

[11] Frenkel D, Clark DE, Li J, Murray CW, B RO, Waszkowycz B, et al. PRO_LIGAND: an approach to de novo molecular design. 4. Application to the design of peptides. J Comput Aided Mol Des. 1995;9:213-25.

[12] Zhu H, Bilgin M, Bangham R, Hall D, Casamayor A, Bertone P, et al. Global analysis of protein activities using proteome chips. Science. 2001;293:2101-5.

[13] Rathert P, Dhayalan A, Murakami M, Zhang X, Tamas R, Jurkowska R, et al. Protein lysine methyltransferase G9a acts on non-histone targets. Nat Chem Biol. 2008;4:344-6.

[14] Filippakopoulos P, Picaud S, Mangos M, Keates T, Lambert JP, Barsyte-Lovejoy D, et al. Histone recognition and large-scale structural analysis of the human bromodomain family. Cell. 2012;149:214-31.

[15] Hoffmann B, Ast T, Polakowski T, Reineke U, Volkmer R. Transformation of a biologically active Peptide into peptoid analogs while retaining biological activity. Protein Pept Lett. 2006;13:829-33.

[16] Scharn D, Wenschuh H, Reineke U, Schneider-Mergener J, Germeroth L. Spatially addressed synthesis of amino- and amino-oxy-substituted 1, 3,5-triazine arrays on polymeric membranes. J Comb Chem. 2000;2:361-9.

[17] Mahrenholz CC, Tapia V, Stigler RD, Volkmer R. A study to assess the cross-

reactivity of cellulose membrane-bound peptides with detection systems: an analysis at the amino acid level. J Pept Sci. 2010;16:297-302.

[18] Ay B, Streitz M, Boisguerin P, Schlosser A, Mahrenholz CC, Schuck SD, et al. Sorting and pooling strategy: a novel tool to map a virus proteome for CD8 T-cell epitopes. Biopolymers. 2007;88:64-75.

[19] Reineke U, Sabat R, Volk HD, Schneider-Mergener J. Mapping of the interleukin-10/interleukin-10 receptor combining site. Protein Sci. 1998;7:951-60.

[20] Kramer A, Keitel T, Winkler K, Stocklein W, Hohne W, Schneider-Mergener J. Molecular basis for the binding promiscuity of an anti-p24 (HIV-1) monoclonal antibody. Cell. 1997;91:799-809.

[21] Tegge W, Frank R, Hofmann F, Dostmann WR. Determination of cyclic nucleotide-dependent protein kinase substrate specificity by the use of peptide libraries on cellulose paper. Biochemistry. 1995;34:10569-77.

[22] Reineke U, Ivascu C, Schlief M, Landgraf C, Gericke S, Zahn G, et al. Identification of distinct antibody epitopes and mimotopes from a peptide array of 5520 randomly generated sequences. J Immunol Methods. 2002;267:37-51.

[23] Tonikian R, Zhang Y, Sazinsky SL, Currell B, Yeh JH, Reva B, et al. A specificity map for the PDZ domain family. PLoS Biol. 2008;6:e239.

[24] Rickles RJ, Botfield MC, Weng Z, Taylor JA, Green OM, Brugge JS, et al. Identification of Src, Fyn, Lyn, PI3K and Abl SH3 domain ligands using phage display libraries. Embo j. 1994;13:5598-604.

[25] Sidhu SS. Phage display in pharmaceutical biotechnology. Curr Opin

Biotechnol. 2000;11:610-6.

[26] Ku J, Schultz PG. Alternate protein frameworks for molecular recognition. Proc Natl Acad Sci U S A. 1995;92:6552-6.

[27] Noren KA, Noren CJ. Construction of high-complexity combinatorial phage display peptide libraries. Methods. 2001;23:169-78.

[28] Willats WG. Phage display: practicalities and prospects. Plant Mol Biol. 2002;50:837-54.

[29] Katz BA. Structural and mechanistic determinants of affinity and specificity of ligands discovered or engineered by phage display. Annu Rev Biophys Biomol Struct. 1997;26:27-45.

[30] Pardridge WM. Drug transport across the blood-brain barrier. J Cereb Blood Flow Metab. 2012;32:1959-72.

[31] Milletti F. Cell-penetrating peptides: classes, origin, and current landscape. Drug Discov Today. 2012;17:850-60.

[32] Koren E, Torchilin VP. Cell-penetrating peptides: breaking through to the other side. Trends Mol Med. 2012;18:385-93.

[33] Choi YS, Lee JY, Suh JS, Lee SJ, Yang VC, Chung CP, et al. Cell penetrating peptides for tumor targeting. Curr Pharm Biotechnol. 2011;12:1166-82.

[34] Sakai N, Takeuchi T, Futaki S, Matile S. Direct observation of anion-mediated translocation of fluorescent oligoarginine carriers into and across bulk liquid and anionic bilayer membranes. Chembiochem. 2005;6:114-22.

[35] Perret F, Nishihara M, Takeuchi T, Futaki S, Lazar AN, Coleman AW, et al.

Anionic fullerenes, calixarenes, coronenes, and pyrenes as activators of oligo/polyarginines in model membranes and live cells. J Am Chem Soc. 2005;127:1114-5.

[36] Verdurmen WP, Brock R. Biological responses towards cationic peptides and drug carriers. Trends Pharmacol Sci. 2011;32:116-24.

[37] Kale AA, Torchilin VP. Enhanced transfection of tumor cells in vivo using "Smart" pH-sensitive TAT-modified pegylated liposomes. J Drug Target. 2007;15:538-45.

[38] Maiolo JR, Ferrer M, Ottinger EA. Effects of cargo molecules on the cellular uptake of arginine-rich cell-penetrating peptides. Biochim Biophys Acta. 2005;1712:161-72.

[39] Park YJ, Chang LC, Liang JF, Moon C, Chung CP, Yang VC. Nontoxic membrane translocation peptide from protamine, low molecular weight protamine (LMWP), for enhanced intracellular protein delivery: in vitro and in vivo study. Faseb j. 2005;19:1555-7.

[40] Watkins CL, Brennan P, Fegan C, Takayama K, Nakase I, Futaki S, et al. Cellular uptake, distribution and cytotoxicity of the hydrophobic cell penetrating peptide sequence PFVYLI linked to the proapoptotic domain peptide PAD. J Control Release. 2009;140:237-44.

[41] Fernandez-Carneado J, Kogan MJ, Pujals S, Giralt E. Amphipathic peptides and drug delivery. Biopolymers. 2004;76:196-203.

[42] Deshayes S, Morris M, Heitz F, Divita G. Delivery of proteins and nucleic

acids using a non-covalent peptide-based strategy. Adv Drug Deliv Rev. 2008;60:537-47.

[43] Bolhassani A. Potential efficacy of cell-penetrating peptides for nucleic acid and drug delivery in cancer. Biochim Biophys Acta. 2011;1816:232-46.

[44] Santra S, Yang H, Dutta D, Stanley JT, Holloway PH, Tan W, et al. TAT conjugated, FITC doped silica nanoparticles for bioimaging applications. Chem Commun (Camb). 2004:2810-1.

[45] Santra S, Yang H, Stanley JT, Holloway PH, Moudgil BM, Walter G, et al. Rapid and effective labeling of brain tissue using TAT-conjugated CdS:Mn/ZnS quantum dots. Chem Commun (Camb). 2005:3144-6.

[46] Hu M, Chen P, Wang J, Scollard DA, Vallis KA, Reilly RM. 123I-labeled HIV-1 tat peptide radioimmunoconjugates are imported into the nucleus of human breast cancer cells and functionally interact in vitro and in vivo with the cyclin-dependent kinase inhibitor, p21(WAF-1/Cip-1). Eur J Nucl Med Mol Imaging. 2007;34:368-77.

[47] Yeh HY, Hwang YC, Yates MV, Mulchandani A, Chen W. Detection of hepatitis a virus by using a combined cell culture-molecular beacon assay. Appl Environ Microbiol. 2008;74:2239-43.

[48] Rothbard JB, Garlington S, Lin Q, Kirschberg T, Kreider E, McGrane PL, et al. Conjugation of arginine oligomers to cyclosporin A facilitates topical delivery and inhibition of inflammation. Nat Med. 2000;6:1253-7.

[49] Dubikovskaya EA, Thorne SH, Pillow TH, Contag CH, Wender PA.

Overcoming multidrug resistance of small-molecule therapeutics through conjugation with releasable octaarginine transporters. Proc Natl Acad Sci U S A. 2008;105:12128-33.

[50] Lindgren M, Rosenthal-Aizman K, Saar K, Eiriksdottir E, Jiang Y, Sassian M, et al. Overcoming methotrexate resistance in breast cancer tumour cells by the use of a new cell-penetrating peptide. Biochem Pharmacol. 2006;71:416-25.

[51] Pauwels EK, Erba P, Mariani G, Gomes CM. Multidrug resistance in cancer: its mechanism and its modulation. Drug News Perspect. 2007;20:371-7.

[52] Wang Z, Ravula R, Cao M, Chow M, Huang Y. Transporter-mediated multidrug resistance and its modulation by Chinese medicines and other herbal products. Curr Drug Discov Technol. 2010;7:54-66.

[53] Pasqualini R, Koivunen E, Ruoslahti E. Alpha v integrins as receptors for tumor targeting by circulating ligands. Nat Biotechnol. 1997;15:542-6.

[54] Doorbar J, Winter G. Isolation of a peptide antagonist to the thrombin receptor using phage display. J Mol Biol. 1994;244:361-9.

[55] McGuire MJ, Samli KN, Johnston SA, Brown KC. In vitro selection of a peptide with high selectivity for cardiomyocytes in vivo. J Mol Biol. 2004;342:171-82.

[56] Samli KN, McGuire MJ, Newgard CB, Johnston SA, Brown KC. Peptide-mediated targeting of the islets of Langerhans. Diabetes. 2005;54:2103-8.

[57] McGuire MJ, Samli KN, Chang YC, Brown KC. Novel ligands for cancer diagnosis: selection of peptide ligands for identification and isolation of B-cell

lymphomas. Exp Hematol. 2006;34:443-52.

[58] Oyama T, Rombel IT, Samli KN, Zhou X, Brown KC. Isolation of multiple cell-binding ligands from different phage displayed-peptide libraries. Biosens Bioelectron. 2006;21:1867-75.

[59] Rajotte D, Arap W, Hagedorn M, Koivunen E, Pasqualini R, Ruoslahti E. Molecular heterogeneity of the vascular endothelium revealed by in vivo phage display. J Clin Invest. 1998;102:430-7.

[60] Rajotte D, Ruoslahti E. Membrane dipeptidase is the receptor for a lung-targeting peptide identified by in vivo phage display. J Biol Chem. 1999;274:11593-8.

[61] Fukumura D, Jain RK. Tumor microenvironment abnormalities: causes, consequences, and strategies to normalize. J Cell Biochem. 2007;101:937-49.

[62] Baluk P, Hashizume H, McDonald DM. Cellular abnormalities of blood vessels as targets in cancer. Curr Opin Genet Dev. 2005;15:102-11.

[63] Arap W, Pasqualini R, Ruoslahti E. Cancer treatment by targeted drug delivery to tumor vasculature in a mouse model. Science. 1998;279:377-80.

[64] Christian S, Pilch J, Akerman ME, Porkka K, Laakkonen P, Ruoslahti E. Nucleolin expressed at the cell surface is a marker of endothelial cells in angiogenic blood vessels. J Cell Biol. 2003;163:871-8.

[65] Laakkonen P, Porkka K, Hoffman JA, Ruoslahti E. A tumor-homing peptide with a targeting specificity related to lymphatic vessels. Nat Med. 2002;8:751-5.

[66] Fogal V, Zhang L, Krajewski S, Ruoslahti E. Mitochondrial/cell-surface

protein p32/gC1qR as a molecular target in tumor cells and tumor stroma. Cancer Res. 2008;68:7210-8.

[67] Javadpour MM, Juban MM, Lo WC, Bishop SM, Alberty JB, Cowell SM, et al. De novo antimicrobial peptides with low mammalian cell toxicity. J Med Chem. 1996;39:3107-13.

[68] Ellerby HM, Arap W, Ellerby LM, Kain R, Andrusiak R, Rio GD, et al. Anti-cancer activity of targeted pro-apoptotic peptides. Nat Med. 1999;5:1032-8.

[69] Agasti SS, Rana S, Park MH, Kim CK, You CC, Rotello VM. Nanoparticles for detection and diagnosis. Adv Drug Deliv Rev. 2010;62:316-28.

[70] So MK, Xu C, Loening AM, Gambhir SS, Rao J. Self-illuminating quantum dot conjugates for in vivo imaging. Nat Biotechnol. 2006;24:339-43.

[71] Wang H, Chen X. Applications for site-directed molecular imaging agents coupled with drug delivery potential. Expert Opin Drug Deliv. 2009;6:745-68.

[72] Wu XL, Kim JH, Koo H, Bae SM, Shin H, Kim MS, et al. Tumor-targeting peptide conjugated pH-responsive micelles as a potential drug carrier for cancer therapy. Bioconjug Chem. 2010;21:208-13.

[73] Kim K, Lee M, Park H, Kim JH, Kim S, Chung H, et al. Cell-permeable and biocompatible polymeric nanoparticles for apoptosis imaging. J Am Chem Soc. 2006;128:3490-1.

[74] Funovics M, Weissleder R, Tung CH. Protease sensors for bioimaging. Anal Bioanal Chem. 2003;377:956-63.

[75] Bremer C, Tung CH, Bogdanov A, Jr., Weissleder R. Imaging of differential

protease expression in breast cancers for detection of aggressive tumor phenotypes. Radiology. 2002;222:814-8.

[76] Mu CJ, Lavan DA, Langer RS, Zetter BR. Self-assembled gold nanoparticle molecular probes for detecting proteolytic activity in vivo. ACS Nano. 2010;4:1511-20.

[77] Lee S, Park K, Kim K, Choi K, Kwon IC. Activatable imaging probes with amplified fluorescent signals. Chem Commun (Camb). 2008:4250-60.

[78] Aina OH, Liu R, Sutcliffe JL, Marik J, Pan CX, Lam KS. From combinatorial chemistry to cancer-targeting peptides. Mol Pharm. 2007;4:631-51.

[79] Holmes TC, de Lacalle S, Su X, Liu G, Rich A, Zhang S. Extensive neurite outgrowth and active synapse formation on self-assembling peptide scaffolds. Proc Natl Acad Sci U S A. 2000;97:6728-33.

[80] Lee JY, Choo JE, Choi YS, Park JB, Min DS, Lee SJ, et al. Assembly of collagen-binding peptide with collagen as a bioactive scaffold for osteogenesis in vitro and in vivo. Biomaterials. 2007;28:4257-67.

[81] Lai CF, Seshadri V, Huang K, Shao JS, Cai J, Vattikuti R, et al. An osteopontin-NADPH oxidase signaling cascade promotes pro-matrix metalloproteinase 9 activation in aortic mesenchymal cells. Circ Res. 2006;98:1479-89.

[82] Rezania A, Healy KE. Biomimetic peptide surfaces that regulate adhesion, spreading, cytoskeletal organization, and mineralization of the matrix deposited by osteoblast-like cells. Biotechnol Prog. 1999;15:19-32.

[83] Dee KC, Andersen TT, Bizios R. Design and function of novel osteoblast-adhesive peptides for chemical modification of biomaterials. J Biomed Mater Res. 1998;40:371-7.

[84] Nelson M, Balasundaram G, Webster TJ. Increased osteoblast adhesion on nanoparticulate crystalline hydroxyapatite functionalized with KRSR. Int J Nanomedicine. 2006;1:339-49.

[85] Geesink RG. Osteoconductive coatings for total joint arthroplasty. Clin Orthop Relat Res. 2002:53-65.

[86] Tanahashi M, Yao T, Kokubo T, Minoda M, Miyamoto T, Nakamura T, et al. Apatite coated on organic polymers by biomimetic process: improvement in its adhesion to substrate by glow-discharge treatment. J Biomed Mater Res. 1995;29:349-57.

[87] Gorski JP. Acidic phosphoproteins from bone matrix: a structural rationalization of their role in biomineralization. Calcif Tissue Int. 1992;50:391-6.

[88] Lee JY, Choo JE, Choi YS, Suh JS, Lee SJ, Chung CP, et al. Osteoblastic differentiation of human bone marrow stromal cells in self-assembled BMP-2 receptor-binding peptide-amphiphiles. Biomaterials. 2009;30:3532-41.

[89] Zhang S, Lockshin C, Cook R, Rich A. Unusually stable beta-sheet formation in an ionic self-complementary oligopeptide. Biopolymers. 1994;34:663-72.

[90] Misawa H, Kobayashi N, Soto-Gutierrez A, Chen Y, Yoshida A, Rivas-Carrillo JD, et al. PuraMatrix facilitates bone regeneration in bone defects of calvaria in mice. Cell Transplant. 2006;15:903-10.

CHAPTER Ⅱ

Peptide-based intracellular delivery of osteoinductive miRNA for efficient regulation in human mesenchymal stem cells

1. LIST OF FIGURES AND TABLES

FIGURES

TABLES

2. ABSTRACT

Stem cell differentiation is modulated by several key molecules, including cytokines, hormones, and engineered peptides. Emerging evidence suggests that microRNA has potential applications in stem cell engineering, such as in osteoblastic differentiation. MicroRNAs (miRNAs) bind to the 3'-untranslated region (UTR) sequence of target mRNA, thereby attenuating protein synthesis. Our goal was to evaluate the delivery of miRNA, i.e., miRNA-29b, to stem cells to promote osteoblastic differentiation because this miRNA is known to target anti-osteogenic factors gene expression. Despite the important role of miRNAs, their application has been limited due to poor cell/tissue penetration. The author attempted to overcome this limitation by using a cell-penetrating peptide (CPP) carrier. Herein, the arginine-rich CPP, called the low-molecular weight protamine (LMWP), is the sequence from natural protamine. The author worked out the difficult problem to transfect into hMSCs by the complex with LMWP, and then the author investigated synthetic double-stranded miR-29b could be induced osteoblast differentiation.

3. INTRODUCTION

MicroRNAs (miRNAs) have emerged as important regulators for various developmental, physiological, and pathological conditions, such as tumorigenesis, viral infection, and cell differentiation and function [1-3]. Most miRNAs are single-stranded small RNA molecules that are approximately 21 or 22 nucleotides in length [2]. They do not encode protein; instead, they regulate the level of target proteins by decreasing messenger RNA (mRNA) levels or inhibiting mRNA translation by binding the 3'UTR of the target mRNA [1]. Although various miRNAs regulate cell differentiation and proliferation, there is only a limited amount of information about the regulatory mechanism of miRNAs in osteoblastic differentiation. In this study, the author used a synthetic, human-derived miRNA-29b (miR-29b), which is one of the most robustly expressed microRNAs during osteoblast differentiation. The miR-29b positively regulates osteoblastic differentiation by down-regulating inhibitory factors of osteogenic signaling pathways and controlling the expression of collagen

in differentiated murine calvaria-derived pre-osteoblasts, e.g., MC3T3 cells [4]. As a consequence of previous reports using animal stem cells, the potential of LMWP as a tool for the intracellular delivery of this miR-29b was evaluated using human stem cells.

The therapeutic applications of oligonucleotides have been hampered in the clinic due to limited stability, poor cellular uptake *in vivo*, and a lack of a reliable delivery method. The main obstacle in the practical application of oligonucleotides as a molecular medicine is the difficulty in delivering these agents across the cell membrane to the cytoplasm, both *in vitro* and *in vivo*, where it can lead sequence-specific mRNA degradation or translational inhibition. Moreover, stem cells, including MSCs, are difficult to transfect [5]. Indeed, hMSCs have been conventionally transfected by several methods, such as electroporation [6], lentiviral vectors [7] and lipid-based transfection methods [8, 9], for the delivery of oligonucleotides such as miRNA or siRNA. However, these methods of gene delivery have their own limitations. Electroporation is not practical *in vivo* [10], and viral vectors risk integrating the viral gene into the host genome [11]. Conjugating or

entrapping the oligonucleotides to or in a nano-carrier, such as a water soluble polymer, cationic lipid, or liposome, is less toxic than using viral vectors; however, there are still problems of low efficiency, and the oligonucleotides must escape the endosome [12, 13]. Therefore, the search for a safe and highly effective delivery system for miRNA-based molecular medicine continues. A promising new approach employing cell-penetrating peptides (CPP) for direct miRNA delivery has been created to meet this challenge. The first CPP was discovered more than a decade ago [14]; since then, the cationic nature of the CPPs has allowed them to electrostatically bind to the phosphate backbone of nucleic acids and thus form a stable complex in which nucleic acids were protected from degradation [15]. CPPs have been shown to effectively deliver DNA [16], miRNA *in vitro* [17] and siRNA was delivered *in vivo* [5]. Additionally, covalently attaching CPPs to other cationic peptides increased their transfection efficiency and prevented DNA neutralization by its negative charge [18].

The author previously reported that a nontoxic, arginine-rich, CPP peptide (VSRRRRRRGGRRRR), called the low molecular weight

protamine (LMWP), possesses cell translocating potential and can effectively deliver large protein molecules to tumors, thereby suppressing tumor growth *in vivo* [19]. Unlike other CPPs, the toxicity profiles of LMWP have already been thoroughly established [19-21]. In a previous study using a dog model, LMWP was neither antigenic nor mutagenic and elicited only minimal complement activation with no detectable hypotensive or toxic responses [20], implying that LMWP could be practically employed as a safe and effective systemic carrier of large molecules, including proteins and gene products, such as therapeutic plasmids. Therefore, LMWP has the potential to overcome the low efficiency of stem cell transfection.

Herein, the author hypothesized LMWP efficiently transduces miRNA directly into human MSCs and induces osteogenic differentiation. Complex creation of LMWP and miRNA-29b, intracellular localization of miRNA-29b by the LMWP/miRNA-29b complex will be demonstrated in this paper. In addition, osteogenic differentiation activity of LMWP/miRNA-29b complex reflected by the suppression of intracellular inhibitory target gene expression will be also detailed discussed in this paper.

4. MATERIALS AND MATHODS

4.1. Synthesis of peptides

The LMWP peptides (VSRRRRRRGGRRRR, the sequence of protamine) corresponding to protamine were prepared in mass quantities using a peptide synthesizer (APEX 396, AAPP TEC, Louisville, KY, USA) based on standard fluoren-9-ylmethoxycarbonyl (F-moc) chemistry. A 2-chlorotrityl chloride resin was pre-swollen in DMF (N,N-dimethyl formamide) and the Fmoc-protecting groups of the resin and amino acids were removed using 29% piperidine in DMF, 10eq. DIPEA (diisopropylethylamine), 5eq. HBTU (2-(1H-Benzotriazol-1-yl)-1, 1, 3, 3-tetramethyluronium hexafluorophosphate), and 5eq. of Fmoc-protected amino acid, calculated according to the loading of the resin. The peptide-resin was dried using methylene chloride. The cleavage and side chain deprotection of the peptide-resin proceeded for 4h using TFA (trifluoroacetic acid)/EDT (1,2-ethanedithiol)/TIS (triisopropylsilane)/H_2O (92.5:2.5:2.5:2.5). The peptide cleavage solutions were triturated with diethylether, and the aqueous solutions

containing peptides were lyophilized. The prepared peptides were purified by reverse-phase high-performance liquid chromatography (Waters AutoPrep system, USA) using a Vydac C18 column and a gradient of water/acetonitrile containing 0.1% TFA. The peptide was characterized in terms of molecular weight by MALDI-TOF and was found to have the expected molecular weight. The purity of the peptides was above 98%.

4.2. Fluorescence labeling

LMWP has only one free amino group on its N-terminal, Val. The reaction was conducted by mixing LMWP with a FITC solution in DMF at pH 9.3 overnight. The FITC labeling of LMWP was conducted by labeling the valine residue of LMWP. The labeling efficiency was monitored by high-pressure liquid chromatography (HPLC) by dual absorbance at 230nm and 480nm. The fluorescently labeled peptides were purified by HPLC (purity > 95%), lyophilized, and then stored at -20°C in the dark until further use.

4.3. MicroRNA expression profiling

Normal hMSC or osteoblastic differentiated cells was given genomic RNAs using TRIzol™ (Invitrogen, CA, USA). The amount of input RNA, labeling, and hybridization conditions were chosen following the recommendations of the manufacturer. The manufacturer developed its procedures that involved dedicated protocols for labeling, equipment for hybridization and scanning, and software for data acquisition. Agilent hybridizations were processed by Ebiogen laboratory (ebiogen co., Korea) according to the manufacturer's instructions. One hundred ng total RNA was pre-treated and hybridized on an 8 x 15K format Agilent human miRNA array. Arrays were washed according to manufacturer's instructions and scanned at a resolution of 5mm using an Agilent 4000B scanner. Data were acquired using Agilent Feature Extraction software version 9.5.3.1.

4.4. MicroRNA target site prediction

A search for predicted target mRNAs was performed using the databases

TargetScan (http://www.targetscan.org/) and PicTar (http://pictar.mdc-berlin.de/). Sequence conservation was examined using the University of California-Santa Cruz's genome browser (http://genome.ucsc.edu/).

4.5. MicroRNA-29b preparation

Human miRNA-29b sequence was obtained from the miRBase Sequence Database (http://microrna.sanger.ac.uk, Release 10.1). The sense strand sequence was the following: hsa-miR-29b, 50-UAGCACCAUUUGAAAUCAGUGUU. The hsa-miR-29b was chemically modified with a thiol group at the 50 end of the sense strand and Tetramethyl-6-Carboxyrhodamine (TAMRA) on the complementary strand. The double-stranded miRNAs were purchased from Bioneer Co. (Korea) with routine process protocol which was set up by the company. Additionally, anti-hsa-miRNA-29b and negative control miRNA (random sequence) were purchased from Ambion Inc., USA.

4.6. Preparation of LMWP/miRNA complexes

The prepared miRNAs were supplemented with 1 volume of reaction buffer (10mM HEPES, 1mM ethylenediamine tetraacetic acid (EDTA), pH 8.0) to adjust the final concentration of the miRNAs to 100nM. The miRNAs were mixed with excess LMWP at a ratio of 1/1-1/10 (-/+) and were incubated for 2h at 4°C to form nanosized disulfide bond-mediated complexes.

4.7. Characterization of LMWP/miRNA complexes

The complex formation was monitored by 2% agarose gel electrophoresis using molecular markers. Following electrophoresis, the gels were stained with 0.5mg/mL ethidium bromide for 20min and analyzed on a UV illuminator to identify the locations of the miRNA. The dispersity of the LMWP/miR-29b was assessed by transmitting electron micrograph (TEM). The complexes were stained with uranyl acetate to examine their morphology. The size distribution and zeta potential of the complexes were measured using a Zetasizer Nano ZS instrument and analyzed using DTS software (Malvern Instruments Limited, Malvern, UK).

The size distribution and zeta potential studies were conducted by dispersing the samples according to the manufacturer's instructions. The instrument measured the electrophoretic mobility and conductivity of the complex and converted it to the zeta-potential using the classical Smoluchowski expression [22]. All measurements were carried out at 25°C. The results are the average of three measurements. Serum stability of naked miR-29b in aqueous solution versus its stability in complex preparations was characterized using 15% polyacrylamide gel electrophoresis. Samples of naked miR-29b in aqueous solution or the LMWP/miR-29b complex were mixed in a 1:1 ratio with fresh serum to give 50% serum concentration. The mixture of the LMWP/miR-29b complex with serum was incubated at 37°C. Aliquots from each mixture of the LMWP/miR-29b or free miR-29b with serum at different incubation times were loaded onto a gel and examined after electrophoresis to visualize intact the miR-29b by staining with ethidium bromide.

4.8. Effect of miRNA transfection strategies on cell viability

A human mesenchymal stem cell line (hMSC, LONZA, Switzerland) was

maintained in MSCGM medium (LONZA, Switzerland). The cell viability was determined using the trypan blue and the 3-(4,5-dimethylthiazol-2-yl)-2,5-diphenyltetrazolium bromide (MTT) colorimetric assay. Before the experiments, the hMSCs were plated in 24-well plates and maintained in antibiotic-free medium for 24h. For lipid-based transfections, miRNAs were mixed with Lipofectamine^{TM} RNAi MAX (Invitrogen, USA) and then added to the cells. LMWP was also delivered in the absence of a transfection reagent by mixing the miRNAs with LMWP in Opti-MEM (Invitrogen, USA; See an above-mentioned protocol "Preparation of LMWP/miRNA complex") and then incubating for 15min at room temperature. The miRNA-LMWP mixtures were directly added to cells and incubated for 4days in MSCGM. At the indicated time, the cells in the 24-well plates were incubated with 0.5 mg/mL MTT for 2h at 37°C. The intensity of the MTT product was measured at 550nm using a microplate reader. Also, cell death was examined by trypan blue exclusion assay, and cells were counted with a hemocytometer. BrdU labeling was quantified using a commercially available ELISA (enzyme-linked immunosorbent assay) kit (Roche, Switzerland).

4.9. Confocal microscopic observation of LMWP and LMWP/miRNA internalization

Either FITC-labeled LMWP complexed with TAMRA-labeled miR-29b or TAMRA labeled miR-29b mixed with Lipofectamine^{TM} RNAi MAX (Invitrogen, USA) was added to cells at a final peptide concentration of 50nM. Following 30min or 5h incubation at 37°C in humidified 5% CO_2, the cells were washed with PBS extensively and then examined by confocal microscopy. Confocal laser scanning microscopy was carried out using an Olympus FV-300 laser scanning microscope operated with FLUOVIEW software (Olympus, Tokyo, Japan). The laser was set at 488nm (green) and 546nm (red) to produce the excitation wavelength for fluorescein. Z-series were taken at a 1-2mm optical section at 2° intervals.

4.10. Flow cytometric analyses of LMWP and LMWP/miRNA internalization

Cells were washed and incubated with either the FITC-labeled LMWP/TAMRA

labeled miR-29b complex or the Lipofectamine™ RNAi MAX/TAMRA-labeled miR-29b complex for 30min or 5h at 37°C in humidified 5% CO_2. After incubation, the cells were washed with PBS and extensively treated with TrypLE™ Express for 10 min to remove surface-bound fluorescence-labeled samples before washing again to avoid artifacts. The cells were analyzed on a FACSCalibur flow cytometer (Beckton Dickinson, CA, USA) equipped with a 488nm air-cooled argon laser. The filter settings for emission were 530/30nm bandpass (FL1) for FITC. The fluorescence of 10,000 vital cells was acquired, and the data were visualized in logarithmic mode.

4.11. Quantitative analysis of osteogenic markers using PCR

Cells were incubated with 50nM of the LMWP/miR-29b complex and miR-29b lipoplex for 48h in MSCGM. At the end of the indicated times, the total RNA was isolated using TRIzol™ (Invitrogen, CA, USA) and then quantified by ultraviolet (UV) spectroscopy. A cDNA library was synthesized using the DNase I-treated total RNA (1mg) by oligo dT priming using the Super Script II pre-amplification

system (Invitrogen, CA, USA). PCR (polymerase chain reaction) was performed using a GeneAmp^{TM} PCR 9700 thermocycler. Real-time quantitative PCR analysis was performed on an ABI PRISM 7500 (Applied Biosystems, CA, USA) by SYBR Green I dye detection. The reactions were assembled following the manufacturer's recommendation. The PCR conditions were as follows: 10s at 95°C, followed by 40 cycles of 5s at 95°C, 34s at the annealing temperature, and 30s at 72°C. The relative cDNA ratio was calculated using the value of threshold cycles. The PCR primer sequences are shown in Table 2.1. The hsa-miR-29b primer set was purchased from EXIQON Co., USA. Human glyceraldehyde-3-phosphate dehydrogenase (GAPDH) was used as reference control to normalize for equal loading of template cDNA.

4.12. Matrix mineralization of hMSCs by LMWP-miR-29b

The cells were grown to confluence in 24-well culture plates and incubated with miR-29b, LMWP/miR-29b complex or miR-29b lipoplex for 7days in mineralization medium containing 20% FBS, 50mg/ml ascorbic acid, 10mM β-

glycerophosphate, and 10^{-7}M dexamethasone. The media were changed once with fresh miR-29b, LMWP/miR-29b and Lipofectamine/miR-29b. The cells were incubated in 2% Alizarin red S (Sigma-Aldrich, Basel, Switzerland) in water for 5min at room temperature, followed by two washes with water and then air drying to visualize the calcium deposits. Matrix mineralization was quantified by extracting the Alizarin red stain with 10% cetylpyridinium chloride (Sigma-Aldrich, USA) at room temperature for 2h. The absorbance of the extracted Alizarin red S stain was measured at 570nm. Cells were stained using the ALP detection kit (Millipore, USA) for 15min at room temperature, followed by two washes with water and air drying. The ALP activity in cell lysates prepared with an ultrasonic cell disrupter was also measured using a commercially available kit (LABOASSAYTM ALP, Wako Pure Chemical Industries, Japan): the activity was assessed as the rate of conversion from p-nitrophenyl phosphate to p-nitrophenol. Additionally, mineralization was visualized under confocal microscopy after the following cell treatment. The hMSCs were seeded at a density of 1×10^{4}/well in 4-well chambered slide glass (Nunc, USA) in MSCGM. One day later, the cells were washed twice with PBS and incubated with miR-29b, LMWP/miR-29b, or

Lipofectamine/miR-29b for 7days in mineralization medium containing 20% FBS, 50mg/ml ascorbic acid, 10mM β-glycerophosphate, and 10^{-7}M dexamethasone, and 1mM Calcein. The medium was changed without miRNAs once. After an appropriate incubation time, cells were washed in PBS and fixed with 10% neutral buffered formalin. The cells were then incubated with Hoechst's dye and imaged using confocal laser scanning microscopy. To examine the effect of the antisense of miR-29b as a mineralization inhibitor, cells were transfected with each sample combined with LMWP for a day. The samples included 50nM LMWP, 50nM control mismatch miRNA, 50nM miR-29b, 50nM anti-miR-29b, and 50nM miR-29b/anti-miR-29b complexes. The cell lysates were examined by western blot using antibodies to detect osteogenesis markers. Additionally, the mineral and ALP staining experiments described above (e.g., Alizarin red S, Calcein, and ALP activity) were also performed to confirm the inhibition effect of mineralization on transfected cells with anti-miR-29b.

4.13. DNA constructs and functional analysis of miR-29b

The method in the present work has been described elsewhere [4,23]. Briefly, the partial segments (200-300 nucleotides) of the mRNA 3‘-UTR containing the miR-29b binding sequences for the HDAC4 (Histone deacetylase 4), CTNNBIP1 (Catenin-β interacting protein 1), DUSP2 (Dual specificity phosphatase 2), COL1A1 (Collagen type 1 alpha 1) and COL5A3 (Collagen type 5 alpha 3) genes were PCR-amplified from human genomic DNA using the forward and reverse primers (Table 2.1). The PCR products were then subcloned into the SpeI-MluI site downstream of the stop codon in the pMIR-REPORT Firefly Luciferase reporter vector (Ambion, USA). The correct orientation of 3‘-UTR fragments in the plasmid DNA constructs were further confirmed by sequencing. Transient transfection of hMSCs (8×10^4 cells/dish) was carried out in 60mm dishes using the LMWP/miR-29b complex. The cells were co-transfected with 200ng of the luciferase constructs 5ng of phRL-null (Promega, USA) Renilla luciferase plasmid, and 100nM microRNAs with LMWP in all transfections for 32h. Luciferase assays were performed using the Dual-luciferase reporter assay system (Promega, USA) based on the manufacturer’s instructions. The luminescent signal was quantified using a luminometer (Glomax; Promega, USA), and each value from the firefly

luciferase construct was normalized by the Renilla luciferase assay.

4.14. Statistical analysis

All experiments were independently repeated at least three times, and the data are presented as the mean ± standard error (SE). The data were analyzed by one way ANOVA followed by Fisher's protected least significant difference (PLSD) post hoc test (StatView; SAS Institute, Cary, NC, USA). *P*-values of <0.05 and <0.01 were considered to be statistically significant.

Table 2.1. The nucleotide sequences of the primers used for constructing the plasmids and osteogenic markers

Gene	Primer sequences
HDAC4	5-GGACTAGTCCCGAAGCTGCTGTTCTCTCCT-3 (Forward)
	5-CGACGCGTCGCACAGCACCCCACTAAGGTT-3 (Reverse)
CTNNBIP1	5-GGACTAGTCCGTGGTAGCAAACCACCGTCT-3 (Forward)
	5-CGACGCGTCGACCAAACCCGCATCTTACTG-3 (Reverse)
DUSP2	5-GGACTAGTCCCACAGCTCTGGCTTTGACTG-3 (Forward)
	5-CGACGCGTCGGGAGGAAGTTGGGGAGAGAG-3 (Reverse)
COL1A1	5-GGACTAGTCCCCCCAAGAACCTGACAACTT-3 (Forward)
	5-CGACGCGTCGTCCCCTCCCAAAGTCTTCTT-3 (Reverse)
COL5A3	5-GGACTAGTCCACTCGGCTCCATCTGCTTTA-3 (Forward)
	5-CGACGCGTCGTGGAATCTCTCACCGTACCC-3 (Reverse)
ALP	5-TGGAGCTTCAGAAGCTCAACACCA-3 (Forward)
	5-ATCTCGTTGTCTGAGTACCAGTCC-3 (Reverse)
OCN	5-CATGAGAGCCCTCACA-3 (Forward)
	5-AGAGCGACACCCTAGAC-3 (Reverse)
OPN	5-ATTCTGGGAGGGCTTGGTT-3 (Forward)
	5-AGTCTGGTCCCGACGATG-3 (Reverse)
TAZ	5-TCCCCACAACTCCAGAAGAC-3 (Forward)
	5-CAAAGTCCCGAGGTCAACAT-3 (Reverse)
GAPDH	5-CGTCTTCACCACCATGGAGA-3 (Forward)
	5-CGGCCATCACGCCACAGTTT-3 (Reverse)

5. RESULTS

5.1. Overview of miRNA array approach

To investigate a specific miRNA that could potentially regulate osteoblastic/osteocytic differentiation, a screening with a miRNA array was utilized. The author first obtained an overview of fluorescent intensity in overall labeled-miRNA samples (Fig. 2.1; left). All the tested miRNAs were analyzed by clustergram. Based on the result of the clustergram, one of the groups was possessed the miRNAs that increased in fold changes in the differentiated (21day)/normal (0day) cells with two exceptions, miRNA-17-5p and miRNA-20a-5p. The author showed the differences of miRNAs values in a red-green heat map (Fig. 2.1; middle) and fold changes by un-differentiated cells in a table (Fig. 2.2; right). The miRNA-29b-3p was the most up-regulated miRNA in the osteogenic induction groups at three week. In analysis using polymerase chain reaction (PCR), miRNA-29b was also elevated in correlated with mRNA levels of osteogenic genes such as alkaline phosphatase (ALP), osteocalcin (OCN) and Runt-related

transcription factor 2 (Runx2) whereas, COL1A1 was decreased which is negative mineralization marker (Fig. 2.2). Thus, miRNA-29b was adopted as internal controls for miRNA quantification using a drug delivery system in the osteogenic differentiation and mineralization. In addition, miRNA-29b was established as a new marker of osteogenic differentiation in a human derived-cell.

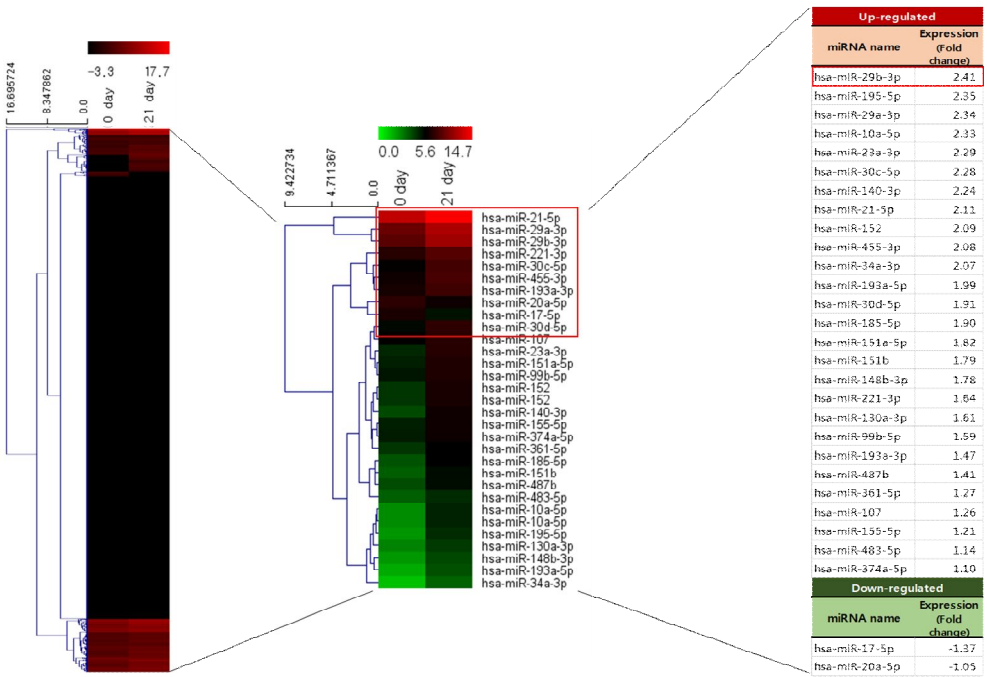

Figure 2.1. The miRNA expression signature during hMSC osteogenic differentiation

Fluorescent intensity of each miRNA on the array chip was shown in a black-red heat map (left figure). Among analyzed miRNAs, a number of miRNAs which were reported osteo-miRNAs were visualized as their detected values in a red-green heat map (middle figure). Log_2 fold changes in the differentiated/normal cells comparison were arranged in a table format (right figure). The miRNA expressions after 21day of osteo-induction (21day) were compared to non-induction control (0day).

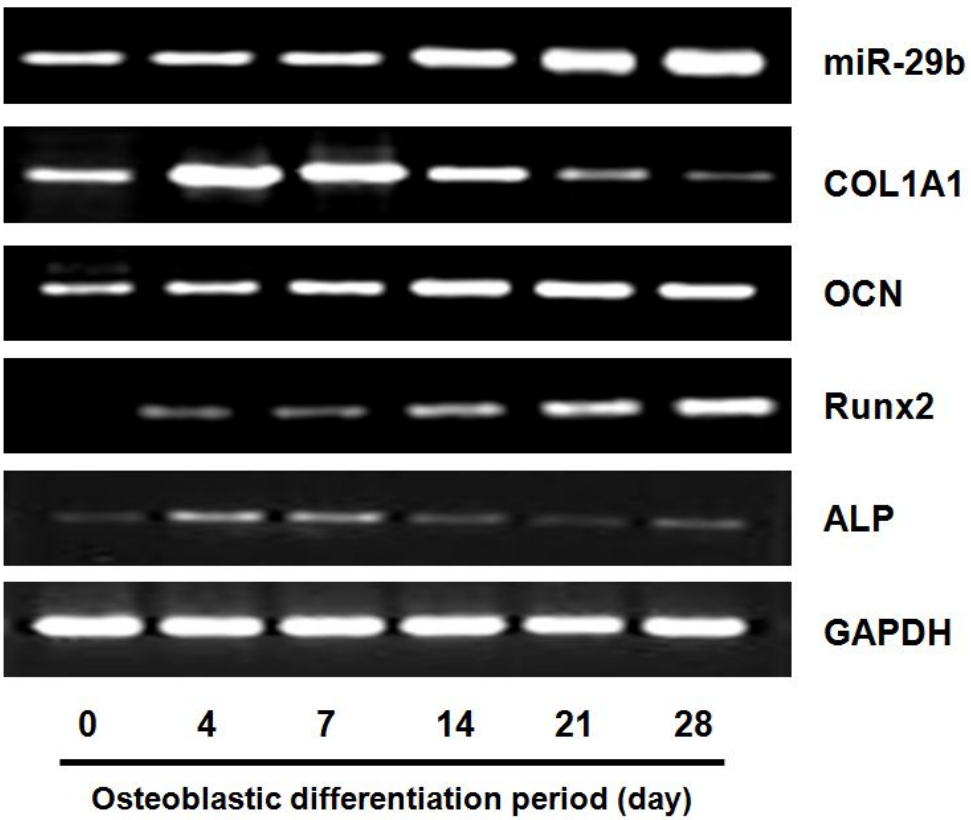

Figure 2.2. Expression of osteogenic markers and miRNA-29b

The mRNA levels of miR-29b, ALP, OCN, Runx2 and COL1A1 for osteogenic differentiation until 28days in hMSCs were investigated using a PCR machine.

5.2. Synthesis and biophysical properties of LMWP/miR-29b complex

The particle size of the LMWP/miR-29b complex decreased in accordance with the increase of (+/- charge ratio up to 5:1 (+/-). The particle size reduction reached a plateau around 30-50 nm in diameter even increase up to 10:1 (+/-) (Fig. 2.3). These results agree with those of other investigators [24]. The LMWP formed a condensed complex with miR-29b, as reflected by the result from gel retardation assay (Fig. 2.4A) and TEM (Fig. 2.4B). Further increase of charge ratio did not provide further reduction in the particle size of the complex. Rather, excess amount of positive charge at the particles has been known to participate in the aggregate creation in the aqueous [25].

As the surface charge ratio of the complex increased, the zeta potential, conductivity as well as mobility accordingly increased from that by the naked miR-29b, indicating high potential in transduction inside the cells (Table 2.2).In addition, the data for the LMWP itself in the Table 2.3 was the one from the dilution (×10). Therefore, the values for the zeta potential, mobility and conductivity have been adjusted in the manuscript. The charge ratio of LMWP/miR-29b was 10:1 (+/-).

The author also examined the stability of miR-29b in the complex when exposed to serum. Incubating free miR-29b in an aqueous solution resulted in the degradation of the oligonucleotides, as indicated by loss of their band in the gel after several hours (Fig. 2.5). The naked miR-29b remains intact during the first 2h incubation; however, its stability is diminished by further incubation in serum. However, the miR-29b in the LMWP complex was protected from degradation for up to 24h, implying that the LMWP/miR-29b complex was stable and protected from digestion in serum; thus, the LMWP might be useful in an *in vivo* application where miR-29b is exposed to serum nucleases.

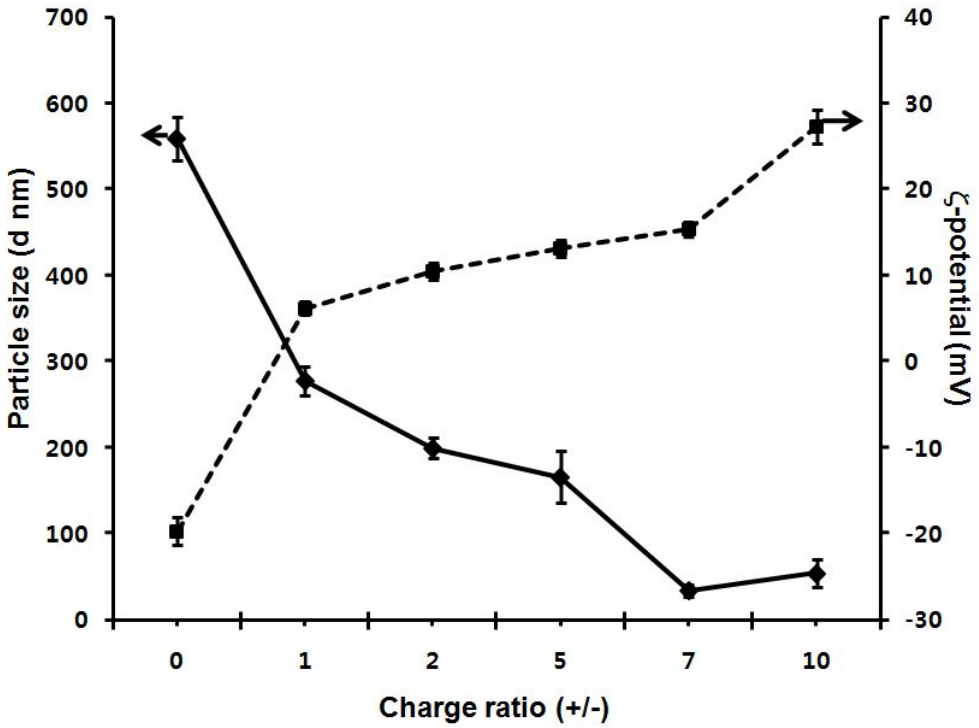

Figure 2.3. Particle size and zeta potential of LMWP/miR-29b complex

Samples were prepared several groups depending on increased charge ratio (+/−) between LMWP and miRNA. The miR-29b concentration was fixed as 50nM.

Table 2.2. Comparison of quantitative particle property between complex and non-complex

The mean particle diameter, zeta potential, mobility and conductivity of the miR-29b, LMWP and LMWP/miR-29b complexes were measured using a dynamic light scattering principle.

	Average size (d nm)	Z-potential (mV)	Mobility (μmcm/Vs)	Conductivity (mS/cm)
miRNA-29b	559.13±25.01	-19.67±1.55	0.017±0.0	-1.54±0.12
LMWP	0.61±0.15	8.86±1.40	0.129±0.01	0.69±0.11
LMWP/miRNA-29b complex	34.32±7.23	27.3±2.0	0.089±0.01	2.14±0.15

Table 2.3. Quantitative particle property of LMWP/miR-29b complex

The mean particle diameter, zeta potential, mobility and conductivity of the LMWP/miR-29b complex were measured as a function of the charge ratio between LMWP and miR-29b. The miR-29b concentration was fixed as 50nM.

miRNA-29b/LMWP charge ratio	Average size (d nm)	Z-potential (mV)	Mobility (μmcm/Vs)	Conductivity (mS/cm)
1:1	277.53±17.1	6.21±0.73	0.021±0.0	0.49±0.06
1:2	199.47±12.0	10.48±1.02	0.087±0.01	0.82±0.08
1:5	165.80±30.0	13.13±1.01	0.089±0.01	1.03±0.08
1:7	34.32±7.23	15.37±0.84	0.087±0.01	1.21±0.07
1:10	54.46±15.46	27.30±2.00	0.040±0.01	2.14±0.15

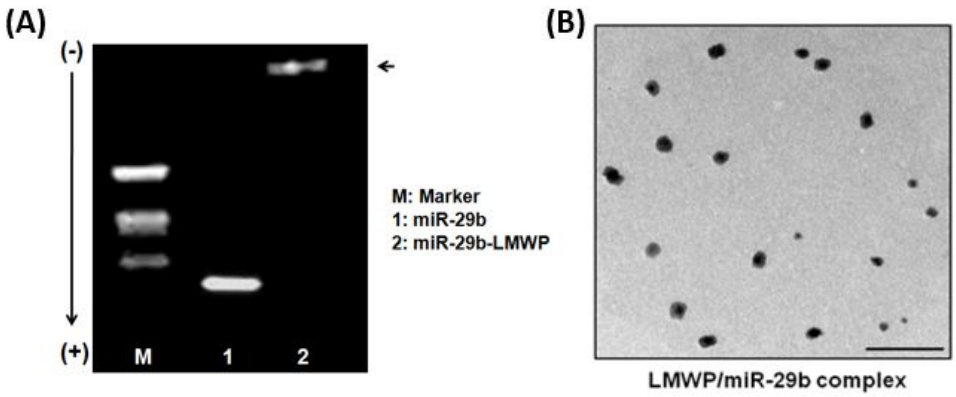

Figure 2.4. Physical characterization of LMWP/miR-29b complex

(A) Gel retardation assay to determine complex formation with 50nM LMWP and 50nM miR-29b. The complex was prepared at a charge ratio of 10:1 (+/-), incubated at room temperature and left for 2h to form complexes. The complex was analyzed on a 2% (w/v) agarose gel by electrophoresis. (B) A transmitting electron micrograph (TEM) of a LMWP/miR-29b complex of 10:1 (+/-). The LMWP/miR-29b complex formed a spherical shape with an average diameter of 35nm. Scale bar; 100μm.

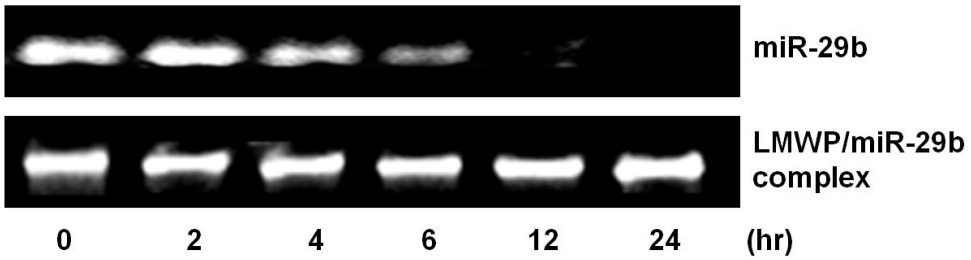

Figure 2.5. Stability assay of LMWP/miR-29b

The miRNA stability test was performed under the presence of serum at 37°C.

5.3. Cell viability after exposure to LMWP/miR-29b complexes

To examine the cell viability after LMWP/miR-29b complex treatment *in vitro*, the author measured DNA synthesis and metabolic activity. Fig. 2.6A demonstrates that there was no significant change in the viability of hMSCs transfected with LMWP/miR-29b complex compared to the miR-29b lipoplex treated cells by MTT. The miRNA and liposomal transfection reagent treated-cells displayed mild toxicity (around 14%). However, the BrdU incorporation assay showed that there was a significant decrease in the DNA synthesis in the miR-29b lipoplex treated-group (Fig. 2.6B). The lipofectamine itself presented significant cytotoxicity due to high percentage of positive charge, while lower cytotoxicity when complex with miR-29b. This is due to the neutralization of the surface charge in the complex when compared to lipofectamine itself. It should be noted that the toxicity of cationic transfection agents has always been a concern in their use as gene carriers. In addition, a greater toxicity for several transfection agents when applied in the absence of genes has been reported [26]. Even the cytotoxicity caused by lipofectamine was alleviated by the complex with miR-29b, the cell death caused

by the lipofectamine complex was marked than that by LMWP/miR-29b complex. The lack of cytotoxicity of LMWP could be advantageous for its use as a delivery carrier of miR-29b to the intracellular target in the stem cells.

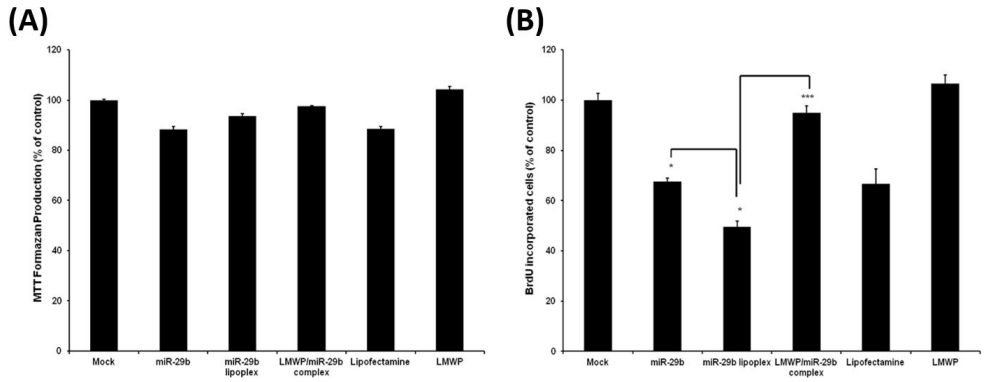

Figure 2.6. Effect of cell viability of LMWP/miR-29b complex in hMSCs

(A) The MTT assay of viable cells. Cytotoxicity of the transfection reagent (Lipofectamine^{TM}), LMWP, free miR-29b, miR-29b lipoplex, and LMWP/miR-29b complex on hMSCs. One dose (50nM) of each compound was incubated with cells for 4days. The number of viable cells remaining in the wells was assessed by MTT assay and then compared with those of cells without treatment in the control wells. (B) The cell proliferation determined by the BrdU labeling method. Data are displayed as mean ± standard error from triplicate experiments (N=4). *$p < 0.05$, as compared to miR-29b treated cells at the same time point. ***$p < 0.01$, as compared to miR-29b lipoplex treated cells at the same time point.

5.4. Cellular delivery of the LMWP/miR-29b complex compared to the miRNA-29b lipoplex

The author labeled the N-terminal of the LMWP with FITC and miR-29b with TAMRA to confirm the ability of the LMWP/miR-29b complex and miR-29b lipoplex to be taken up by hMSCs using FACS and confocal microscope 0.5h or 5h post-transfection. Table 2.4 shows the percentage of cells that had taken up complexes, as measured by the mean fluorescence intensity of these cells. Fig. 2.7 was showed that LMWP had the ability to transfect the cells with miR-29. The mean of fluorescence intensity of the LMWP/miR-29b complex-treated cells ('Mean value' in Table 2.4) was higher compared to the LMWP-treated (positive control) cells. However, the percentage of positive cells ('M1% gated' in Table 2.4) was similar between the LMWP/miR-29b complex-treated cells and the LMWP treated cells (96.96% vs. 98.69% in the figures detected FL1 wavelength). The author visualized the internalized LMWP/miR-29b complex to more precisely understand this cell internalization event mediated by the LMWP peptide (Fig. 2.8A). The fluorescence signal indicated that the miR-29b complex with LMWP

was largely distributed in the cytosol within 0.5h of post-transfection. The fluorescence signal was also observed in the peri-nucleus, indicating fast localization of the LMWP/miR-29b complex inside the cells.

The author quantified the transfection efficiency between the LMWP/miR-29b complex and the miR-29b lipoplex after 5h (Fig. 2.8B). The cationic lipids, which are known to be highly efficient transfection reagents, insufficiently transfected the miRNA transfer into the cells within 5h of treatment, while miRNA delivery using LMWP increased about 6.5-fold at the same incubation time. The FACS results agreed well with the confocal microscopy observations; the LMWP/miR-29b complexes showed clearly increasing translocation in a time-dependent manner. Overall, the cell uptake studies clearly demonstrate that LMWP can effectively deliver miRNA-29b to the cytoplasm and show the possibility to occur high biological activity at low doses.

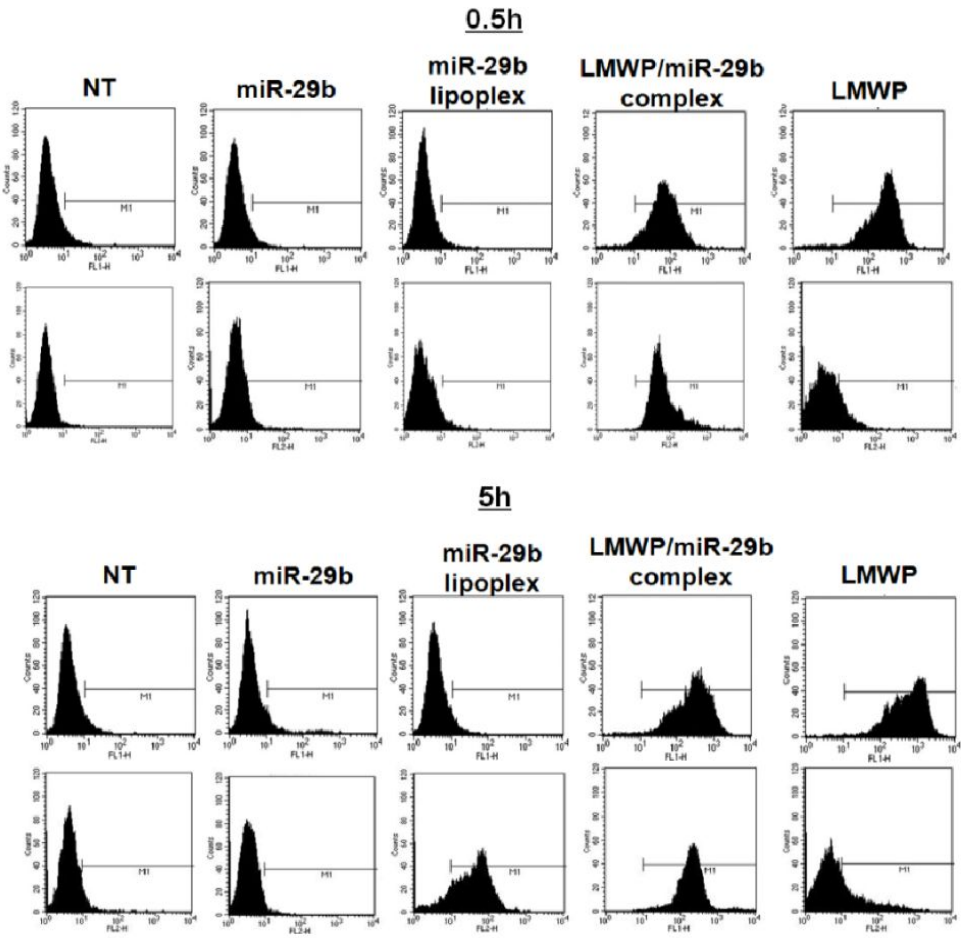

Figure 2.7. FACS analysis of cellular uptake of LMWP/miR-29b complex

50nM TAMRA-labeled miR-29b, FITC-labeled LMWP, TAMRA-labeled miR-29b lipoplex, and FITC-labeled LMWP/TAMRA-labeled miR-29b complex were treated to hMSCs and then, analyzed using FACSCalibur. (Upper panel: sample treatment for 0.5h, Bottom panel: sample treatment for 5h).

Table 2.4. The quantitative intracellular localization of LMWP/miR-29b complex using FACSCalibur

By setting the gate, M1 permeable cells are marked to show the difference in the populations of negative control cells and cells that have taken up the LMWP/miR-29b complex, whereas the M1 gated cells of the LMWP/miR-29b complex are similar to those of the LMWP alone. The amount of LMWP/miR-29b complex was quantified as the percentage of cells within the M1 gate multiplied by the mean fluorescence intensity of those cells.

Cell uptake for 0.5h				Cell uptake for 5h			
GROUP	MEAN	GEO MEAN	M1 % Gated	GROUP	MEAN	GEO MEAN	M1 % Gated
Mock	4.78	4.05	5.22	Mock	4.78	4.05	5.22
Lipofectamine	4.74	4.00	4.96	Lipofectamine	4.80	4.13	5.45
miR-29b	4.59	3.91	4.37	miR-29b	6.16	3.93	5.2
miR-29b lipoplex	4.34	3.74	3.36	miR-29b lipoplex	4.71	4	4.77
LMWP/miR-29b complex	84.30	60.46	96.96	LMWP/miR-29b complex	387.15	258.69	99.36
LMWP	295.60	219.18	98.69	LMWP	765.20	522.18	99.65

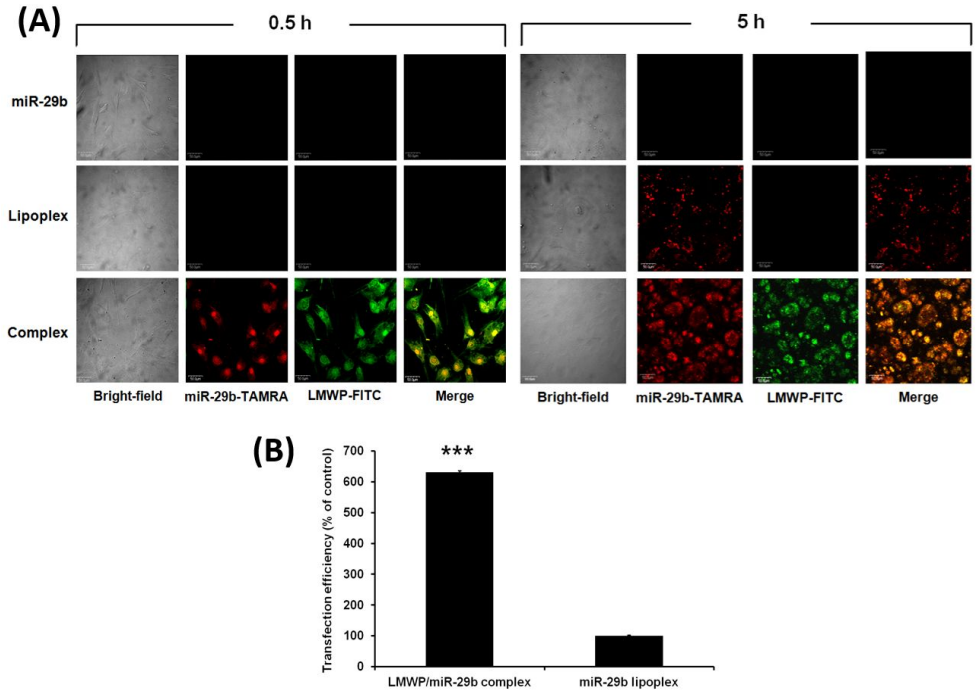

Figure 2.8. Image of intracellular localization of LMWP/miR-29b complex

(A) Cellular localization of 50nM fluorescence-dual-labeled LMWP/miR-29b complex in hMSCs. Cellular localization was monitored by confocal microscopy. (B) A comparison of the transfection efficiencies of miR-29b lipoplexes and LMWP/miR-29b complexes in the cells at 5h. Data are displayed as mean ± standard error from triplicate experiments (N=4). ***$p < 0.01$, as compared to miR-29b lipoplex treated cells at the same time point.

5.5. Targeting of negative regulators in osteoblastic differentiation by the LMWP/miR-29b complex

A previous study identified that the expression of hsa-miR-29b was increased during osteogenesis [27], therefore, the author examined two databases (TargetScan, miRanda and PicTar) to search for miR-29b targets with a high probability to inhibit osteoblast differentiation. Five putative miR-29 targets were selected for this study: HDAC4, CTNNBIP1, DUSP2, COL1A1 and COL5A3. The complementary pairing between the miR-29b "seed region" and the 3'-UTR of target genes is highly conserved in vertebrate species, including humans. The expression of these target genes was monitored by encoded luciferase. The miR-29b reduced the luciferase activity of the target genes, indicating suppressed mRNA translation (Fig. 2.9). The results indicated that miR-29b not only targeted HDAC4 but also targeted CTNNBIP1 and DUSP2, factors involved in the inhibition of osteoblastic differentiation. The miR-29b was predicted to target a large number of collagen genes, which was counter-intuitive to the well-established requirement of ECM synthesis to promote osteoblastic differentiation. There are

three putative binding sites for miR-29b in the COL1A1 mRNA 3'-UTR. Transfecting cells with the LMWP/miR-29b complex showed that ectopic miR-29b in human MSCs significantly repressed the luciferase activity of reporter plasmids carrying the COL1A1 and COL5A3, a minor component of bone tissue, 3'-UTRs. The author concludes from these results that miR-29b inhibits the expression of multiple negative regulators of osteogenesis by mediating translational repression, thereby facilitating the progression of differentiation.

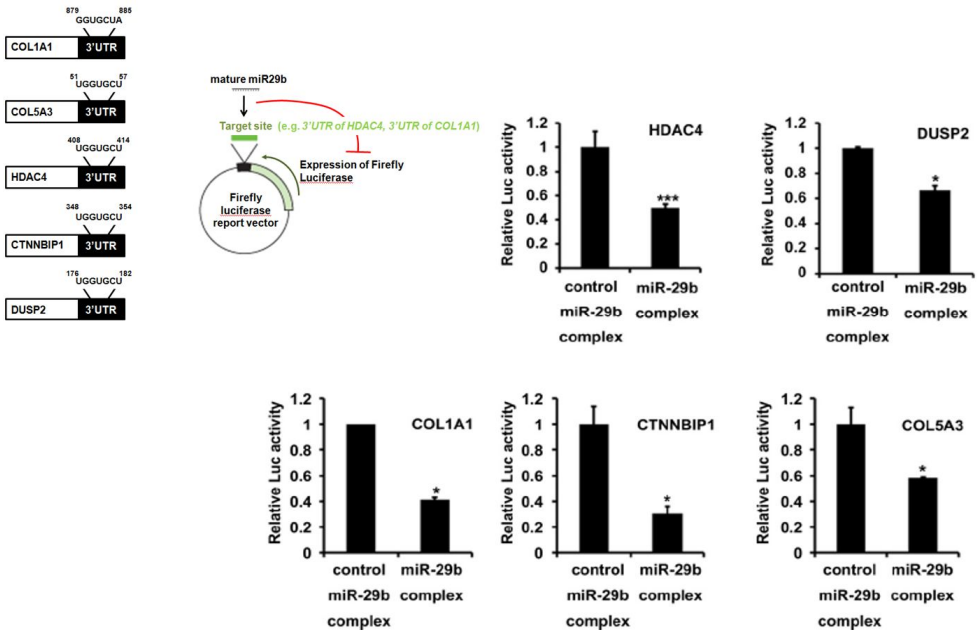

Figure 2.9. Inhibitory translation of miR-29b targeted genes by LMWP/miR-29b complex

One putative target site of miR-29b predicted by the TargetScan program contained the 3'-UTRs of HDAC4 CTNNBIP1, DUSP2 and collagen family members, such as COL1A1 and COL5A3 mRNA. The hMSCs were co-transfected with 50nM miR-29b RNA or negative control miRNA (negative control miR), phRL-null (*Renilla* plasmid), and the luciferase constructs (firefly) carrying the 3'-UTRs of HDAC4 CTNNBIP1, DUSP2, COL1A1 and COL5A3. Luciferase assays were performed 36h after transfection. The ratio of the reporter Firefly luciferase to the control *Renilla* luciferase in relative luminescence units was plotted. Data are displayed as mean ± standard error from triplicate experiments (N=4). *$p < 0.05$ or ***$p < 0.01$, as compared to control miR-29b complex at the same time point.

5.6. Osteogenic-specific gene expression of the LMWP/miR-29b complex

Osteogenic gene markers such as ALP, COL1A1, OPN, TAZ, Runx2 and OCN were measured by RT-PCR and real-time PCR to confirm the functional activity of the miR-29b on osteoblastic differentiation in hMSCs (Fig. 2.2). Transfection by the LMWP/miR-29b complex increased the mRNA levels of all osteogenic markers, except COL1A1, at 48h compared to the levels at 24h in a concentrationdependent manner, which exceeded the mRNA increases from the miR-29b lipoplex (Fig. 2.10A). Additionally, the levels of osteogenic markers increased with the miR-29b concentration, indicating the activation of osteogenesis by the transfected miR-29b (Fig. 2.10B). However, COL1A1 protein expression, which is known not only as one of the target genes of miR-29b that is conserved among vertebrate species but also, ironically, as the factor for promoting osteogenesis, decreased from the transfection point onward. Since the action induced mineralization is only involved collagen genes, the author suggested confirmed osteogenic markers (ALP, OCN, OPN and Runx2) showed redundancy by mineral production. Therefore, the reduction of COL1A1 mRNA had not

affected mineralization. Consequently, the LMWP/miR-29b complex induces osteogenic differentiation by increasing the expression of osteogenic genes and that the LMWP/miR-29b complex was more effective at inducing osteogenic differentiation than the lipoplex.

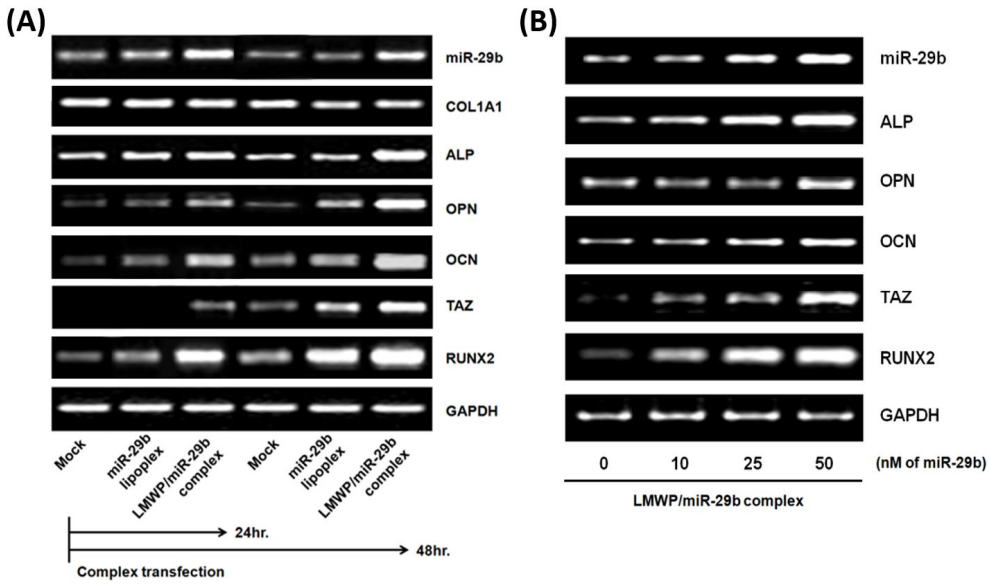

Figure 2.10. Expression level of osteogenic markers by LMWP/miR-29b complex

(A) The gene expression induced by the LMWP/miR-29b complex with respect to transfection time. (B) After 48h transfection with various concentrations of the LMWP/miR-29b complex, the osteogenic markers were detected by RT-PCR.

5.7. Osteoblastic differentiation of hMSCs by LMWP/miR-29b complex

The author determined whether the LMWP/miR-29b complex was able to induce osteoblastic differentiation in hMSCs. Compared to the cells without treatment and those with miR-29b alone, cells treated with the miR-29b lipoplex showed increased expression of ALP (Fig. 2.11A). Furthermore, the LMWP/miR-29b-treated cells had significantly higher ALP expression than the miR-29b lipoplextreated cells, which also increased with the applied concentration (Fig. 2.11B). Similarly, calcein stainwas evident in cells treated with the LMWP/miR-29b complex, while marginal expression of calcein in the control cells without treatment and in cells treated with native miR-29b (Fig. 2.12A; upper panel and 2.12B). The ALP expression was increased in both the miR-29b lipoplex-treated and the LMWP/miR-29b-treated hMSCs (Fig. 2.11), but the LMWP/miR-29b treated hMSCs cells strongly induced calcium deposition by Alizarin red S staining for up to 14 days (Fig. 2.12A; bottom panel and Fig. 2.12C) and staining of calcein. Together, these results not only suggest that LMWP carries oligonucleotides such as miRNAs more efficiently than the liposomal carrier but also confirms that the

miR-29b supports osteoblastic differentiation at multiple concentrations within a short time to induce complete osteogenesis.

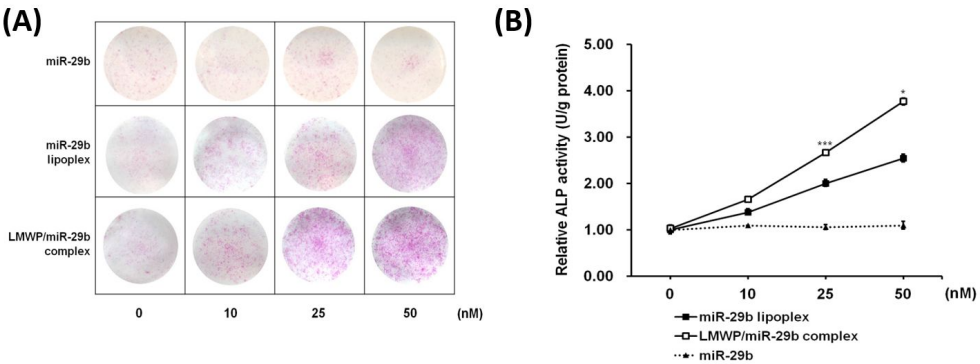

Figure 2.11. Effect of ALP expression by LMWP/miR-29b complex

(A) The hMSCs were treated with various concentrations of the miR-29b, miR-29b lipoplex or the LMWP/miR-29b complex for 10days in osteogenic media containing 20% FBS, 50μg/ml ascorbic acid, 10mM β-glycerophosphate and 10^{-7}M dexamethasone and were stained for alkaline phosphatase detection kit. (B) The stained area exhibiting ALP activity was quantified. Data are displayed as mean ± standard error from triplicate experiments (N=4). *p < 0.05 or ***p < 0.01, as compared to miR-29b lipoplex at the same time point.

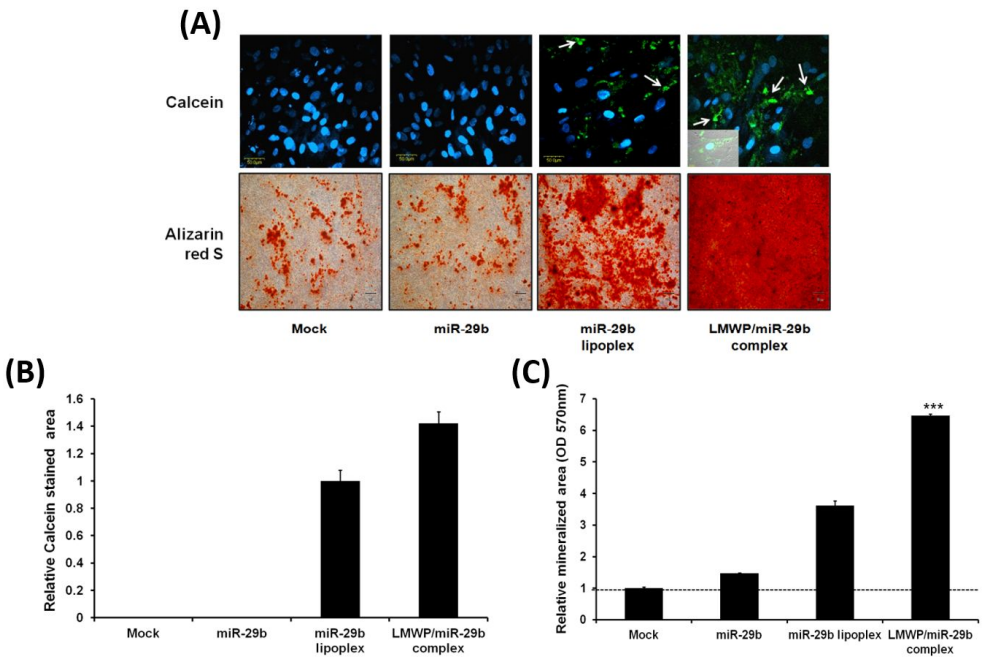

Figure 2.12. Effect of calcium deposition by LMWP/miR-29b complex

(A) Cultured with 50nM miR-29b, miR-29b lipoplex or LMWP/miR-29b complex, the cells were visualized using confocal laser scanning microscopy with Calcein dye (Blue: nuclei, Green: calcein) and the Alizarin red S to show newly created calcium. The quantification of the calcified areas performed (B) Calcein and (C) Alizarin red S staining. Data are displayed as mean ± standard error from triplicate experiments (N=4). *$p < 0.05$ or ***$p < 0.01$, as compared to miR-29b lipoplex at the same time point.

5.8. Inhibition of osteoblastic differentiation by anti-miR-29b

To examine whether these osteoblastic differentiation was specifically induced by the addition of the miR-29b sequence, the anti-miR-29b was administered in combination with miR-29b. The mismatched sequence of miR-29b as control miR-29b, miR-29b, anti-miR-29b and miR-29b with anti-miR-29b were complexed with LMWP and applied to the hMSCs. Complementary to the activation of the osteogenic effect by miR-29b, the addition of anti miR-29b abolished the expression of osteogenic markers, i.e., phosphorylated Smad1/5/8 (pSmad1/5/8), Runx2, ALP and phosphorylated TAZ (pTAZ), which antagonized the osteogenic effect of miR-29b *in vitro* (Fig. 2.13A). Compared with the negative controls, the anti-miR-29b treated cells clearly repressed both pSmad1/5/8 and pTAZ, which are classical markers of osteoblast differentiation and direct targets for Runx2, a master regulator of osteoblastic differentiation. Meanwhile, the COL1A1 protein level was not significantly changed by western blot. Additionally, the cotreatment of hMSCs with each miRNA and its corresponding anti miR-29b reversed the miRNA's inhibitory effects on osteogenic differentiation. The inhibition of miR-29b's

function by anti-miR-29b in the post-translational stage significantly reduced the expression of miR-29b-induced ALP activity (Fig. 2.13B, upper panel). Furthermore, the anti-miR-29b has no effect on the miR-29b induced calcium deposition, as seen by Alizarin red S staining (Fig. 2.13B, middle panel) and calcein staining (Fig. 2.13B, bottom panel). The quantification of ALP activity and Alizarin red S staining revealed up to 50% reductions by anti-miR-29b compared with that by the miR-29b (Fig. 2.13C). These results suggest that human derived miR-29b has direct specificity in osteoblastic differentiation by down-regulating target inhibitory gene expression in hMSCs.

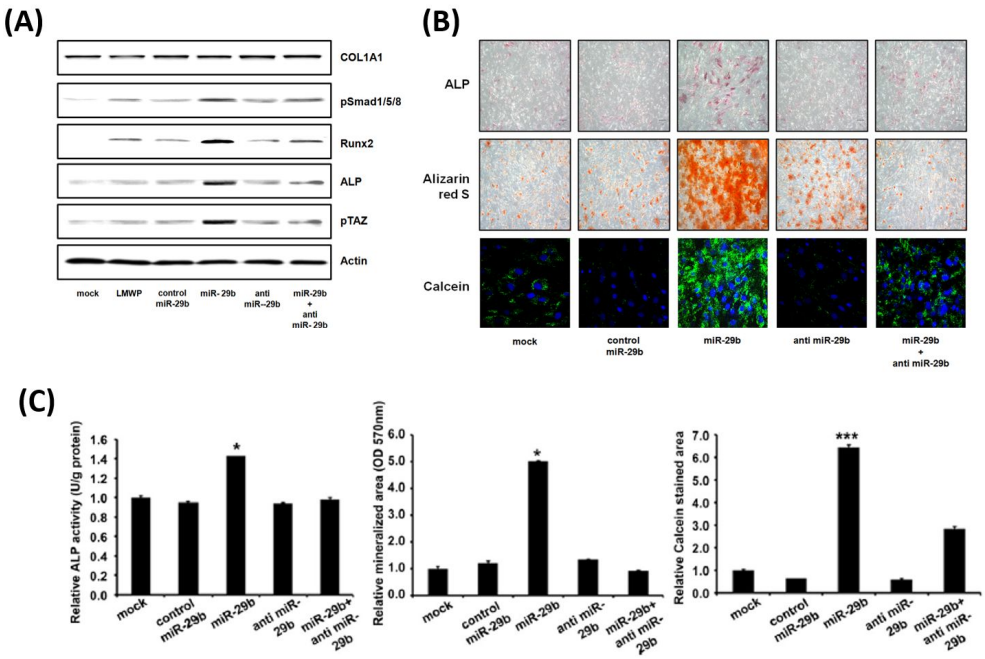

Figure 2.13. Evaluation of the functionality of miR-29b as an osteo-miRNA by anti-miR-29b

(A) The hMSCs were transfected with 50nM miR-29b, control mismatched miR-29b (control miRNA) or anti-miR-29b using LMWP. Western blot analysis was performed inducing osteogenesis for 14days 36h after transfection. (B) The cells cultured with the LMWP/miR-29b complex were visualized using confocal laser scanning microscopy after staining with Calcein (Blue: nuclei, Green: Calcein), alizarin red S to show newly created calcium and detected ALP activity. (C) The stained area by Calcein, Alizarin red S and ALP were quantified. Data are displayed as mean ± standard error from triplicate experiments (N=4). *$p < 0.05$ or ***$p < 0.01$, as compared to anti miR-29b complex at the same time point.

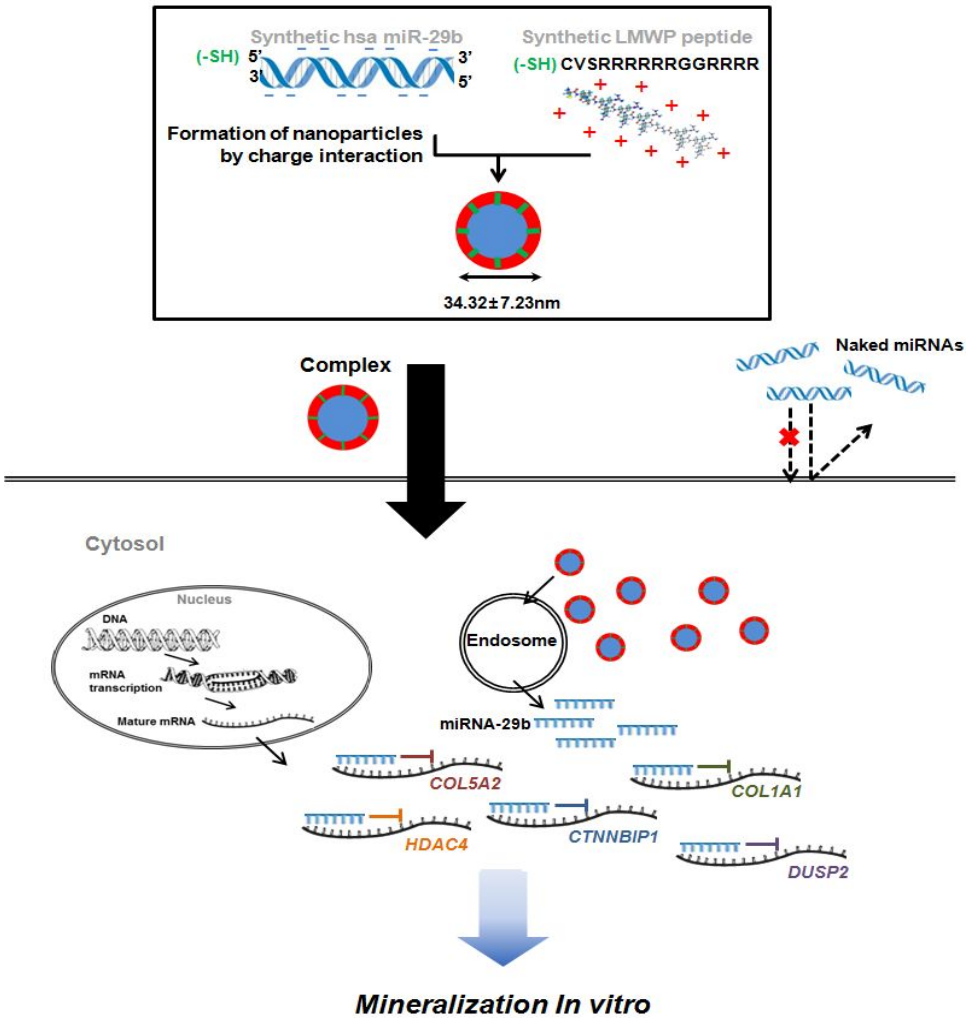

Figure 2.14. Scheme of the mechanism of LMWP/miR-29b complex on the targeting anti-osteogenic genes

The LMWP/miR-29b complex promotes osteogenesis by directly down-regulating known inhibitors of osteoblast differentiation, HDAC4, CTNNBIP1, DUSP2, COL1A1 and COL5A3 proteins through binding to target 3'-UTR sequences in their mRNAs. Thus, LMWP/miR-29b complex is a key regulator of development of the osteoblast phenotype by targeting anti-osteogenic factors and efficient modulating bone extracellular matrix proteins.

6. DISCUSSION

Design of effective carriers requires many important characteristics, including the ability to deliver oligonucleotides efficiently into the target cells, the stability in living systems and the biocompatibility with reduced toxicity. For this reason, this study was designed to create dense spherical complex with non-cytotoxic CPP, LMWP, to prevent the degradation of miRNAs by complexing them. In this study, the positive charged-cell penetrating peptide, LMWP, helped to condense the size of the miRNA complexes. The two inherent properties of LMWPs make them attractive as a gene delivery vehicle: i) they have a large positive charge due to the presence of arginine residues, which enables to interact with negatively charged oligonucleotides, such as DNA and RNA, via electrostatic interaction, and then the surface of complex replaces positive charge with negative one, ii) they could act as nuclear localization signals that benefit the nuclear targeting of genes of interest as TAT does [28]. In the initial part of this study, we investigated the ability of LMWP to deliver linear double-stranded RNA in the nanoparticle by complex formation.

Transfection reagents administered systemically have been known to have adverse effects; for example, lipoplexes applied intravenously or by inhalation via the lungs result in an inflammatory response. Eventually, the toxicity of lipoplex could diminish both the transfection efficiency and the transgene expression [13,29]. Conversely, knowledge about the toxic effects and tissue damage following local administration of lipoplexes to various tissues still limits its application [29]. Additionally, oligonucleotide induced toxicity may be due to the polyanionic nature and the cytokine secretion, e.g., interleukin family [30] due to the inflammatory reaction. Clearly, the transfection data (Fig. 2.6; the cytotoxicity results) obtained with the LMWP/miR-29b complex can only be properly interpreted by taking into account the potentially toxic effect of the complexes on the cells.

In this case, nanosized complexes (50-100nm) were created due to the effect of charge-charge interactions. Zeta potentials more positive than -30 mV and more negative than +30 mV are normally considered stable for colloidal dispersions [31]. In our study, the innate value of the zeta potential of the miRNA is -19.67 mV, while the LMWP/miR-29b complex showed a highly positive zeta potential value,

27.3 mV, due to the presence of LMWP which is positively charged, suggesting that the complexly shaped over-coating LMWP around miRNAs forms a stable suspension and would be easier for parenteral administration in further *in vivo* studies. Increasing LMWP content created more dense complexes due to the cooperative effect and stronger ionic interactions, as confirmed by the particle size analysis. This finding is in agreement with results obtained with oligonucleotide/peptide in our previous study [24,32]. Chemical conjugation secures the penetration of cargo molecules into cells; however, complexation of the miRNA with excess LMWP is advantageous in preserving its stability while guiding its translocating capability because miRNA has highly negative charges compared to other proteins and is even susceptible to digestion when exposed to serum due to the presence of nucleases (Fig. 2.5). The electrostatic and dynamic character of the LMWP/miR-29b complex is a dominant factor responsible for their recognition and uptake by cells (Table. 2.4). The electrophoretic mobility of nanoparticles to a potential at a hydrodynamic plane of shear is called the zeta potential [33], and it provides information concerning charge beyond the hydro-dynamically stagnant layer. However, the conductivity offers information on the

amount of mobile counter charges inside the stagnant layer. Therefore, the electrical characterization of the complex as a cell-penetrating vehicle is quantified both by measuring the stream of charge matter with charge (zeta potential) and without charge (conductivity). Meanwhile, polyarginine peptides possess cell translocation activity and an internalization pathway similar to those of TAT_{47-57} [34]. LMWP, which consists of two clusters of arginine sequences similar to those of TAT_{47-57}, showed comparable translocation capacity [19]. Several hypotheses have been suggested to account for the mechanisms of CPP-mediated cell transduction, including the formation of hydrogen bonds between the guanidine head group in the arginine residues with the phospholipids on the cell membrane and the interaction of the arginine residue with the extracellular matrix glycosaminoglycans, such as heparin sulfate or chondroitin sulfate. The guanidinium head group of arginine is the central structural feature required for peptide uptake. But, heptamers of citrulline, an isotere of arginine with nitrogen of guanidine replaced by oxygen, are unable to enter cells [35]. Although the translocation mechanism is still unclear, LMWP mediated cell transduction could well be related to one or all of these mechanisms. The LMWP peptide possesses

two major advantages over TAT_{47-57}. Extensive and conclusive animal studies on the LMWP peptides have confirmed that they actually possess significantly reduced antigenicity, mutagenicity, and complement activating activity, as well as fewer other cationic, polymer associated, hemodynamic/hematologic toxic effects than the parent protamine, a clinical drug approved by the U.S. Food and Drug Administration [19-21]. Additionally, an important prerequisite for miRNA-mediated systemic gene silencing is that the inhibitory effects must be specific (rather than non-specific "off target" effects). There might be an argument that material toxicity against target gene suppression alone can result in osteogenesis by miR-29b inhibition, similar to the off-target effects, which agrees with our previous study (Fig. 2.6) [32]. Based on this concern, the peptide LMWP alone and other toxic transfecting agent were employed to monitor the possible non-specific effects on osteogenic markers as a consequence of cytotoxicity. However, LMWP alone did not affect cell viability (Fig. 2.6) nor did it suppress osteogenic marker levels in cells (Fig. 2.13). The specific increases in osteogenic gene expression by the LMWP/miR-29b complex were compared to the presence of LMWP alone, control mismatch miR-29b, miR-29b and anti-miR-29b (Fig. 2.13). Therefore, the

suppression of osteogenic marker levels is primarily from specific miR-29b delivered by LMWP.

Our study indicates that miR-29b targets several inhibitory genes to osteogenesis, such as HDAC4, CTNNBIP1, and DUSP2, which impinge on signal transduction pathways promoting osteogenesis (e.g., Smads, ERK, p38 MAPK, and Wnt). All of these factors are known to be involved in inhibiting osteoblast differentiation [36-38]. For example, CTNNBIP1 (also known as ICAT) inhibits β-catenin-mediated transcription by binding to β-catenin and preventing interactions with TCF/LEF factors [26]. The DUSP2 inactivates and anchors ERK within the nucleus [24] and blocks an inhibitor of ERK signaling during osteoblast differentiation [25]. HDAC4 negatively regulates chondrocytes and osteoblasts [39,40]. In a previous study, HDAC4 and Runx2 interacted in the context of transfected cell lines, and the interaction interfered with Runx2 DNA binding, as seen in both the EMSA assays and the chromatin immuno-precipitations. These observations suggest that the phenotypic effects of HDAC4 could be linked to its ability to interfere with Runx2 [41-43]. Not only the importance of these miR-29b targets in controlling osteogenesis, but we show that exogenous introduction of

miR-29b promotes osteoblastic differentiation, as reflected by increased levels of osteogenic marker genes, including Runx2 and alkaline phosphatase. Hence, the ability of miR-29b to promote osteoblast differentiation can be attributed to the intracellular delivery by LMWP thereby relieving the negative effects of anti-osteogenic cell signaling pathways.

According to published studies, the action of type I collagen on osteogenesis is controversial. Collagen within the extracellular matrix is essential for promoting osteoblastic differentiation as early marker [44,45], but collagen fibrils interfere with calcium deposition at late stage of osteogenesis [46,47]. We examined gene expression by differentiation time to evaluate the association between miR-29b and osteogenic marker genes including COL1A1. The figure was seen shown type I collagen decreased by processing osteogenic differentiation at contrast with miR-29b and other osteoblastic differentiation makers (Fig. 2.2). Also, previous publication showed that even rhBMP-2, as the strong osteogenic inducer has an inhibitory effect on collagen synthesis for early osteogenesis [48]. The attenuation of collagen synthesis by miR-29b may allow ordered collagen fibril maturation to facilitate mineral deposition [49]. In bone tissues, collagens are the major

extracellular matrix (ECM) proteins with about 95% type I and 5% type V collagens assembled into hetero fibrils [50]. Genetic modification in the appropriate formulating of collagen fibrils results in specific bone disorders [51,52]. Thus, the biological role of miR-29b as a mineralization-inducer may be to protect bones from fibrosis and/or to restrict type I collagen protein accumulation to facilitate ordered deposition of mineral associated with collagen fibrils. The result of our studies showed that miR-29b does not repress collagen protein (Fig. 2.13) in immature osteoblasts but rather causes decreased collagen mRNA levels (Fig. 2.10A) after transfection with miR-29b, which may be explained by alternative mRNA splicing that results in different collagen 3'-UTRs. Although animal miRNAs mainly inhibit translation, they can also induce significant degradation of mRNA targets [53].

In this study, LMWP could efficiently deliver miR-29b into human mesenchymal stem cells, and target anti-osteogenic genes to regulate osteoblastic differentiation *in vitro* (Fig. 2.14). This differentiation strategy using LMWP/miR-29b may be applicable to stem cell based osteogenesis thus deserve further investigation *in vivo*.

7. CONCLUSION

Our study suggests that miR-29b promotes osteoblast differentiation by targeting and interfering with negative regulators of osteogenic pathways. The author demonstrated that LMWP is a potent non-toxic cell-penetrating carrier for miR-29b and that mineralization effects of the LMWP/miR-29b complex in human MSCs are potentially applicable as a stem-cell differentiation tool. The stem cell based osteogenesis strategy using LMWP/miR-29b may be applicable to bone regeneration and deserves further investigation *in vivo*.

8. REFERENCES

[1] Hobert O. Gene regulation by transcription factors and microRNAs. Science. 2008;319:1785-6.

[2] Kloosterman WP, Plasterk RH. The diverse functions of microRNAs in animal development and disease. Dev Cell. 2006;11:441-50.

[3] Stefani G, Slack FJ. Small non-coding RNAs in animal development. Nat Rev Mol Cell Biol. 2008;9:219-30.

[4] Li Z, Hassan MQ, Jafferji M, Aqeilan RI, Garzon R, Croce CM, et al. Biological functions of miR-29b contribute to positive regulation of osteoblast differentiation. J Biol Chem. 2009;284:15676-84.

[5] Eguchi A, Meade BR, Chang YC, Fredrickson CT, Willert K, Puri N, et al. Efficient siRNA delivery into primary cells by a peptide transduction domain-dsRNA binding domain fusion protein. Nat Biotechnol. 2009;27:567-71.

[6] Wohlbold L, van der Kuip H, Moehring A, Granot G, Oren M, Vornlocher HP, et al. All common p210 and p190 Bcr-abl variants can be targeted by RNA interference. Leukemia. 2005;19:290-2.

[7] Rangatia J, Bonnet D. Transient or long-term silencing of BCR-ABL alone induces cell cycle and proliferation arrest, apoptosis and differentiation. Leukemia. 2006;20:68-76.

[8] Zhelev Z, Bakalova R, Ohba H, Ewis A, Ishikawa M, Shinohara Y, et al. Suppression of bcr-abl synthesis by siRNAs or tyrosine kinase activity by Glivec

alters different oncogenes, apoptotic/antiapoptotic genes and cell proliferation factors (microarray study). FEBS Lett. 2004;570:195-204.

[9] Wilda M, Fuchs U, Wossmann W, Borkhardt A. Killing of leukemic cells with a BCR/ABL fusion gene by RNA interference (RNAi). Oncogene. 2002;21:5716-24.

[10] Li JM, Meng S, Wei BJ, Xu RH, Zhang K, Wang LN, et al. TAT Peptides Mediated Small Interfering RNA Delivery to Huh-7 Cells and Efficiently Inhibited Hepatitis C Virus RNA Replication. Intervirology. 2009;52:135-40.

[11] Hatefi A, Canine BF. Perspectives in vector development for systemic cancer gene therapy. Gene Ther Mol Biol. 2009;13:15-9.

[12] Pirollo KF, Zon G, Rait A, Zhou Q, Yu W, Hogrefe R, et al. Tumor-targeting nanoimmunoliposome complex for short interfering RNA delivery. Hum Gene Ther. 2006;17:117-24.

[13] Chien PY, Wang J, Carbonaro D, Lei S, Miller B, Sheikh S, et al. Novel cationic cardiolipin analogue-based liposome for efficient DNA and small interfering RNA delivery *in vitro* and *in vivo*. Cancer Gene Ther. 2005;12:321-8.

[14] Derossi D, Joliot AH, Chassaing G, Prochiantz A. The third helix of the Antennapedia homeodomain translocates through biological membranes. J Biol Chem. 1994;269:10444-50.

[15] Morris MC, Deshayes S, Heitz F, Divita G. Cell-penetrating peptides: from molecular mechanisms to therapeutics. Biol Cell. 2008;100:201-17.

[16] Heitz F, Morris MC, Divita G. Twenty years of cell-penetrating peptides: from molecular mechanisms to therapeutics. Br J Pharmacol. 2009;157:195-206.

[17] Crombez L, Aldrian-Herrada G, Konate K, Nguyen QN, McMaster GK, Brasseur R, et al. A new potent secondary amphipathic cell-penetrating peptide for siRNA delivery into mammalian cells. Mol Ther. 2009;17:95-103.

[18] Ishihara T, Goto M, Kodera K, Kanazawa H, Murakami Y, Mizushima Y, et al. Intracellular delivery of siRNA by cell-penetrating peptides modified with cationic oligopeptides. Drug Deliv. 2009;16:153-9.

[19] Park YJ, Chang LC, Liang JF, Moon C, Chung CP, Yang VC. Nontoxic membrane translocation peptide from protamine, low molecular weight protamine (LMWP), for enhanced intracellular protein delivery: *in vitro* and *in vivo* study. FASEB J. 2005;19:1555-7.

[20] Lee LM, Chang LC, Wrobleski S, Wakefield TW, Yang VC. Low molecular weight protamine as nontoxic heparin/low molecular weight heparin antidote (III): preliminary *in vivo* evaluation of efficacy and toxicity using a canine model. AAPS PharmSci. 2001;3:E19.

[21] Tsui B, Singh VK, Liang JF, Yang VC. Reduced reactivity towards anti-protamine antibodies of a low molecular weight protamine analogue. Thromb Res. 2001;101:417-20.

[22] Camp JP, Capitano AT. Size-dependent mobile surface charge model of cell electrophoresis. Biophys Chem. 2005;113:115-22.

[23] Lee K, Kim JH, Kwon OB, An K, Ryu J, Cho K, et al. An Activity-Regulated microRNA, miR-188, Controls Dendritic Plasticity and Synaptic Transmission by Downregulating Neuropilin-2. J Neurosci. 2012;32:5678-87.

[24] Park YJ, Liang JF, Ko KS, Kim SW, Yang VC. Low molecular weight protamine as an efficient and nontoxic gene carrier: *in vitro* study. The journal of gene medicine. 2003;5:700-11.

[25] Goparaju GN. Evaluation of cationic peptide-plasmid DNA complexes for gene delivery. UMI Dissertation Publishing, 2008. p. 219.

[26] Morgan DM, Larvin VL, Pearson JD. Biochemical characterisation of polycation-induced cytotoxicity to human vascular endothelial cells. J Cell Sci. 1989;94 (Pt 3):553-9.

[27] Goff LA, Boucher S, Ricupero CL, Fenstermacher S, Swerdel M, Chase LG, et al. Differentiating human multipotent mesenchymal stromal cells regulate microRNAs: prediction of microRNA regulation by PDGF during osteogenesis. Exp Hematol. 2008;36:1354-69.

[28] Chugh A, Eudes F. Translocation and nuclear accumulation of monomer and dimer of HIV-1 Tat basic domain in triticale mesophyll protoplasts. Biochim Biophys Acta. 2007;1768:419-26.

[29] Bauer M, Kristensen BW, Meyer M, Gasser T, Widmer HR, Zimmer J, et al. Toxic effects of lipid-mediated gene transfer in ventral mesencephalic explant cultures. Basic Clin Pharmacol Toxicol. 2006;98:395-400.

[30] Boe S, Longva AS, Hovig E. Photochemically induced gene silencing using small interfering RNA molecules in combination with lipid carriers. Oligonucleotides. 2007;17:166-73.

[31] Li D, Muller MB, Gilje S, Kaner RB, Wallace GG. Processable aqueous

dispersions of graphene nanosheets. Nat Nanotechnol. 2008;3:101-5.

[32] Choi YS, Lee JY, Suh JS, Kwon YM, Lee SJ, Chung JK, et al. The systemic delivery of siRNAs by a cell penetrating peptide, low molecular weight protamine. Biomaterials. 2010;31:1429-43.

[33] Froude VE, Zhu Y. Dielectrophoresis of functionalized lipid unilamellar vesicles (liposomes) with contrasting surface constructs. J Phys Chem B. 2009;113:1552-8.

[34] Tung CH, Mueller S, Weissleder R. Novel branching membrane translocational peptide as gene delivery vector. Bioorg Med Chem. 2002;10:3609-14.

[35] Schmidt N, Mishra A, Lai GH, Wong GC. Arginine-rich cell-penetrating peptides. FEBS Lett. 2010;584:1806-13.

[36] Kang JS, Alliston T, Delston R, Derynck R. Repression of Runx2 function by TGF-beta through recruitment of class II histone deacetylases by Smad3. EMBO J. 2005;24:2543-55.

[37] Maeda S, Hayashi M, Komiya S, Imamura T, Miyazono K. Endogenous TGF-beta signaling suppresses maturation of osteoblastic mesenchymal cells. EMBO J. 2004;23:552-63.

[38] Jeon EJ, Lee KY, Choi NS, Lee MH, Kim HN, Jin YH, et al. Bone morphogenetic protein-2 stimulates Runx2 acetylation. J Biol Chem. 2006;281:16502-11.

[39] Tuddenham L, Wheeler G, Ntounia-Fousara S, Waters J, Hajihosseini MK,

Clark I, et al. The cartilage specific microRNA-140 targets histone deacetylase 4 in mouse cells. FEBS Lett. 2006;580:4214-7.

[40] Olson EN, Vega RB, Matsuda K, Oh J, Barbosa AC, Yang XL, et al. Histone deacetylase 4 controls chondrocyte hypertrophy during skeletogenesis. Cell. 2004;119:555-66.

[41] Vega RB, Matsuda K, Oh J, Barbosa AC, Yang X, Meadows E, et al. Histone deacetylase 4 controls chondrocyte hypertrophy during skeletogenesis. Cell. 2004;119:555-66.

[42] Bartel DP. MicroRNAs: genomics, biogenesis, mechanism, and function. Cell. 2004;116:281-97.

[43] Sun X, Wei L, Chen Q, Terek RM. HDAC4 represses vascular endothelial growth factor expression in chondrosarcoma by modulating RUNX2 activity. J Biol Chem. 2009;284:21881-90.

[44] Pelaez D, Arita N, Cheung HS. Extracellular signal-regulated kinase (ERK) dictates osteogenic and/or chondrogenic lineage commitment of mesenchymal stem cells under dynamic compression. Biochem Biophys Res Commun. 2012;417:1286-91.

[45] Lin H, Yang G, Tan J, Tuan RS. Influence of decellularized matrix derived from human mesenchymal stem cells on their proliferation, migration and multi-lineage differentiation potential. Biomaterials. 2012;33:4480-9.

[46] Price PA, Toroian D, Lim JE. Mineralization by inhibitor exclusion: the calcification of collagen with fetuin. J Biol Chem. 2009;284:17092-101.

[47] Fornoni A, Cornacchia F, Howard GA, Roos BA, Striker GE, Striker LJ. Cyclosporin A affects extracellular matrix synthesis and degradation by mouse MC3T3-E1 osteoblasts *in vitro*. Nephrol Dial Transplant. 2001;16:500-5.

[48] Zhao M, Berry JE, Somerman MJ. Bone morphogenetic protein-2 inhibits differentiation and mineralization of cementoblasts *in vitro*. J Dent Res. 2003;82:23-7.

[49] Glimcher MJ. Mechanism of calcification: role of collagen fibrils and collagen-phosphoprotein complexes *in vitro* and *in vivo*. Anat Rec. 1989;224:139-53.

[50] Wenstrup RJ, Florer JB, Davidson JM, Phillips CL, Pfeiffer BJ, Menezes DW, et al. Murine model of the Ehlers-Danlos syndrome. col5a1 haploinsufficiency disrupts collagen fibril assembly at multiple stages. J Biol Chem. 2006;281:12888-95.

[51] Stewart TL, Roschger P, Misof BM, Mann V, Fratzl P, Klaushofer K, et al. Association of COLIA1 Sp1 alleles with defective bone nodule formation *in vitro* and abnormal bone mineralization *in vivo*. Calcif Tissue Int. 2005;77:113-8.

[52] Sarathchandra P, Pope FM, Kayser MV, Ali SY. A light and electron microscopic study of osteogenesis imperfecta bone samples, with reference to collagen chemistry and clinical phenotype. J Pathol. 2000;192:385-95.

[53] Wu L, Fan J, Belasco JG. MicroRNAs direct rapid deadenylation of mRNA. Proc Natl Acad Sci U S A. 2006;103:4034-9.

CHAPTER Ⅲ

Intracellular targeting of bioactive peptide probe for synchronous dual effects; molecular imaging and restoring

1. LIST OF FIGURES AND TABLES

FIGURES

TABLE

2. ABSTRACT

Targeting tissues/cells using probing materials to detect diseases such as cancer and inflammatory disease has been attempted with some success. Most of the molecular targets used in diagnosis and therapy were identified through the discovery of intracellular signaling pathways. Among intracellular signaling processes, the ubiquitination of proteins, and thereby their proteasomal degradation, is important because it plays a role in most diseases involving alterations to a component of the ubiquitination system, particularly E3 ligases, which have selective target-binding affinity and are key to the success of regulating the disorder. The regulation and monitoring of E3 ligases can be achieved using peptides containing protein-protein binding motifs. The author generated a human protein-derived peptide that could target Smurf1, a member of the E3 ligase family, by competitively binding to osteo-Smads. To effectively deliver it into cells, the peptide was further modified with a cell-penetrating peptide. The peptide contains two fluorescent dyes: fluorescein isothiocyanate (FITC) as a fluorophore and black hole quencher-1 (BHQ-1) as a fluorescence quencher. When the target Smurf1

combined with complementary sequences in the peptide probe, the distance between the fluorophore and BHQ-1 increased via a conformational change, resulting in the recovery of the fluorescence signal. Simultaneously, the degradation of Smad1/5/8 was blocked by the binding of the peptide probe to Smurf1, leading to the potentiation of the osteogenic pathway, which was reflected by an increase in the expression of osteoinductive genes. Possible future applications of the peptide probe include its integration into imaging tools for the diagnosis of Smurf1-overexpressing diseases.

3. INTRODUCTION

Noninvasive simultaneous imaging and treatment, termed theragnostics, has been attempted with some success for diseases such as cancer and inflammatory disease [1, 2]. Such imaging has typically relied on the specific enzymatic activity expressed by a substrate target previously conjugated to an activatable probe [3-5]. For example, in the case of rheumatic arthritis, a matrix metalloproteinase (MMP)-3-specific substrate-modified polymer has been evaluated as a near-infrared fluorescent (NIRF) probe [6]. Prior to enzyme activation, target enzyme-protein binding occurs; therefore, it might be more advantageous for early detection if the probe design were based on protein-protein binding. Target-specific molecular binding is a widespread phenomenon in biology and is the basis of numerous practical applications directed at analysis, imaging, and therapy. The formation of a stable covalent bond between a synthetic probe molecule and a specific site on a target protein has many potential applications in biomedical science [7]. A particularly interesting type of synthetic probe molecule is peptide ligands, the strongest of which typically bind to receptors with micromolar dissociation

constants and may depend on processes other than simple binding to produce images [8].

Herein, the E3 ubiquitin enzyme system was used as a protein-binding target. Ubiquitination is a natural proteasomal degradation reaction responsible for processing aged or abnormal proteins for removal. Dysfunctional or overactive ubiquitination can cause progression to a disease state. The ligation of ubiquitin in the ubiquitin-proteasome system (UPS) is mediated by the E1-E2-E3 enzymatic cascade [9]. A donor ubiquitin is activated by an activating enzyme, E1, after which the thioester bond between the ubiquitin C-terminus and a cysteine on the E1 is transferred to the active cysteine of an E2 conjugating enzyme. The final bond formation between the ubiquitin C-terminus and its target is mediated by an E3 ligase [10, 11]. Numerous studies have identified E3 ligases as key molecules in many diseases involving the UPS [12-14]. Smurf1, an E3 ubiquitin ligase that belongs to the HECT class of ubiquitin ligases, specifically binds to Smad1/5/8 proteins, thus facilitating Smad1/5/8 degradation by the proteosome [15]. Smads, particularly Smad1/5/8, are associated with osteogenesis. In most inflammatory diseases, such as rheumatic arthritis, osteoporosis, other bone resorption diseases,

and cancer, the overexpression of Smurfs is significant. In inflammatory diseases, osteogenesis is impaired due to the degradation of Smad1/5/8 proteins. The role of the E3 ubiquitin-ligating enzyme is based on specific binding to target proteins, which induces proteosomal degradation. Here, the author designed a peptide motif as a therapeutic tool to block the proteosomal degradation of Smad1/5/8 by binding an E3 ligase to Smad1/5/8 in Smurf1-overexpressing cells and tissues. LIM mineralization protein 1 (LMP1) is a recently identified intracellular protein that has been demonstrated to stimulate osteoblast differentiation and create mineralized nodules in rat calvarial osteoblasts *in vitro* [16]. Although the exact mechanism or key domain for the osteogenic action of LMP1 is unknown, LMP1 has been shown to bind to Smurf1 [15, 17].

The author hypothesized that a specific domain sequence of LMP1 could be prepared via peptide synthesis and would mimic LMP1 activity. This synthetic peptide had to fulfill three essential requirements: i) it must retain the same chemical and physical properties of LMP1; ii) it must possess well-defined Smurf1-binding strength (i.e., greater than that between Smurf1 and Smad1/5/8); and iii) it must be able to be transduced into cells and bind to intracellular Smurf1,

thereby blocking the proteosomal degradation of Smad1/5/8. To this regard, the author identified new cell-penetrating peptide (CPP) sequence derived from human bone morphogenetic protein 4 (BMP4) to deliver the LMP1 domain peptide into the cells. The blocked proteosomal degradation of Smad1/5/8 would be reflected by increased osteogenesis. In addition, it would be advantageous if this binding could be monitored. The alteration of the peptide conformation by target binding would also be detected using fluorescence resonance energy transfer (FRET) imaging based on the fluorescent dye and its quenching dye becoming conjugated to each end of the peptide. Initially, there is no fluorescence, but a conformational change can expand the distance between both dyes. Herein, our peptide probe was conjugated to black hole quencher (BHQ) 1 and a fluorescent dye, leading to an absence of fluorescence until the probe reached Smurf1, which then activated the probe only after the binding of Smurf1 to the Smurf1-binding peptide (SBP) sequence compensated for the interference by BHQ1. The peptide motif, i.e., the peptide probe, offers a convenient, rapid, specific, and sensitive means of monitoring analytes and indicating the presence of specific target substrates through a signal that is generally proportional to the concentration or activity of the

target. The synthesis of the peptide, its binding to Smurf1, and its monitoring *in vitro* and *in vivo*, e.g., in rheumatic arthritis (RA) cells overexpressing Smurf1, will be discussed in this manuscript.

4. MATERIALS AND METHODS

4.1. Synthetic peptides

Peptides were automatically synthesized by sequentially coupling amino acids to preloaded 2-chlorotrityl chloride resin using a peptide synthesizer (Apex 396, AAPPTec, USA). Peptide precipitates were purified to homogeneity using reverse-phase high-performance liquid chromatography with a Vydac C18 column (Grace & Co.-Conn, USA) with a linear gradient of acetonitrile in H_2O, with both solutions containing 0.1% TFA. The peptides were eluted under gradient conditions consisting of 5−60% acetonitrile with a flow rate of 20ml/min for 60min and monitoring at 230nm. Each peptide was characterized using MALDI-TOF mass spectrometry. The purity of the peptides was greater than 95%.

4.2. Peptide labeling

Purified peptides were prepared at 20μM in phosphate-buffered saline (pH 7.5).

EZ-Link Sulfo-NHS-Biotin (Pierce, USA) was mixed with the peptide solutions to achieve a Sulfo-NHS-Biotin: peptide molar ratio of 20:1. After 2h of shaking at room temperature, the reaction was terminated via the addition of lysine to a final concentration of 20μM. Unreacted free biotin was removed by ultrafiltration, and the concentrated labeled peptides were stored at -20°C until use.

These peptides were automatically synthesized using the Fmoc strategy with a peptide synthesizer (Apex 396; AAPPTEC). The desired resin-linked product had only one free amino group at its N-terminus; therefore, reactions were conducted by mixing peptides with fluorescein isothiocyanate (FITC) solution in DMF at pH 9.3 overnight. The labeling efficiency was monitored using HPLC with dual absorbance at 230 and 488nm. The fluorescently labeled peptides were purified using HPLC (purity > 95%), lyophilized, and stored at -20°C in the dark until further use.

To obtain bioconjugated peptides for quenching assays, 1-ethyl-3-(3-dimethylaminopropyl) carbodiimide (EDC; 5mM) was added to the above fluorescently labeled peptide solutions, and the solutions were shaken for approximately 15min. Then, n-hydroxysulfo-succinimide (NHS; 5mM) was added

to the solutions to prepare fluorescently labeled peptides conjugated to BHQ-1 via an EDC–NHS coupling reaction for 40min. The quenched peptides were purified using HPLC (purity > 95%), lyophilized, and stored at -20℃ in the dark until further use. The quenching of FRET by a reaction between the synthetic peptides and the Smurf1 protein was investigated by imaging using an LAS 3000 Imaging System (Fuji Co., Japan), a confocal microscope (Olympus, Japan) and FACSCalibur (BD, USA).

4.3. Dot blot assay for screening of synthetic bioactive candidates

A nitrocellulose membrane (PALL life sciences, USA) was pre-wetted with Tris-buffered saline (TBS: 20mM Tris-HCl; pH7.6, 150mM NaCl) and partially dried. Peptides dissolved in water were immobilized to the membrane using a vacuum pump for 20h. Purified Smurf1 protein (Origene, USA) or Heparin (Sigma Chemical Co., MO, USA) was loaded on the immobilized peptides for 90min. The membrane was then blocked in 0.5% Tween 20 in TBS (TBST) with 5% nonfat dry milk powder for 1 h at room temperature. The applied peptides were incubated for

4 h at room temperature with primary antibody to each loaded proteins in the blocking buffer (1:1000) and washed 3 × 10 min with TBST. Incubation with HRP-conjugated secondary antibody (1:5000) in TBST for 1h at room temperature was followed by washing. Visualization of proteins with chemiluminescent reagents was recorded by exposure to enhanced chemiluminescence (ECL) membrane using MicroChemi (DNR Bio-imaging systems, USA).

4.4. Binding affinity analysis

A total of 20µl of purified Smurf1 protein (50µg/ml) was blotted onto a nitrocellulose membrane in slot blot wells, and the wells were blocked in TBST for 30min. Biotinylated peptides were incubated with Smurf1 in the slot blot wells for 90min. The wells were washed, and the blots were blocked with TBST containing 0.5% Tween 20. The blots were then incubated with peroxidase-labeled avidin (Sigma-Aldrich, USA) for 1h. After washing, the blots were incubated with ECL substrate solution, and the membranes were exposed to X-ray film for signal detection.

The Smurf1 protein was amine-coupled to the sensor chip with N-ethyl-N′-(dimethylaminopropyl) carbodiimide/N-hydroxy succinimide (EDC/NHS) using 10mM acetate (pH 4.5) as a coupling buffer and HBS-EP as a running buffer. Typical immobilization levels were approximately 27,500 resonance units (RU). The first flow channel was left unmodified, and Smurf1 protein was immobilized in the second flow channel. All the compounds were dissolved in sterilized distilled water (DW) to form 1mM stock solutions. The assay was performed in an e-tube format. The peptides and Smad1 recombinant protein (Abnova Co., Taipei, Taiwan) were prepared in running buffer and were tested in triplicate at a concentration of 10μM. The flow rate was 5μl/min, and the analysis temperature was 37°C. The test peptides and negative controls were injected in a cycle with a contact time of 420s and a dissociation time of 60s, followed by an extra wash of the flow system with 50mM NaOH. The assay was preceded by priming the system three times with running buffer and three start-up cycles with injections of running buffer.

4.5. Culture, differentiation, and Smurf1 overexpression in hMSCs

A human mesenchymal stem cell (hMSC) line (Lonza, USA) was maintained as a monolayer culture in a humidified incubator (95% air and 5% CO_2) at 37°C in a petri dish (Nunc International, USA) containing MSCGM™ Bullet Kit® medium (Lonza, USA). The medium was changed twice per week. When 70–80% confluence was reached, cells were passaged, and cells at passage 4 were used in the following experiments.

For osteogenic differentiation, hMSCs were cultured in osteogenic medium composed of the MSCGM™ Bullet Kit® medium supplemented with 50mM ascorbate-2-phosphate, 1μM dexamethasone and 10mM β-glycerophosphate. The medium was changed three times per week. Additionally, recombinant TNFα protein (10ng/ml, R&D Systems, USA) was used to treat the cells under osteogenic conditions for 72h, and 10μM each peptide was subsequently added for 2h.

For hSmurf1 overexpression, when cells reached 90% confluence, the cDNA expression plasmid, a pCMV-FLAG-tagged Smurf1 (F-Smurf1) was transiently transfected into the cells using the Lipofectamine™ 2000 transfection reagent (Invitrogen, USA) according to the manufacturer's instructions. The total amount

of transfected plasmids in each group was equalized via the addition of an empty vector. BHQ-1-conjugated FITC-labeled peptides were used to treat the hSmurf1-overexpressing hMSCs. After 1h, the cells were analyzed using the LAS 3000 imaging system and a fluorometer.

4.6. Activity of synthetic peptides using protein A-based immunoprecipitation

Human mesenchymal stem cells were treated with MG132 (Calbiochem, USA) for 4h. After treatment, peptides were added for 1.5h. Cell lysates were incubated with anti-Smad1/5/8 antibody for ubiquitination assay or anti-Smurf1 antibody for investigating peptide affinity to Smurf1-Smad1/5/8 complex and then, Protein A/G-agarose beads (Santa Cruz, USA) overnight at 4°C. The immunoprecipitates were washed with 50mM Tris-HCl buffer (pH 8.0) containing 150mM NaCl, 0.1% Tween 20, 0.05% deoxycholate, and 0.1% SDS to remove unbound protein, resuspended in 5× sample buffer, and subjected to Western blot analysis with an anti-ubiquitin antibody, Smad1/5/8 or Smad7.

4.7. Intracellular translocation of synthetic peptides

FITC-labeled peptides were added to cells at a final peptide concentration of 100μM. Following 20- and 80-min incubations at 37°C in humidified 5% CO_2, the cells were washed with PBS. To observe the intracellular localization of peptides, the cells were further incubated with Hoechst 33342 (Molecular Probes, USA) to visualize the nucleus of non-fixed cells. Confocal laser-scanning microscopy was performed using an Olympus FV-300 laser-scanning microscope with FLUOVIEW software (Olympus, Japan).

For flow cytometric analyses, the cells treated with peptides were washed with PBS, treated with TrypLE™ Express for 10min to remove surface-bound FITC-labeled samples, and washed again to avoid artifacts. The cells were washed twice with PBS and were then resuspended in PBS. The analysis was conducted using a FACSCalibur flow cytometer (Becton Dickinson, CA) equipped with a 488nm air-cooled argon laser. The fluorescence of 10,000 live cells was acquired, and the data were visualized in logarithmic mode.

4.8. Osteogenic differentiation analysis

Alkaline phosphatase (ALP) activity was measured by staining cells with a mixed solution of naphthol and Fast Red Violet according to the manufacturer's instructions for the ALP staining kit (Chemicon, USA). Calcium phosphate precipitates from the cell cultures were stained with Alizarin Red S. The wells were photographed with an Olympus inverted microscope. In addition, osteogenically differentiated cells were identified by observing fluorescent Calcein AM (Sigma-Aldrich, USA) by confocal microscopy. An adaptation of the protocol described in [18] was followed. Intracellular proteins from cells treated with peptides were separated into nuclear and cytoplasmic extracts using NE-PER® Reagent (Pierce, IL, USA). After the cells were lysed according to the manufacturer's instructions, the protein concentrations were determined using a Bradford protein assay kit (Bio-Rad, USA), and the proteins were transferred to nitrocellulose membranes. The membranes were washed three times and were incubated with the primary antibodies anti-Erk1/2 (1:2000), anti-phospho-Erk1/2 (1:1000), anti-Smad1/5/8 (1:2000), anti-phospho-Smad1/5/8 (1:1000), anti-Smurf1 (1:1000), anti-actin

(1:8000), anti-lamin B (1:5000), and anti-Runx2 (1:2000). Protein bands were visualized with a chemiluminescence reagent (West-Zol®; Intron, Korea).

4.9. Quantitative analysis of osteogenic marker expression by synthetic peptides

Human mesenchymal stem cells were incubated with 10μM each peptides for 14days in mineralization medium. At the end of the indicated time, total RNA was isolated using TRIzol® (Invitrogen, USA). After reverse transcription, a real-time quantitative PCR analysis was performed in an ABI PRISM 7500 (Applied Biosystems, CA, USA) using SYBR Green I dye detection. The reactions were performed following the manufacturer's recommendations. The PCR primer sequences were as follows: 1) human ALP: TGGAGCTTCAGAAGCTCAACACCA and ATCTCGTTGTCTGAGTACCAGTCC; 2) human osteocalcin: CATGAGAGCCCTCACA and AGAGCGACACCCTAGAC; and 3) human Runx2: CAGACCAGCAGCACTCCATA and CAGCGTCAACACCATCATTC. Human GAPDH (CGTCTTCACCACCATGGAGA and CGGCCATCACGCCACAGTTT) was

used as a control to normalize for equal loading of the cDNA template.

4.10. *In vivo* biofluorescence imaging

To induce experimental rheumatic arthritis (RA), female Lewis rats (7weeks old) were subcutaneously injected at the base of their tails and into their right paws with 200μg of bovine type II collagen (Sigma-Aldrich, USA) in 125μl of 0.1M acetic acid emulsified in an equal volume of complete Freund's adjuvant (Difco, USA) containing 2mg/ml Mycobacterium tuberculosis H37 RA. The rats were again challenged with the same antigen preparation 7days later. Before the injection, the animals were anesthetized with ether, and the injections were performed with a 15-gauge needle. Disease developed approximately 11days after the second immunization.

The rats were anesthetized intraperitoneally with Zoletil 50 (tiletamine 25mg/kg and zolazepam 25mg/kg; Virbac, France), followed by an intraarticular injection of 100mM quenched peptide probes suspended in 200μl of PBS 21days after the induction of CIA (Collagen-induced arthritis). The fluorescence intensity

in the ankle joints of two hind limbs was visualized with an LAS 3000 imaging system (Fuji Co., Japan). After an exposure time of 1/2sec, the fluorescence signal intensity was detected in the ankle joints and paws. Images were generated using MultiGauge software (Fuji Co., Japan).

4.11. Immunohistomorphologic evaluation

After biofluorescence imaging, the rats were sacrificed, and the knee joints, calvariae, and hind limbs were removed, fixed for 1day in 10% buffered formalin, decalcified for 3days in Calci-Clear Rapid (National Diagnostics, USA), and embedded in paraffin. Paraffin-embedded sections (3μm) obtained from each tissue from normal and arthritic animal models were stained with hematoxylin and eosin. Each calvaria was stained with Calcein AM (Sigma-Aldrich, USA) following the manufacturer's instructions. Rabbit anti-human Smurf1 was developed using anti-rabbit Alexa Fluor 546 (Molecular Probes, USA), and mouse anti-TNFα was detected with anti-mouse Alexa Fluor 488 (Molecular Probes, USA).

4.12. *In vitro* quenching analysis

NIH3T3 and HOS (ATCC, USA) were cultured in α-minimal essential medium supplemented with 10% fetal bovine serum (GIBCO, USA). The BHQ-1 conjugated FITC-hBCPP-SBP was treated the cells and after 1h, the cells were analyzed using FACSCalibur and confocal microscope.

4.13. Histomorphologic evaluation

After bio fluorescence imaging, the rats were sacrificed, and the knees joints, calvarias and hindlimbs were removed, fixed for 1day in 10% buffered formalin, decalcified for 3days in Calci-Clear rapid (National diagnostics, USA), and embedded in paraffin**.** Sections (3μm) of paraffin-embedded each tissue obtained from animal models of normal and arthritis was stained with hematoxylin and eosin. Each calvarias were stained Calcein AM (Sigma, USA) by manufacture's instruction.

4.14. Statistical analysis

All the data are presented as the means ± standard error (SE) for all the controls and experiments (N = the total number of independent cultures). The data were analyzed using a one-way analysis of variance (ANOVA) followed by Fisher's protected least-significant difference (PLSD) post hoc test (StatView; SAS Institute, USA). *p*-values < 0.05 were considered significant.

5. RESULTS

5.1. Screening of protein-derived potential motifs as bioactive peptides

With two aims to identify bioactive peptides that possess highly penetrating and high binding affinity to Smurf1, the candidates were synthesized based on F-moc chemistry. Epitope mapping as a strategy for searching the most potential motif is a very useful tool for screening a known protein sequence for active regions. The peptides are generated by shifting a frame of a distinct peptide length of a protein sequence of interest. In this study, Epitope semi-mapping consists of peptides with a reported bioactive motif and a framedesign (e.g., frameshift) of random segmentation. To find the most bioactive motif bound with Smurf1, four domains were designed by including WW interaction site of LMP1 (APSVSLNKTARPFGA, ADPPRYTFAP, ADPPRYTFAPSVSLNKTARPFGAPPPADSAP and GAPPPADSAP). Fig. 3.1 is showed parent molecule, theoretical pI-values, net charge and molecular weight as well as each sequence of the domains. The binding affinity of the Smurf1 binding domains was determined, respectively (Fig. 3.2). Among the domains, Smurf1 binding domain-test peptide 4 (SBD-TP4) revealed the maximum binding affinity with Smurf1 even 0.1μM. With selecting two candidates, SBD-TP3 and SBD-TP4, having good Smurf1 binding ability,

functional assay was performed using FACSCalibur. However, the peptides were not penetrating into cells (Fig. 3.2A). To elucidate indirect osteogenic differentiation through binding with Smurf1, the domains were synthesized containing Tat sequence as a common cell penetrating motif. After osteogenic differentiation, SBD-TP3 and SBD-TP4 significantly showed remarkable effectiveness in mineralization compared to the not-treated group (Fig. 3.2B). Therefore, a key domain that could be inducing mineralization through the strong binding to Smurf1 was selected to SBD-TP4.

Second, for selecting a motif as using a cell penetrating peptide, the amino acid sequence of the domains corresponded to heparin binding residues of human BMP2-derived motif (HBD-TP1-3; SCKRH, RKRLSSCKRH and QAKHKQRKRLSSCKRH) and BMP4 (HBD-TP4-6; NCRRH, RKKNPNCRRH and SPKHHSQRARKKNPNCRRH) (Fig. 3.4). The synthetic domains were consisted of positively charged (Arg, Lys and His) and hydrophobic (Phe and Asp) amino acids. The BMP4-derived motifs were possessed more increasing binding affinity to heparin than the BMP2-derived motifs. Among them, the HBD-TP5 peptide significantly showed the most outstanding affinity to heparin (Fig. 3.5). To investigate effect of the domains in cell viability, viable cells were detected using MTT assay. The hMSCs were treated with the peptides (0, 1, 10, 100μM) for 0, 24,

48, 72h in complete media. The cell growth increased in a time-dependent manner, however there was no significant change in cell viability for the peptides treated hMSCs (Fig. 3.6A). In addition, in the penetrating ability of heparin binding domains, HBD-TP2 and HBD-TP5 were remarkably increased compared to not-treated cells. Especially, the fluorescent mean value of HBD-TP5 (447.56) was higher than that of HBD-TP2 (209.66) (Fig. 3.6B), suggesting that the HBD-TP5 sequence is essential for the heparin binding affinity. These results indicate the HBD-TP5 have the potential to penetrate a bioactive domain such as SBD-TP4 into cells. Without affecting cell viability, and therefore has the potential to use as a cell penetrating peptide.

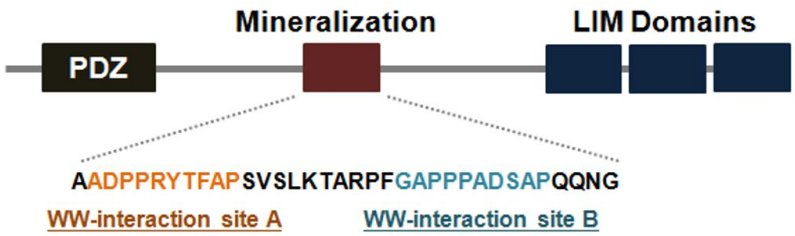

Peptide	Parent molecule	Iso-electric point	Sequence	Net charge/ Mw (Da)
SBD-TP1	hLMP-1	11.49	APSVSLNKTARPFGA	2 / 1515.73
SBD-TP2	hLMP-1	6.69	ADPPRYTFAP	0 / 1134.26
SBD-TP3	hLMP-1	9.71	ADPPRYTFAPSVSLNKTARPFGAPPPADSAP	1 / 3196.57
SBD-TP4	hLMP-1	3.1	GAPPPADSAP	-1 / 878.94

* The WW-interaction sites are underlined.

Figure 3.1. Synthetic peptides used for screening the most potential Smurf1 binding motifs

Sequence alignment of four peptides obtained from partially WW-interaction domains of LMP-1. Parent molecule, theoretical pI-value, peptide sequence and molecular weight as well as net charge are shown. SBD: Smurf1 binding domain, TP: Test peptide, hLMP-1: Human LIM mineralization protein 1

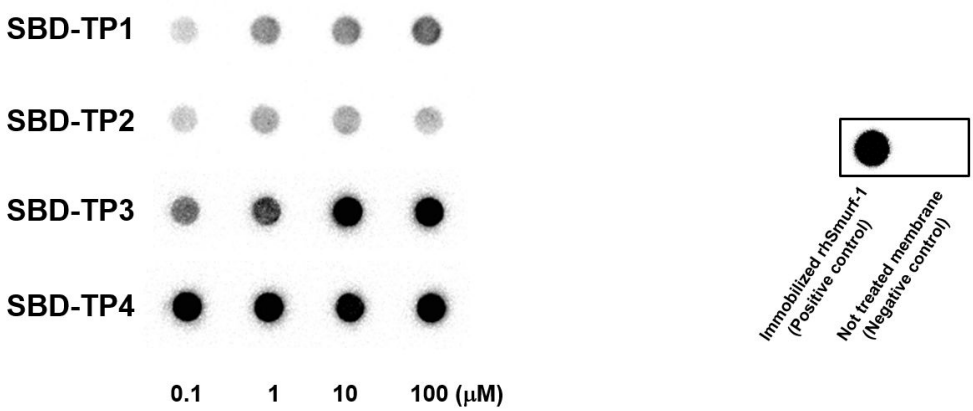

Figure 3.2. Epitope semi-mapping of Smurf1 binding domains using Dot blotting

Image of the membrane after incubation with a Smurf1 protein on SBD peptides was detected by dot blot.

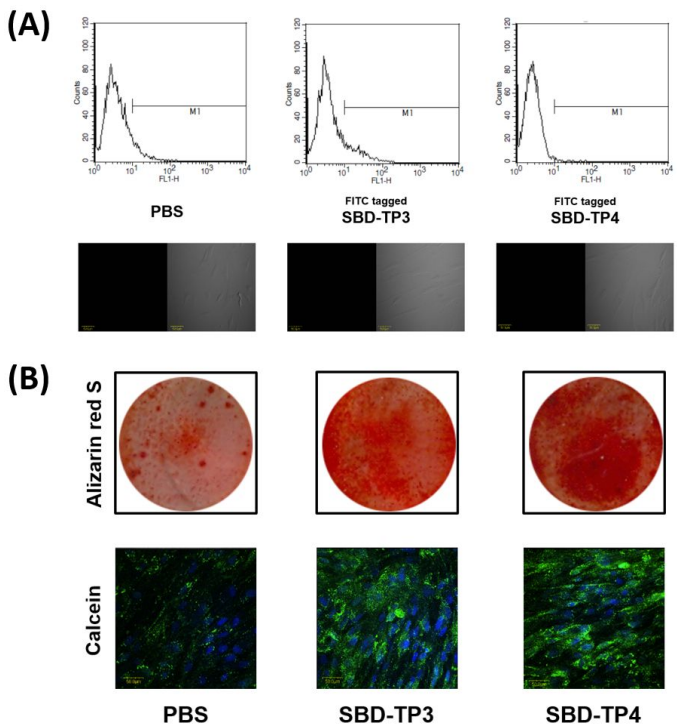

Figure 3.3. Internalization and mineralization ability of the selected two peptides

(A) The intracellular distribution of SBD-TP3 and SBD-TP4 was measured using FACSCalibur and confocal microscope. (B) Matrix mineralization ability of SBD-TP3 and SBD-TP4 was detected by Alizarin red S staining and Calcein AM staining.

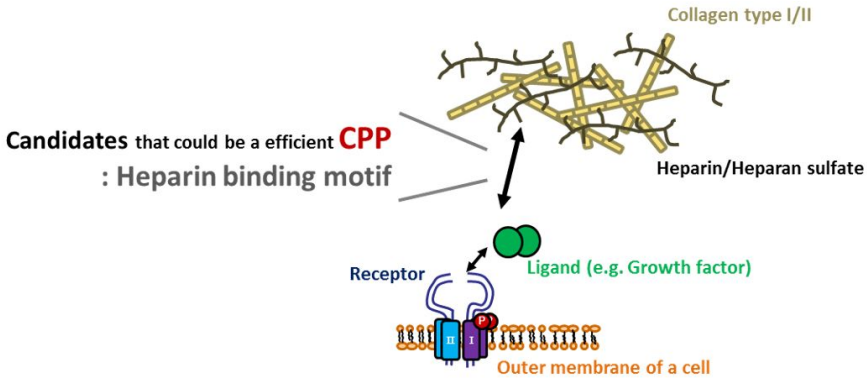

Peptide	Parent molecule	Iso-electric point	Sequence	Net charge/ Mw (Da)
HBD-TP1	hBMP-2	10.11	SCKRH	2 / 629.73
HBD-TP2	hBMP-2	12.14	RKRLSSCKRH	5 / 1398.70
HBD-TP3	hBMP-2	12.17	QAKHKQRKRLSSCKRH	7.1 / 2119.53
HBD-TP4	hBMP-4	10.9	NCRRH	2 / 684.7
HBD-TP5	hBMP-4	12.14	RKKNPNCRRH	5 / 1308.53
HBD-TP6	hBMP-4	12.42	SPKHHSQRARKKNPNCRRH	7.2 / 2337.66

* The heparin binding domains are underlined.

Figure 3.4. Synthetic peptides used for screening the most potential heparin binding motifs

Sequence alignment of six peptides obtained from partially heparin binding domains of BMP2 or BMP4. The sequence consist of positively charged amino acids such as Arg, Lys and His, as well as the hydrophobic amino acids Asp and Phe. Parent molecule, theoretical pI-value, peptide sequence and molecular weight as well as net charge are shown. HBD: Heparin binding domain, TP: Test peptide, hBMP2: Human bone morphogenetic protein 2, hBMP4: Human bone morphogenetic protein 4

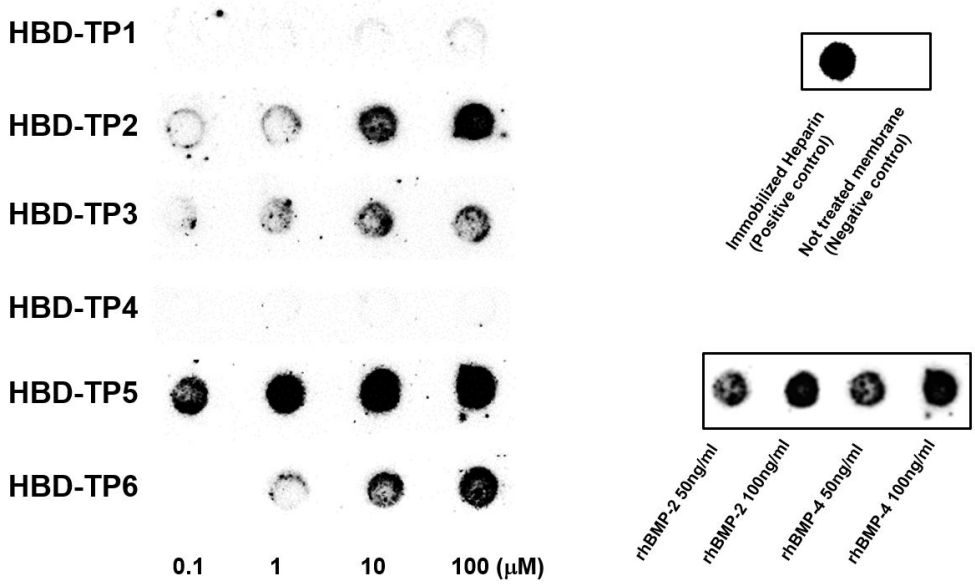

Figure 3.5. Epitope semi-mapping of Heparin binding domains using Dot blotting

Image of the membrane after incubation with Heparin on HBD peptides was detected by dot blot.

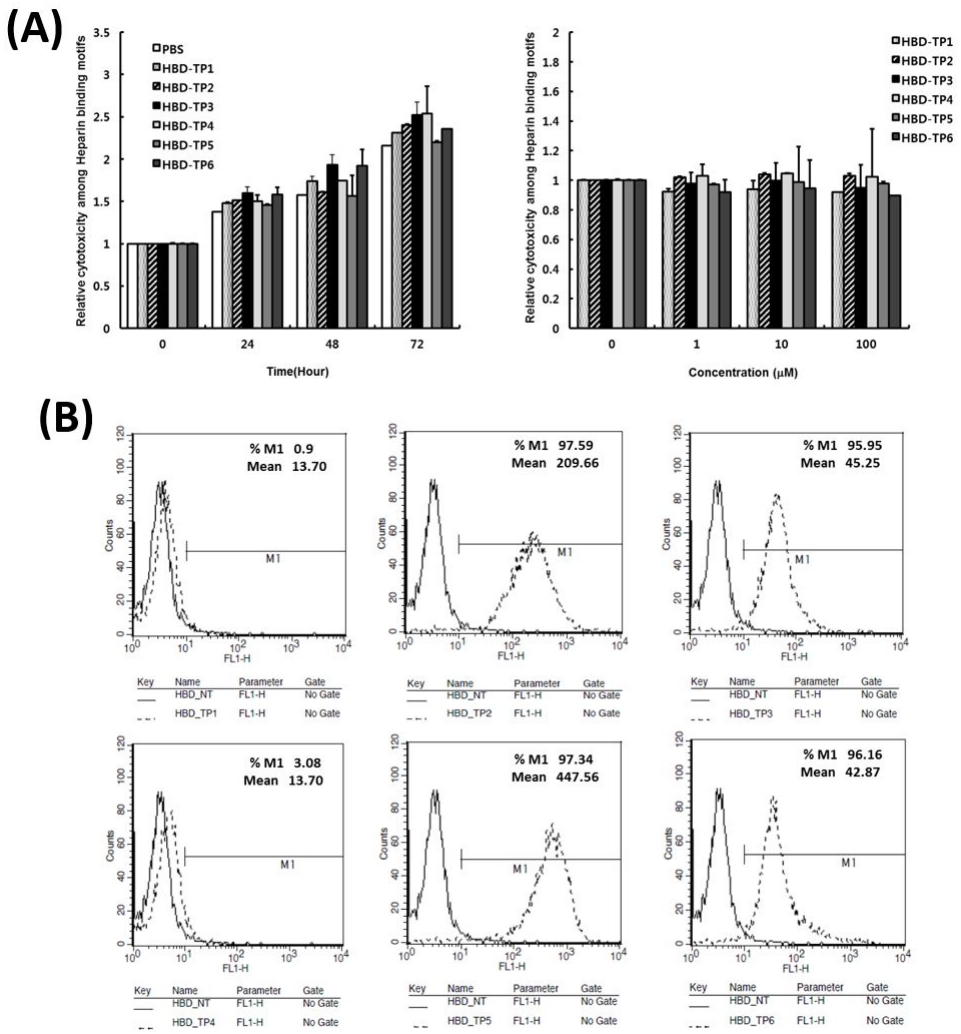

Figure 3.6. Verification of the functionality of heparin binding domains as a cell penetrating peptide

(A) Effect of HBD peptides on cell viability was analyzed by MTT assay on increased incubation times and various concentrations. (B) Intracellular transduction ability of HBD peptides compared to not-treated cells was measured using FACSCalibur.

5.2. Internalization of the human-derived cell-penetrating domain

Fig. 3.7 shows that our CPP penetrated cells as efficiently as the well-known, virus-derived, cell-permeable Tat peptide, in marked contrast to the penetration ability of the control, polyglutamic acid (PGA; CGGGEEEEEEEEEEE). In less than 20min, our hBCPP was observed to primarily localize to the cytosol, with a minority of the hBCPP located at perinuclear sites, similar to the localization of Tat (left panel). After 80min, both hBCPP and Tat translocated through the cell membrane and accumulated in the cytoplasm and nucleus, with the majority of both internalized peptides found in the nucleus (right panel), demonstrating an unprecedented efficiency of cellular internalization of both hBCPP and Tat_{47-57}. As expected, no SBP was observed in the cytoplasm or nuclei of the hMSCs, whereas the peptide probe containing the SBP linked to hBCPP successfully penetrated the hMSCs. In addition, FACS analysis was showed the results in correlated with images of confocal microscopy (Fig. 3.8).

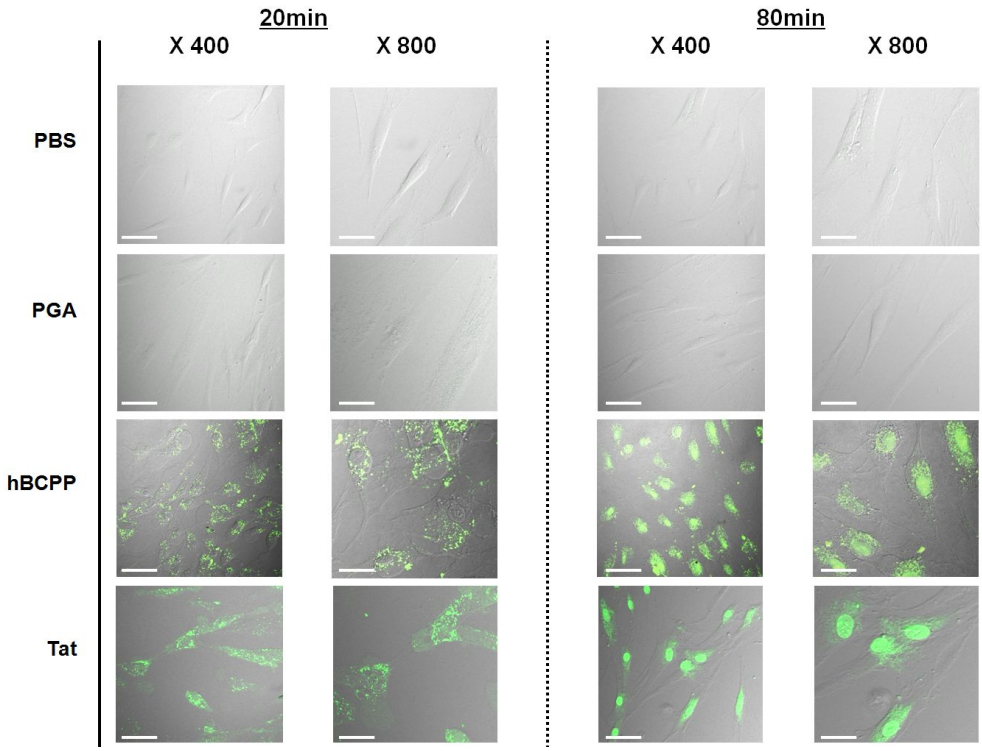

Figure 3.7. Intracellular translocation of the hBCPP chosen as a cell penetrating peptide

The human BMP4-derived cell penetrating peptide (hBCPP), Tat as a positive control, and polyglutamic acid (PGA) as a negative control were added (10μM), and the cells were incubated for either 20 or 80min, washed twice with PBS, and placed in growth medium. Live cells were then visualized under a confocal microscope. Fluorescence-labeled peptides are shown in green.

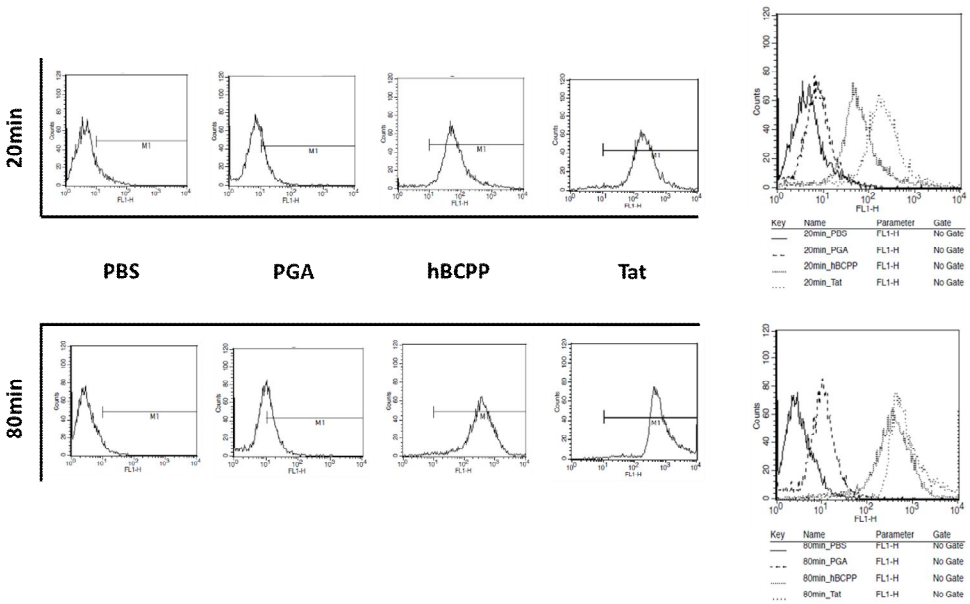

Figure 3.8. Intracellular uptake ability of the hBCPP depends on incubation times

The hBCPP, Tat, and PGA were added (10μM), and the cells were incubated for either 20 or 80min, washed twice with PBS. After trypsinization, the cells were washed twice with PBS and immediately observed by FACSCalibur.

5.3. Binding affinity between hBCPP-SBP and Smurf1

In this study, the author created a peptide sequence to bind a target protein as an osteogenesis inducer and to probe activity via the synthesis and linkage of two short domains. A cell-penetrating SBP was prepared using Fmoc solid-phase peptide synthesis. The peptide was composed of two motifs: an LMP1-derived Smurf1 binding motif (SBP; GAPPPADSAP) and a newly identified CPP, which was reported by the author and co-workers who discovered human BMP4, termed human BMP-derived CPP (hBCPP; RKKNPNCRRH). The latter peptide was linked to the N-terminal region of the former sequence during peptide synthesis, representing a strategy for functionalizing a non-penetrating peptide, which features a simple method for internalizing an intracellular sequence using a CPP. The peptides were analyzed by mass spectrometry. SBP [M+Na]+: 897.91 (calculated), 901.2 (found); hBCPP-SBP [M+Na]+: 2446.73 (calculated), 2445.7 (found); hBCPP [M+H]+: 1585.82 (calculated), 1585.7 (found) (Fig. 3.9).

To confirm the identity and concentration dependency of the SBP peptide for binding to Smurf1, the author performed a slot blot assay. The results showed that

not only did binding occur between Smurf1 and peptides containing the LMP-1-derived motif but the nitrocellulose membranes also became thick at increasing concentrations of the peptides (Fig. 3.10A). To examine the binding activity of the synthesized peptides, the author measured the binding affinity of purified Smurf1 protein to our fusion peptide containing the cell-penetrating SBP using a surface plasmon resonance (SPR) assay. Although the cell-penetrating peptide had negligible binding affinity for the Smurf1 protein, the SBP bound strongly to the Smurf1 protein, which was added to a CM5 chip at a typical flow rate (10μl/min) (Fig. 3.10B). The apparent binding constants (K_A) for the LMP-1-derived SBP, hBCPP-SBP and hBCPP were calculated to be $1.036\times10^{8}(M^{-1})$, $1.237\times10^{7}(M^{-1})$, and $4.129\times10^{5}(M^{-1})$, respectively. Accordingly, the apparent dissociation constants (K_D) were 96.6, 80.8, and 2422nM for SBP, hBCPP-SBP, and hBCPP, respectively. In contrast, the K_D for Smad1, which is known to bind strongly to Smurf1 during the ubiquitination process in the osteogenic pathway, was 298nM (Table 3.1). Based on the calculated binding constants, the author concluded that SBP interacted more powerfully with Smurf1 than with Smad1; therefore, LMP-1 may compete with Smad1/5/8 for binding to Smurf1, thus inhibiting the targeting of

Smad1/5/8 for ubiquitination. These relatively high binding affinities raised the possibility that Smurf1 interactions may have biological importance. These results are consistent with the above binding analysis, showing that the hBCPP-SBP identified in our study contains an LMP domain critical for inhibiting Smurf1, which is further activated by the addition of hBCPP.

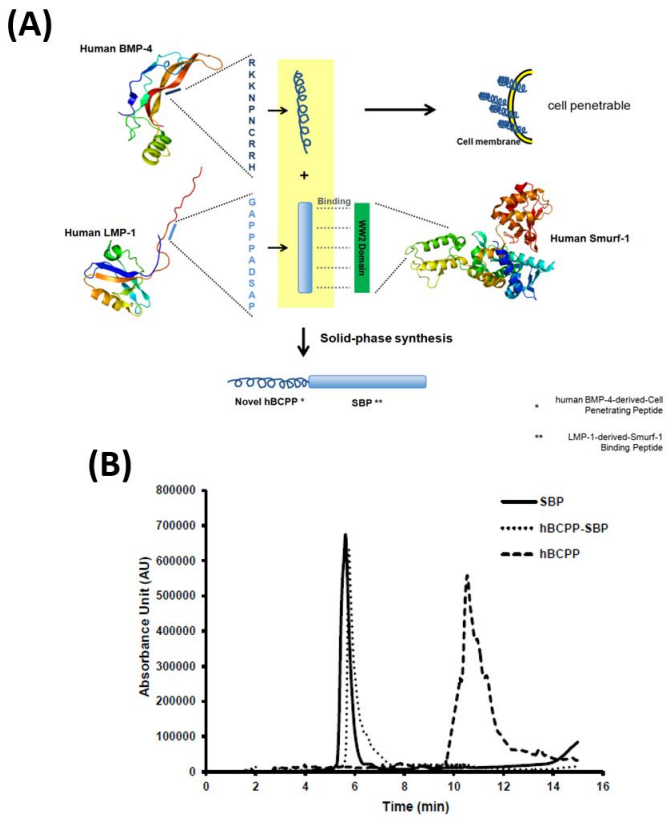

Figure 3.9. Design, synthesis and purification of the SBP, hBCPP-SBP and hBCPP

(A) Peptide design and fabrication using Fmoc solid-phase peptide synthesis**.** (B) Analysis and purification of SBP, hBCPP-SBP and hBCPP by a C18 column using a high performance liquid chromatography.

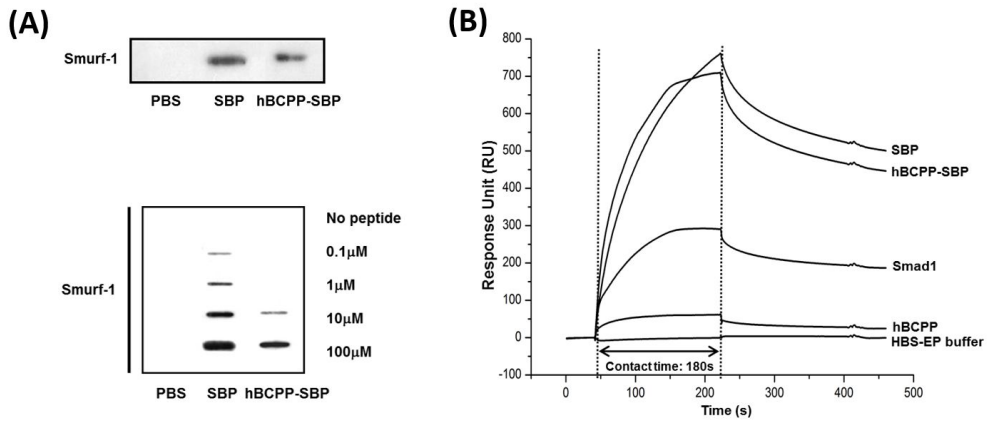

Figure 3.10. Smurf1 binding ability of the SBP and hBCPP-SBP

(A) Assessment of the binding of SBP and hBCPP-SBP, which contains a WW domain-interacting binding site, to Smurf1 using a slot blot assay. (B) Sensorgram of the specific binding of immobilized Smurf1 to 1μM of each peptide using SPR assays.

Table 3.1. Kinetic parameters of the binding of Smurf1 to SBP, hBCPP-SBP, hBCPP, and Smad1

Interacting proteins	K_D (M)	K_A (M^{-1})	K_a ($M^{-1}S^{-1}$)	K_d (S^{-1})	Rmax (RU)
recombinant Smurf1-SBP	9.657×10^{-8}	1.036×10^{8}	6671	6.442×10^{-4}	1371.5
recombinant Smurf1-hBCPP-SBP	8.080×10^{-8}	1.237×10^{7}	7321	5.916×10^{-4}	1475.0
recombinant Smurf1-hBCPP	2.422×10^{-6}	4.129×10^{5}	2447	5.927×10^{-3}	22.4
recombinant Smurf1-Smad1	2.980×10^{-7}	3.360×10^{6}	3548	1.057×10^{-3}	348.6

The rate constants of the association and dissociation reactions and the equilibrium dissociation constants of the interactions were determined from surface plasmon resonance measurements with the BIAevaluation software 4.0.

5.4. Effect of cell viability of the peptides

To investigate whether the synthetic peptides affects cell viability, cytotoxicity was measured after the peptides treatment. The hMSCs were treated with various concentration of SBP, hBCPP-SBP and hBCPP for 0, 24, 48, 72h in complete media and the cell viability was detected by MTT assay (Fig. 3.11). The cell viability increased in a time-dependent manner, but there was no significant change in cell growth for SBP, hBCPP-SBP or hBCPP treated hMSCs.

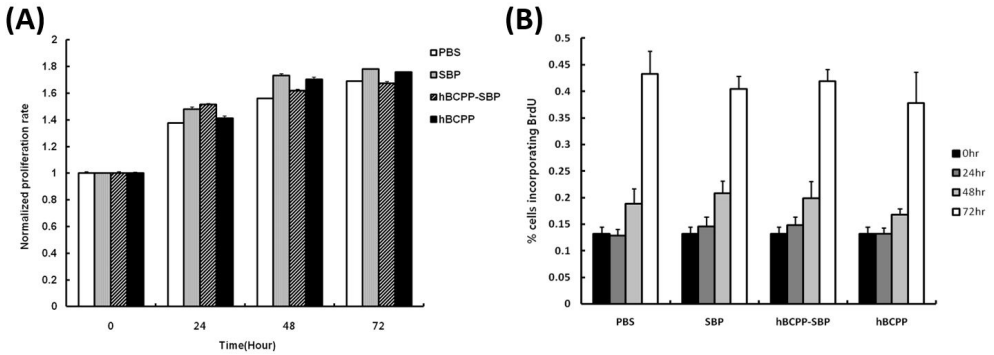

Figure 3.11. Effect of the SBP, hBCPP-SBP and hBCPP on cell viability

(A) Cytotoxicity testing of peptides after 3-[4,5-Dimethylthiazol-2-yl](C-2,5-diphenyltetrazolium bromide (MTT) treatment for 72h and (B) 5-Bromo-2´-Deoxyuridine (BrdU) assays demonstrating that cells treated with SBP, hBCPP-SBP, or hBCPP exhibited virtually identical viability to untreated cells. The values are expressed as the means ± SD. Each experiment was performed in triplicate.

5.5. Regulation of biological activity by the binding of hBCPP-SBP to targets

Smurf1 is a member of the HECT family of E3 ligases, and it contains a C2 domain at the N-terminus, two WW domains in the middle for mediating protein-protein interactions and a HECT domain at the C-terminus [19]. Smurf1 has been reported to interact with Smad1, Smad5, Runx2 and Smad7 through specific motifs. These interactions result in the ubiquitination and subsequent proteasomal degradation of target proteins. Most of the Smads related to BMP signaling bind to the WW domains of Smurf1, and this interaction could be suggested as the canonical Smurf1-substrate interaction. Recently, the involvement of Smurf1's C2 domain in substrate interaction was reported one of non-canonical pathways. Smurf1's C2 domain is important for its plasma membrane localization [20]. For example, Smad7, a member of TGFβ signal pathway, ubiquitination and translocation from nucleus to cytoplasm was considered to occur around TGFβ receptor, during which the membrane localization of Smurf1 by its C2 domain was indispensable [21]. Significant inhibition of Smad1/5/8 ubiquitination was observed in the presence of hBCPP-SBP (Fig. 3.12A), demonstrating that this

peptide inhibited the Smurf1-mediated digestion of Smad1/5/8. To elucidate whether the hBCPP-SBP affects Smurf1-Smad1/5/8 complex status, the peptide was treated to Smurf1-overexpressed hMSCs after MG132 treatment. Due to SBP does not have intracellular translocation ability, bound Smad1/5/8 to Smurf1 did not occur any changes. While the levels of Smad1/5/8 was decreased depending on increasing hBCPP-SBP concentration. Furthermore, hBCPP-SBP was determined that does not affect other binding of Smurf1-substrate (e.g., Smurf1-Smad7 interaction through C2 domain) (Fig. 3.12B). It should be noted that the identification of oligopeptide domains in functional proteins may represent a valuable alternative for alleviating the shortcomings of protein therapy using protein-protein interaction (PPI) concept.

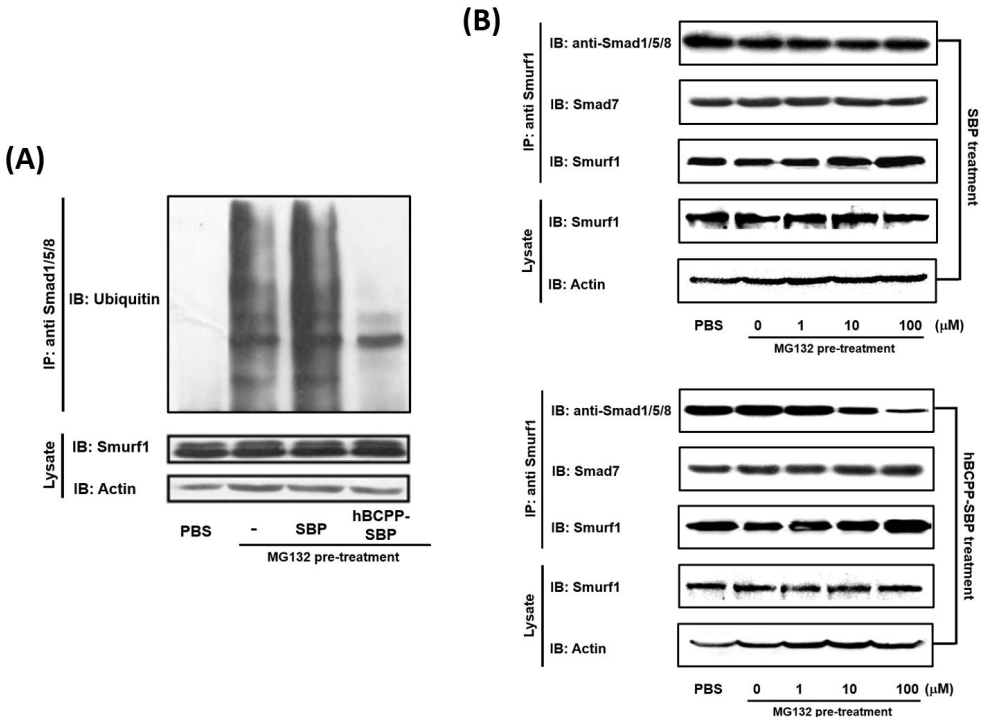

Figure 3.12. *In vitro* protein-peptide interaction between Smurf1 and hBCPP-SBP

(A) Effect of hBCPP-SBP on ubiquitin proteosomal degradation of Smad1/5/8 by Smurf1 was detected using Western blot analysis after immunoprecipitation of intracellular proteins bound Smurf1. (B) In normal condition that exists as Smurf1-Smad1/5/8 complex, competitive binding affinity by treating hBCPP-SBP was investigated using Smad1/5/8 antibody following immnuprecipitation and then, Smad7, that can binds C2 domain in Smurf1, antibody was used for observing specific binding of hBCPP-SBP to WW interaction motif in Smurf1.

5.6. Internalization of hBCPP-SBP by cells via the human-derived cell-penetrating domain

The internalization of the hBCPP-SBP was monitored using confocal microscopy after incubating the peptides with the cells for 20 or 80min. The hBCPP-SBP consisted of the hBCPP as a cell penetrating peptide accumulated in the nucleus for the extended period (Fig. 3.13). As aforementioned, the author described the ability of this CPP to enter cells and determined its subcellular localization (Fig. 3.7). In Fig. 3.4, SBP domain absolutely possesses osteogenic activity but, it was not possible to intracellular transduction. The results were showed hBCPP invests cell penetrating ability to SBP. Therefore, hBCPP-SBP has dual effects, osteogenic activity and penetrating activity.

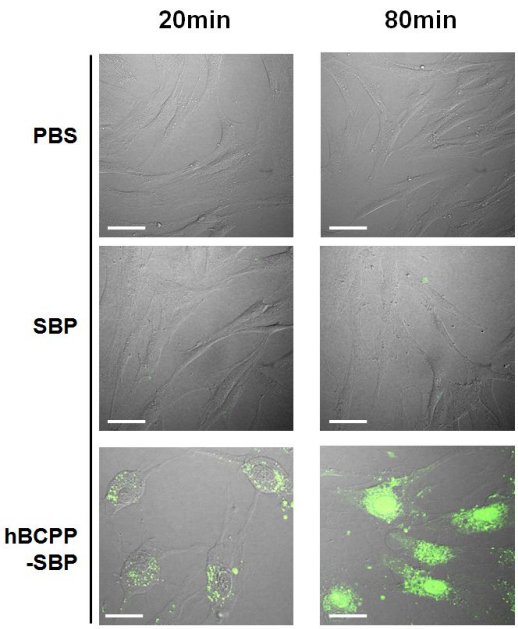

Figure 3.13. Intracellular translocation of SBP and hBCPP-SBP

The uptake of hBCPP-SBP by hMSCs was assessed observation of the cellular localization of fluorescein isothiocyanate (FITC)-labeled SBP and hBCPP-SBP in hMSCs using Confocal microscopy. Scale bar: 50μm, magnification: 800×.

5.7. Indirect evaluation of the restoration of Smad1/5/8 by hBCPP-SBP: increased osteogenic differentiation

To examine whether blocking Smurf1 using cell-permeable SBP would stimulate osteogenesis, the author incubated the hBCPP-SBP fusion peptide with stem cells under differentiation conditions. The author then investigated the expression of osteogenic markers using real-time RT-PCR with primer sets specifically designed to detect the osteogenic differentiation of hMSCs using hBCPP-SBP. ALP mRNA was detected only in the hBCPP-SBP-treated cells; no ALP mRNA was detected in the control peptide-treated cells. The hBCPP-SBP-treated cells showed a 2-fold increase in osteocalcin (OCN) gene expression ($P < 0.001$) and a 2.5-fold increase in Runx2 gene expression ($P < 0.001$), indicating that hBCPP-SBP induced cellular responsiveness to osteogenic stimulation under differentiation conditions. This response was observed after 3days but was more prominent 7days after treatment (data not shown). These findings also confirmed the results of the RT-PCR analysis. More specifically, the ALP, OCN, and Runx2 mRNA levels were prominently increased in the cells treated with hBCPP-SBP

(Fig. 3.14). Moreover, a relevant physiological question is whether these mechanisms are active in undifferentiated hMSCs, which initiate adult osteogenesis. In these cells, the author investigated whether the interaction between hBCPP-SBP and Smurf1 resulted in an increased activation of the osteogenic pathway. The author measured the levels of phosphorylated Smad1/5/8, Runx2, and Smurf1 in the cytoplasm and nucleus. The cells treated with hBCPP-SBP showed a significantly greater increase in the levels of osteogenic signaling molecules than the cells treated with SBP alone hBCPP (Fig. 3.15), indicating that the peptide could stimulate the osteogenic response at early stages. As a result, alizarin red S, alkaline phosphatase, and Calcein AM staining (Fig. 3.16) demonstrated accelerated osteogenic nodule formation and mineralization in the cells transfected with hBCPP-SBP compared with those transfected with SBP without hBCPP, which lacked the capacity for translocation.

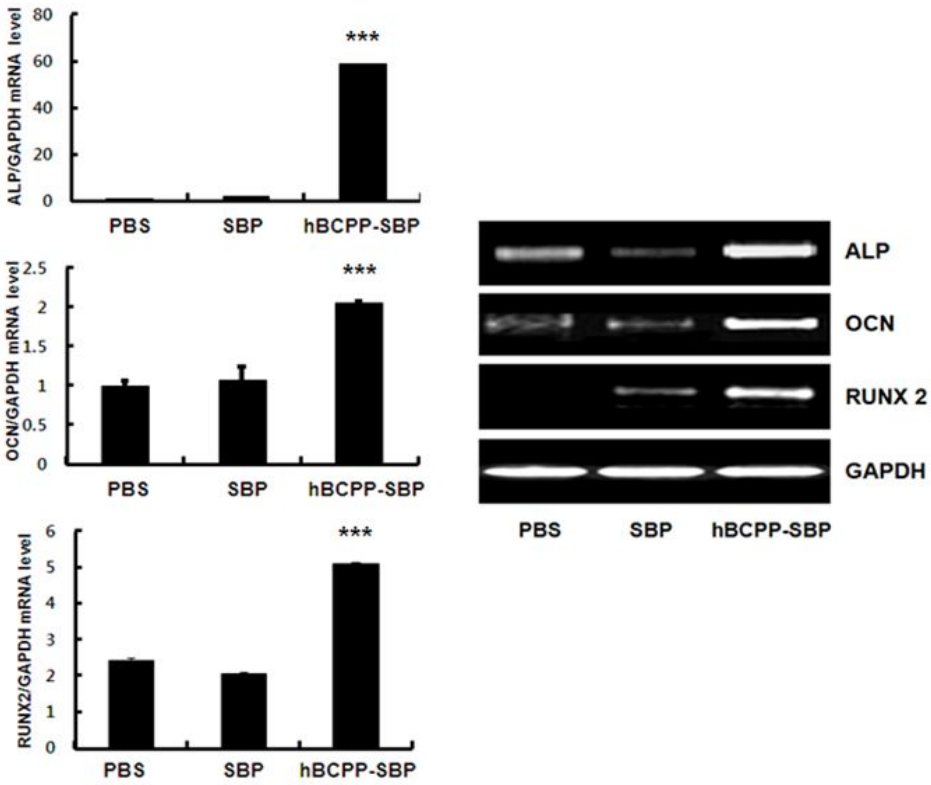

Figure 3.14. Osteogenic-specific gene expression by SBP and hBCPP-SBP treatment

Examination of hMSCs treated with SBP and hBCPP-SBP under osteogenic differentiation condition. The mRNA levels of ALP, OCN, and Runx2 were measured using quantitative real-time PCR and the PCR products were photographed under UV light.

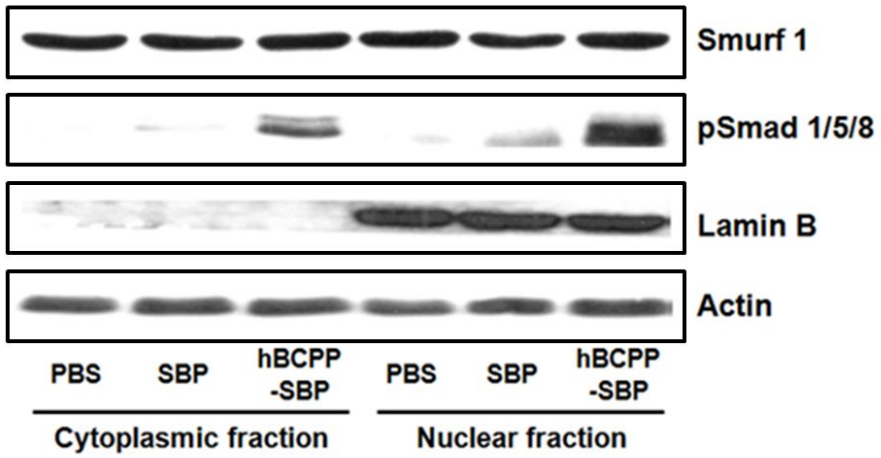

Figure 3.15. Restoring of Smad1/5/8 phosphorylation by SBP and hBCPP-SBP treatment

Western blotting was performed to determine the protein levels of osteogenic signal transduction molecules in each cell fraction.

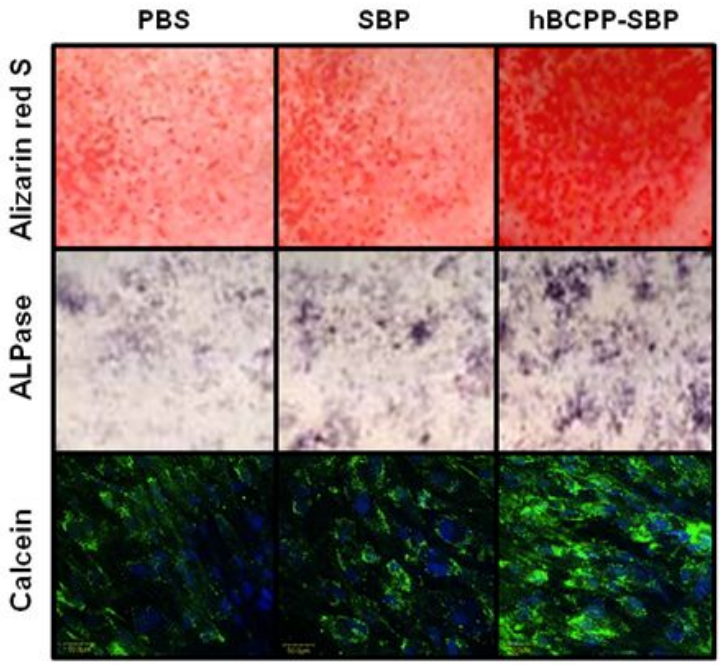

Figure 3.16. Matrix mineralization by SBP and hBCPP-SBP treatment

Differentiated hMSCs were stained with 2% Alizarin red S, with ALP detection kit, and with Calcein AM. The data are presented as the means ± the standard error of the mean (***, *p*-value < 0.01).

5.8. Visualizing the expression of Smurf1 *in vitro* using the hBCPP-SBP probe

The peptides were further modified with an activatable fluorescent dye to examine the binding interaction between the SBP sequence and Smurf1 via a FRET quenching strategy. BHQ-1 was able to quench the fluorescence of FITC with high efficiency. The fluorescence of the hBCPP and SBP peptides was inactive because the fluorescent dye and BHQ-1 were located close to each other; however, their fluorescence became activated after Smurf1 treatment due to the sequestration of BHQ-1 caused by its binding to Smurf1 and SBP (Fig. 3.17A). Furthermore, pSmurf1 was transfected into hMSCs caused the cells to overexpress Smurf1 mRNA. The fluorescence intensity was proportional to the pSmurf1 concentration, indicating that the prepared peptide probe might be useful for measuring RA-associated bone loss (Fig. 3.17B). The critical osteogenic markers Runx2 and OCN were decreased in the Smurf1-overexpressing cells, but hBCPP-SBP caused a greater increase in these markers than that induced by Smurf1 alone (Fig. 3.17C). This result is most likely a consequence of the conformational change in the peptides induced by the relatively large Smurf1 molecule. To investigate the

following results *in vitro*, the author performed a FRET assay using Smurf1-positive human osteosarcoma (HOS) cells and Smurf1-negative mouse fibroblasts (NIH3T3) (Fig. 3.18). The fluorescence signal was restored in quenched hBCPP-SBP-treated HOS cells, but it was not restored in the NIH3T3 cells. In addition, quenched SBP-treated HOS and NIH3T3 cells exhibited no fluorescence because SBP was unable to penetrate the cell membrane by itself. Because hBCPP did not bind Smurf1, the recovery of the fluorescence signal was not observed in any of the peptide-treated cells.

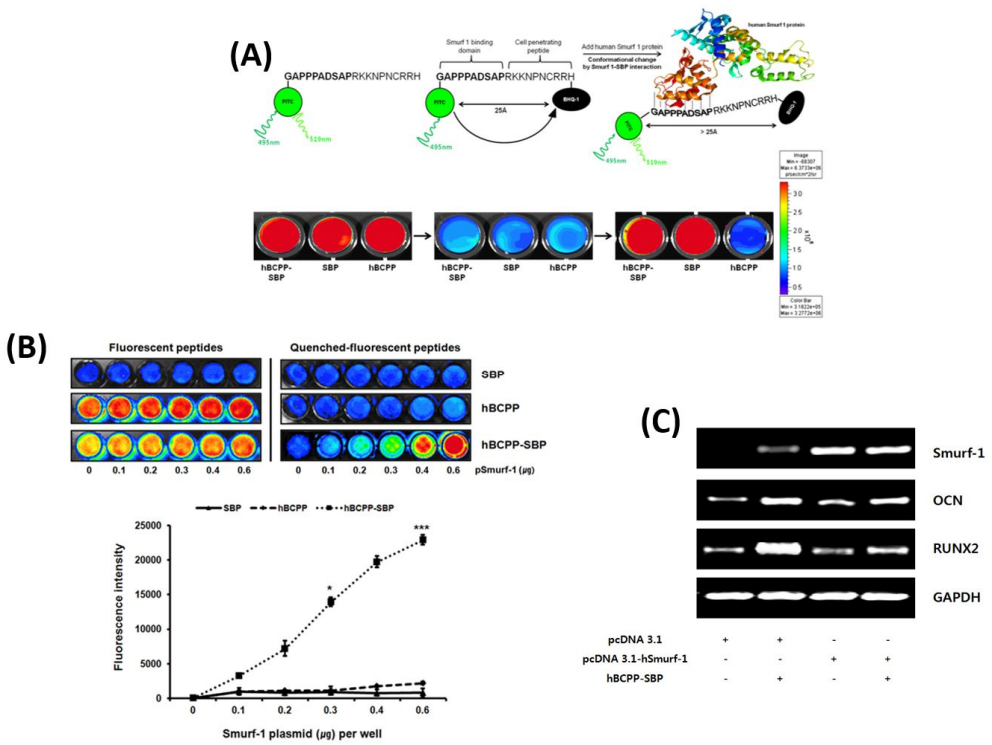

Figure 3.17. *In vitro* visualization based on FRET of fluorescence labeled SBP, hBCPP-SBP and hBCPP

(A) Fluorescence imaging of fluorescence labeled peptides (light emitted; left panel), BHQ-1-conjugated fluorescence labeled peptides (middle panel), and the recovery of peptide fluorescence due to a conformational change induced by the Smurf1 protein (light re-emitted; right panel). (B) Smurf1-overexpressing hMSCs were treated with various concentrations of the quenched fluorescent peptides, and the fluorescence was detected at 488 nm using the LAS3000. The fluorescence intensity was quantified using a fluorometer. The data are presented as the means ± the standard error of the mean (*, *p*-value < 0.05, ***, *p*-value < 0.01). (C) In the Smurf1-overexpressing hMSCs, the expression of Smurf1, ALP, OCN, COL1, and Runx2 mRNA was determined using PCR analysis.

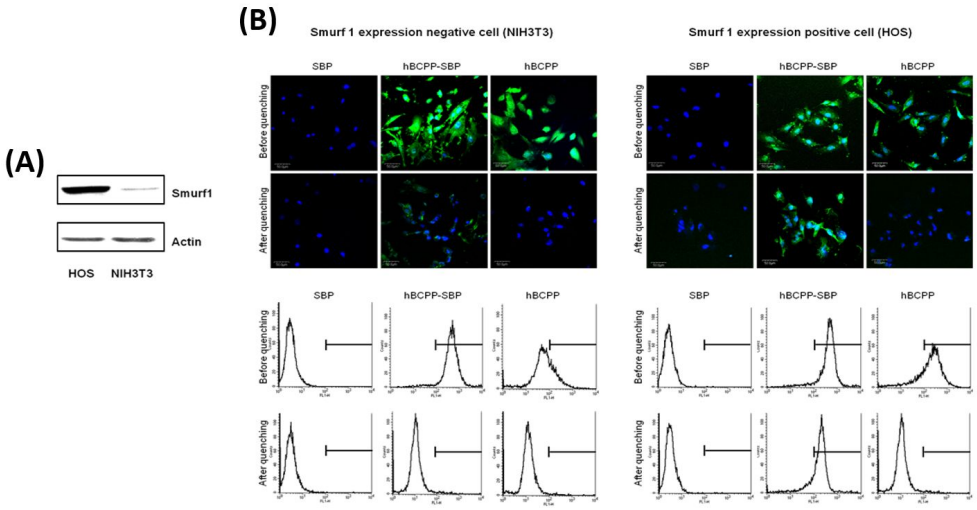

Figure 3.18. Observation of dequenched SBP, hBCPP-SBP and hBCPP by endogenous Smurf1 level

(A) Two cells were chosen as negative and positive cells in accordance with Smurf1 endogenous level. (B) Confocal microscopy imaging analysis and flow cytometry were performed using the BHQ-1 conjugated fluorescence labeled peptides to target endogenous Smurf-1 on NIH3T3 or HOS. The BHQ-1 conjugated peptides were incubated on 2h, 200μM. Fluorescence signals was significantly activated on HOS/hBCPP-SBP compared to others not contain SBP sequence or not able to penetrate into cells. By contrast, the BHQ-1 conjugated hBCPP-SBP on NIH3T3 was not reversible fluorescence signal after quenched. HOS: Human osteosarcoma cell line, NIH3T3: Mouse embryonic fibroblast cell line, BHQ-1: Black hole quencher-1.

5.9. Visualizing the expression of Smurf1 using the hBCPP-SBP probe: an *in vivo* rheumatic arthritis model

As the results in Fig. 3.16 show, hBCPP-SBP exhibited osteogenic-inducing ability. The author therefore investigated whether hBCPP-SBP could induce osteogenesis by binding to Smurf1 *in vitr*o. To confirm the *in vitro* probing action by the protein binding of hBCPP-SBP that was observed in Smurf1-overexpressing cells, the efficacy of hBCPP-SBP as a diagnostic probe was further investigated in an experimental rat model of RA. The increase in fluorescence intensity by re-excitation in hBCPP-SBP-treated cells was positively correlated with the transfected pSmurf1 volume. In contrast, the transfection of the two other peptides produced no significant difference in the fluorescence intensity. Also, the author stimulated hMSCs with TNFα in the presence of hBCPP-SBP. The TNFα-treated hMSCs exhibited significant Smurf1 expression (Fig. 3.19), but the Smad1 protein level was decreased without hBCPP-SBP. In contrast, the decreased Smad1 levels returned to normal in the cells treated with hBCPP-SBP compared with the level in cells treated only with hBCPP-SBP. Taken together, these results suggest that

hBCPP-SBP interacts with the TNFα signaling pathway, specifically with Smurf1, to inhibit Smad1/5/8 degradation.

Twenty-one days after the initial immunization, the severity of the bone damage and inflammation in the RA model rats was histologically examined with CIA after sacrifice. Joints in the hind paws, cranial bone, and knees exhibited severe bone degradation (Fig. 3.20A and B), and the synovial cavity of the knees was crowded with inflammatory cells, which were stained blue by eosin (Fig. 3.20C). Severe swelling of the hind paws induced by arthritis was associated with significant increases in the TNFα and Smurf1 protein levels compared with the control rats (Fig. 3.21A and B). Therefore, hBCPP-SBP was used in the RA model as a diagnostic drug because hBCPP-SBP is a Smurf1-specific binding peptide. To test this hypothesis that hBCPP-SBP may have clinical utility as a diagnostic drug, the author administered general anesthesia to RA rats, injected their hind paws with the quenched fluorescent SBP, hBCPP, and hBCPP-SBP peptides, and examined the fluorescence. The author detected a higher re-excitation level after treatment with hBCPP-SBP compared with SBP or hBCPP (Fig. 3.21C). Therefore, based on the findings that TNFα promoted inflammation in rats with CIA, which was correlated

with bone loss, and that Smurf1 induced TNFα expression, the author hypothesized that hBCPP-SBP could also induce osteogenesis by targeting Smurf1 and that the role of the probe was to bind to Smurf1. Although other reports have demonstrated detection using enzymatic cleavage, the present study was the first to use intracellular target-binding-mediated specific detection. To measure whether hBCPP-SBP had the potential to restore bone loss and promote bone formation, hMSCs were cultured with hBCPP-SBP supplementation. Our hypothesis was that the hindered binding of Smad1/5/8 by the peptide probe would induce osteogenic gene expression, thereby increasing bone formation (Fig. 3.16). In this regard, SBP also has potential as a therapeutic molecule because it induces bone formation and facilitates the diagnosis of RA (Fig. 3.21C). In future studies, the author would need to observe bone restoration *in vivo* through the systemic inhibition of Smurf1 via immunization by hBCPP-SBP, a Smad1/5/8 (osteo-Smads) degradation-interfering peptide.

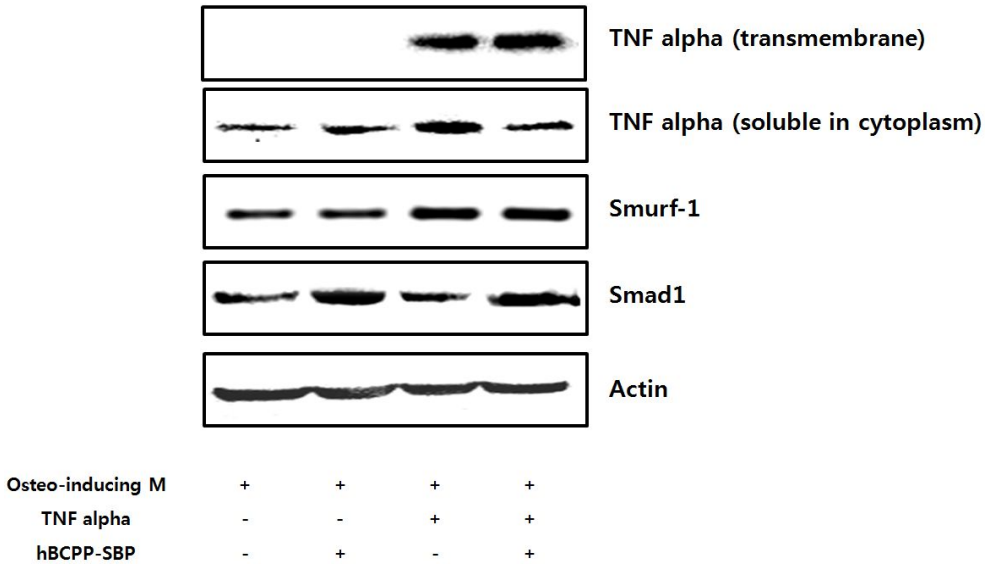

Figure 3.19. *In vitro* effect of hBCPP-SBP by TNFα treatment for mimicking rheumatic arthritis

TNFα-treated hMSCs were co-treated with hBCPP-SBP and were cultured under osteogenic differentiation condition for 72h and then protein were isolated from the cells. In TNFα-treated cells, the expression of two variant forms of TNFα and of the Smurf1, total Smad1, Runx2, and pErk1/2 proteins was assessed using Western blot analysis.

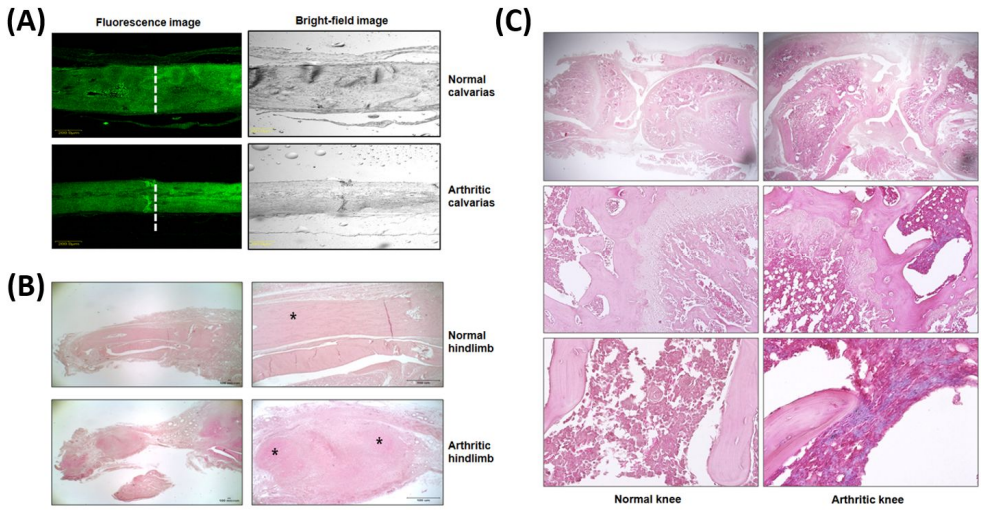

Figure 3.20. Representative histopathology of normal rats versus arthritis diseased rats

(A) Calcein stained calvarias to examine the difference of bone thick between both. (B) The paw joint tissues were stained with H&E (Magnification 12.5×; left 40×; right, Asterisks indicate hard tissues like a bone). (C) The knee tissues were stained with H&E for histopathological examination and inflammatory mononuclear cells (12.5×; upper, 100×; middle, 200×; middle, original magnification). H&E: Hematoxylin and eosin.

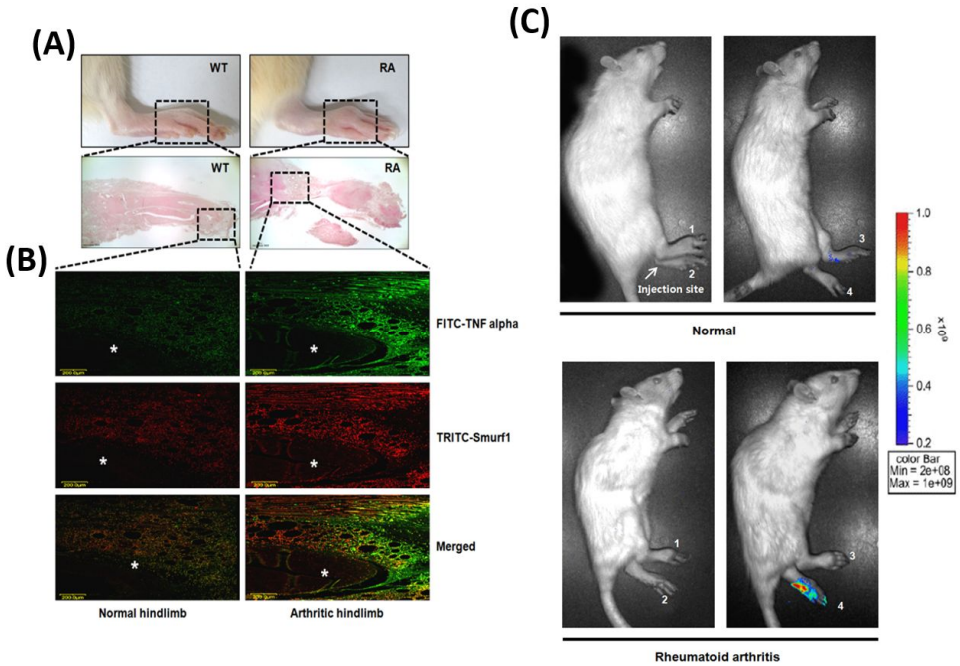

Figure 3.21. ***In vivo*** **molecular imaging on the rheumatoid tissue**

(A) Gross appearance of normal (WT, upper left) and arthritic (RA, upper right) hindpaws. The paw joint tissues were stained with H&E for histopathological examination. Magnification: 12.5×. (B) Immunofluorescence staining of the hind limbs was performed using antibodies against TNFα and Smurf1. The white asterisk indicates the bone area. (C) Verification of the Smurf1-peptide probe interaction in the hind limbs of arthritic rats using *in vivo* biofluorescence imaging. The rats were immunized with collagen on days 0 and 7 to generate CIA, and the normal rats were intraarticularly injected with quenched peptides on day 21. The biofluorescence images of the hind limbs of individual animals show the location and magnitude of the emitted light 2h after the peptide probe administration. Whole-body images are displayed as pseudocolored fluorescence intensity images overlaid with bright-field images of the rat body. 1: Smurf1 non-binding peptide (SNBP; PAATAAAITS); 2: SBP; 3: hBCPP; 4: hBCPP-SBP.

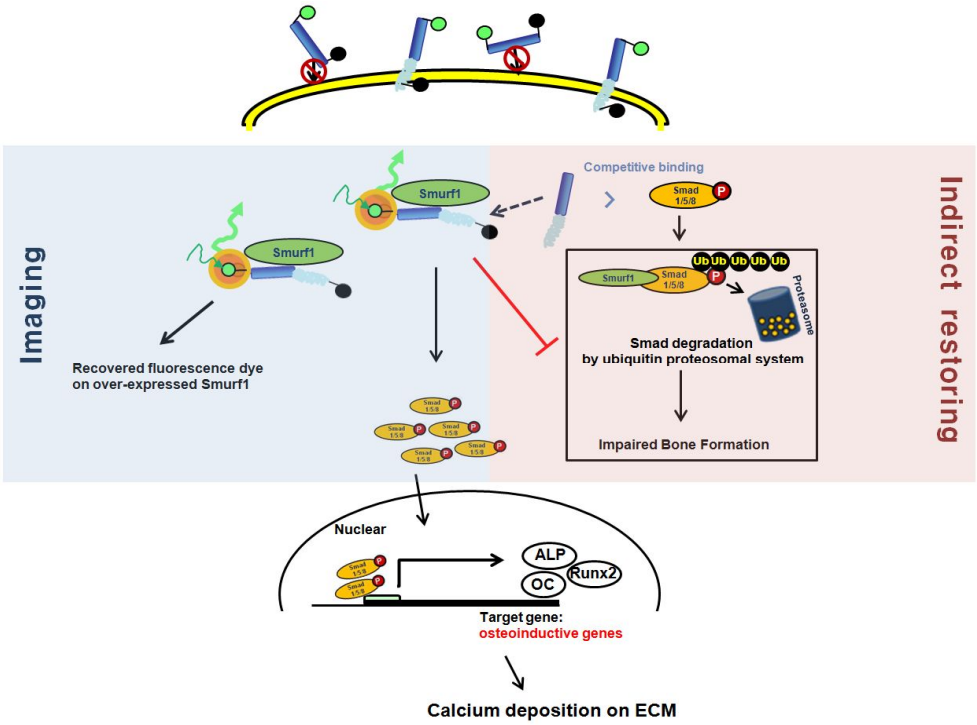

Figure 3.22. Scheme of stem cell imaging and restoring using the peptide probe

The figure is showed overall concept of the dual effects, imaging, and stem cell restoration using the ubiquitin-proteosome system (UPS)-based peptide probe

6. DISCUSSION

The ubiquitin-mediated proteasomal degradation pathway is the major intracellular mechanism for degrading many short-lived regulatory proteins, and it plays a major role in disease progression. The UPS is a critical intracellular regulator of pathologic pain, and UPS-mediated protein degradation is required for the maintenance of chronic pain, inflammation, and joint destruction, particularly in RA [22]. Smurf1 is a member of the HECT family of E3 ligases, and it has been reported to strongly bind to osteogenic transcription factors, including Smad1, Smad5, Smad6, Smad7, and Runx2 [18, 23-27]. These strong interactions result in the ubiquitination of target proteins, followed by the degradation of these proteins by proteasomes. The overexpression of Smurf1 causes degenerative musculoskeletal diseases, such as osteoarthritis, and it is a symptom of osteoporosis. Previously published data suggested that the interaction between Smurf1 and LMP-1 prevents the ubiquitination of Smad1/5/8, key intracellular messengers in the osteogenic pathway [23]. In a previous study, the viral gene (Ad5F35LMP-1)-mediated delivery of whole LMP-1 into hMSCs treated with

BMP-2 resulted in an increase in the level of phosphorylated Smad1 in the cytoplasm [28]. Furthermore, the author reported that the interaction between Smurf1 and LMP-1 or Smad1/5/8 was based on the presence of a unique motif in LMP-1, SBP, which binds the WW2 domain of Smurf1. The ability of LMP-1 to block the binding of Smurf1 to Smad1/5/8 resulted in an increase in the retention of Smad1/5/8 in the cytosol, leading to a potentiation of the cellular response to osteogenic signaling (Fig. 3.15). Moreover, the author used Smurf1-overexpressing MSCs and a rat arthritis model in that study and observed that the fluorescence intensity increased in a Smurf1 concentration-dependent manner (Fig. 3.17) [29]. The hMSCs were compared with other cell line such as HOS and NIH3T3 and demonstrated higher expression of the Smurf1 (Fig. 3.18). The increased Smurf1 expression itself can be one of the reasons of using the hMSCs to visualize the binding with the peptides. In addition, as stem cell has the capacity of multidirectional differentiation by the addition of the stimulatory factor, the author used the hMSCs with the overexpression of the Smurf1. This overexpression was anticipated to mimic the diseased/inflammatory condition and the author confirmed the restoration of its original osteogenic activity by the treatment of peptide probe,

at least *in vitro* condition. As a result, by using hMSCs with overexpression of Smurf1, the author could described the hBCPP-SBP involves restoring of hMSC as well as the rheumatic arthritis diagnostic probe for binding with Smurf1.

In previous studies, diagnostic methods of detecting RA by measuring the enzymatic activity of MMPs have been successfully created [6, 26, 28, 30]. However, the presence of MMP-mediated aggrecan and collagen type II degeneration might represent a turning point in the reversibility of cartilage degradation in patients with RA; thus, the enzymes have been limited to earlier RA detection [31]. To overcome the disadvantages of these RA imaging systems, the author attempted to create a fluorescence-based peptide probe containing both a Smurf1-binding domain for theranosis and a human-derived heparin-binding domain for cell permeability in hMSCs. The delivery of diagnostic probes has been hampered by low permeability through target tissues. It is noteworthy that our target-binding strategy, which employs a cell-permeable peptide Smurf1 probe, is also applicable to the universal ubiquitin system, which is a prerequisite for proteosomal disease regulation. Furthermore, protein-protein binding by affinity occurred indirectly in our strategy to induce osteogenesis via osteo-Smads retention.

Similar to the SBP probe used in this study, fluorescence-based biosensors are useful tools for the detection of biomolecules *in vitro* and *in vivo*. Fluorescence is sensitive and specific, and it lends itself to nondestructive imaging. As such, high-resolution imaging and the real-time measurement of fluorescent biosensors have provided valuable information about the spatial and temporal localization of a wide variety of intracellular targets. These techniques have proven to be an effective means of visualizing dynamic processes and monitoring enzymatic activities in living cells, and they are useful tools for drug discovery as well [6, 50, 32]. To transduce ligand binding into a detectable optical signal, fluorescence-based biosensors bear a sensing moiety that is either genetically or chemically coupled to a fluorescent probe. The spectral properties of this probe undergo measurable changes upon target recognition using fluorescence technologies for monitoring target recognition, i.e., FRET-based or environmentally sensitive technologies. FRET requires the emission spectrum of the fluorophore and the absorption spectrum of the quencher to overlap, with an effective distance between the labeling dyes of 20–100Å. During contact quenching, the fluorophore and the quencher must be close to each other to form a ground-state complex that does not

emit light [1]. In previous study, the distance between two amino acids that means the length of a peptide bond has been known 1.27Å in primary structure. In secondary structure, on the other hand, amino acids spaced three and four apart in the sequence are spatially quite close to one another in a α helix. The pitch of the α helix, which is equal to the product of the translation (1.5 Å) and the number of residues per turn (3.6mer), is 5.4 Å [33]. According to the above theory, the hBCPP-SBP contained 20mer has been calculated the overall length, about 25Å. Furthermore, the fluorescence labeled on a synthetic peptide probe undergoes an enzyme activity or protein-protein binding-dependent conformational change such that the distance between the adopter and the donor [34]. This change in distance results in a change in FRET efficiency that manifests itself as a change in emission ratio. In this study, Smurf1 binding motif was specifically dequenched by binding Smurf1 protein ex vitro/vivo, but the hBCPP not contained 'Smurf1 binding motif' was not changed its fluorescence level (Fig. 3.17). The result was consistent with *in vivo* noninvasive imaging data (Fig. 3.21). Taken together, the re-emission of inactivated fluorescent peptide indicates a slight variation of distance based on conformational change of each structure by binding Smurf1 binding motif to the

target protein, Smurf1. Moreover, fluorescent biosensors may be designed to probe an enzymatic activity, recognize a specific target, or recognize a specific conformation; thus, they are referred to as activity-, ligand-, or affinity-based, respectively. In this study, the author produced a probe that could specifically recognize its target; the resulting conformational change produced a specific fluorescent signal. However, the Smurf1-binding motif could not mediate the penetration of the cell due to its anionic charge. Therefore, the author synthesized a probe fused to a cell-penetrating domain.

Cationic CPPs are generally rich in arginine or lysine [35]. CPP peptides which possess protein transduction domains (PTDs), are suitable candidates for the delivery of relatively large molecules, such as nucleic acids, peptides, proteins, and even paramagnetic particles up to 200 nm in diameter [18, 35, 36]. These short CPP peptides have been reported to translocate across lipid bilayers in an energy-independent manner [37]. Polyarginine peptides possess cell translocation activity and an internalization pathway similar to that of Tat_{47-57} [38]. hBCPP, which consists of two clusters of cationic amino acid sequences similar to those of Tat_{47-57}, showed translocation capacity comparable to that of Tat peptide [35]. However,

most identified CPPs are from nonhuman species or viruses, which lack established biocompatibility. In this study, the author identified a cell-permeable peptide based on the human growth factor BMP-4; this peptide may be safer than the related viral molecule (Fig. 3.11). Interactions between heparin and hBCPP are based on ionic interactions between positively charged residues (Arg and Lys) and negatively charged groups on heparin (the sulfate groups of glucosamine or the carboxylate group of iduronic acid) [38]. Most arginine-rich peptides can interact not only with heparin sulfate but also with the lipid bilayer of cell membranes. The author chose a sequence rich in arginine and lysine residues to promote high heparin-binding affinity. In our previous study, the biological role in hMSCs of the heparin-binding domain of BMP-4 (hBCPP) was compared to that of BMP-4 [39]. The surface of BMP-4 contains a cluster of basic residues, including Lys-16, Arg-23, and His-24, which constitute binding sites for heparin and other sulfated substrates [7, 40]. In this regard, it would be advantageous if the heparin-binding motif alone could at least partially mimic the role of the growth factor. BMP-4, a member of the BMP family, is involved in bone and cartilage development [41, 42] and osteogenic differentiation [43, 44]. The author therefore investigated whether hBCPP could

promote hMSC differentiation in a manner similar to that of BMP-4. hBCPP increased osteoblastic differentiation without affecting cell proliferation or DNA synthesis (Fig. 3.11).

The author identified a small peptide domain in the LMP-1 protein that competitively bound to Smurf1 to block ubiquitin ligase activity, thus inhibiting proteosomal degradation. The author was also able to monitor the intracellular binding of the peptide to the target. The peptide was further modified by the addition of a new cell-penetrating peptide derived from a human molecule to enable its efficient internalization into cells. Identified human-derived cell-permeable peptide carriers have potential applications in drug delivery systems and in stem cell engineering for tissue regenerative procedures. Although further analyses are needed to verify its ability to maintain bioactivity, hBCPP-SBP has potential applications as a detection molecule for early-stage RA and, incidentally, as a component of bone tissue engineering tools in combination with bioimaging for bone restoration purposes.

7. CONCLUSION

In this study, a cell-permeable peptide probe that can specifically bind to an intracellular target enzyme in the UPS was generated. The peptide probe was bound to an intracellular model target, Smurf1, and this binding was monitored using on/off fluorescence imaging. This fluorescent peptide probe can be used for *in vitro* and *in vivo* affinity-based imaging, which can be performed in parallel with the real-time monitoring of disease processes. The author envisions that this peptide probe might be integrated into systems for the targeting, imaging, and tracking of therapeutic drugs to develop dual-function nanomolecules for noninvasive diagnosis. In addition, this peptide may prove advantageous for restoring normal cell function in Smurf1-overexpressing inflammatory diseases, such as osteoarthritis (Fig. 3.22).

8. REFERENCES

[1] Kim EM, Park EH, Cheong SJ, Lee CM, Kim DW, Jeong HJ, et al. Characterization, biodistribution and small-animal SPECT of I-125-labeled c-Met binding peptide in mice bearing c-Met receptor tyrosine kinase-positive tumor xenografts. Nucl Med Biol. 2009;36:371-8.

[2] Czernin J, Weber WA, Herschman HR. Molecular imaging in the development of cancer therapeutics. Annu Rev Med. 2006;57:99-118.

[3] Blanco-Mezquita T, Martinez-Garcia C, Proenca R, Zieske JD, Bonini S, Lambiase A, et al. Nerve growth factor promotes corneal epithelial migration by enhancing expression of matrix metalloprotease-9. Invest Ophthalmol Vis Sci. 2013;54:3880-90.

[4] Zhou Q, Gil-Krzewska A, Peruzzi G, Borrego F. Matrix metalloproteinases inhibition promotes the polyfunctionality of human natural killer cells in therapeutic antibody-based anti-tumour immunotherapy. Clin Exp Immunol. 2013;173:131-9.

[5] Akhatib B, Onnerfjord P, Gawri R, Ouellet J, Jarzem P, Heinegard D, et al. Chondroadherin fragmentation mediated by the protease HTRA1 distinguishes human intervertebral disc degeneration from normal aging. J Biol Chem. 2013;288:19280-7.

[6] Ryu JH, Lee A, Chu JU, Koo H, Ko CY, Kim HS, et al. Early diagnosis of arthritis in mice with collagen-induced arthritis, using a fluorogenic matrix

metalloproteinase 3-specific polymeric probe. Arthritis Rheum. 2011;63:3824-32.

[7] Marquez BV, Beck HE, Aweda TA, Phinney B, Holsclaw C, Jewell W, et al. Enhancing peptide ligand binding to vascular endothelial growth factor by covalent bond formation. Bioconjug Chem. 2012;16:1080-9.

[8] Ehrlich A, Ray P, Luker KE, Lolis EJ, Luker GD. Allosteric peptide regulators of chemokine receptors CXCR4 and CXCR7. Biochem Pharmacol. 2013;86:1263-71.

[9] Tian M, Xie Q. Non-26S proteasome proteolytic role of ubiquitin in plant endocytosis and endosomal trafficking(F). J Integr Plant Biol. 2013;55:54-63.

[10] Schulman BA, Harper JW. Ubiquitin-like protein activation by E1 enzymes: the apex for downstream signalling pathways. Nat Rev Mol Cell Biol. 2009;10:319-31.

[11] Ye Y, Rape M. Building ubiquitin chains: E2 enzymes at work. Nat Rev Mol Cell Biol. 2009;10:755-64.

[12] Wang Z, Nie Z, Chen W, Zhou Z, Kong Q, Seth AK, et al. RNF115/BCA2 E3 ubiquitin ligase promotes breast cancer cell proliferation through targeting p21(Waf1/Cip1) for ubiquitin-mediated degradation. Neoplasia. 2013;15:1028-35.

[13] Schnetzke U, Fischer M, Spies-Weisshart B, Zirm E, Hochhaus A, Muller JP, et al. The E3 ubiquitin ligase TRAF2 can contribute to TNF-alpha resistance in FLT3-ITD-positive AML cells. Leuk Res. 2013;37:1557-64.

[14] Pan WW, Zhou JJ, Yu C, Xu Y, Guo LJ, Zhang HY, et al. Ubiquitin E3 ligase CRL4(CDT2/DCAF2) as a potential chemotherapeutic target for ovarian surface

epithelial cancer. J Biol Chem. 2013;288:29680-91.

[15] Sangadala S, Boden SD, Viggeswarapu M, Liu Y, Titus L. LIM mineralization protein-1 potentiates bone morphogenetic protein responsiveness via a novel interaction with Smurf1 resulting in decreased ubiquitination of Smads. J Biol Chem. 2006;281:17212-9.

[16] Boden SD, Liu Y, Hair GA, Helms JA, Hu D, Racine M, et al. LMP-1, a LIM-domain protein, mediates BMP-6 effects on bone formation. Endocrinology. 1998;139:5125-34.

[17] Sangadala S, Boden SD, Metpally RP, Reddy BV. Modeling and analysis of molecularinteraction between Smurf1-WW2 domain and various isoforms of LIM mineralization protein. Proteins. 2007;68:690-701.

[18] Suh JS, Lee JY, Choi YS, Yu F, Yang V, Lee SJ, et al. Efficient labeling of mesenchymal stem cells using cell permeable magnetic nanoparticles. Biochem Biophys Res Commun. 2009;379:669-75.

[19] Bernassola, F., Karin, M., Ciechanover, A., and Melino, G. The HECT family of E3 ubiquitin ligases: multiple players in cancer development. Cancer cell. 2008;14:10-21.

[20] Tian, M., Bai, C., Lin, Q., Lin, H., Liu, M., Ding, F., et al. Binding of RhoA by the C2 domain of E3 ligase Smurf1 is essential for Smurf1-regulated RhoA ubiquitination and cell protrusive activity. FEBS Lett. 2011;585:2199-2204.

[21] Suzuki C1, Murakami G, Fukuchi M, Shimanuki T, Shikauchi Y, Imamura T, et al. Smurf1 regulates the inhibitory activity of Smad7 by targeting Smad7 to the

plasma membrane. J Biol Chem. 2002;399:19-25.

[22] Ahmed AS, Li J, Ahmed M, Hua L, Yakovleva T, Ossipov MH, et al. Attenuation of pain and inflammation in adjuvant-induced arthritis by the proteasome inhibitor MG132. Arthritis Rheum. 2010;62:2160-9.

[23] Guo R, Yamashita M, Zhang Q, Zhou Q, Chen D, Reynolds DG, et al. Ubiquitin ligase Smurf1 mediates tumor necrosis factor-induced systemic bone loss by promoting proteasomal degradation of bone morphogenetic signaling proteins. J Biol Chem. 2008;283:23084-92.

[24] Hanyu A, Ishidou Y, Ebisawa T, Shimanuki T, Imamura T, Miyazono K. The N domain of Smad7 is essential for specific inhibition of transforming growth factor-beta signaling. J Cell Biol. 2001;155:1017-27.

[25] Ito Y, Bringas P, Jr., Mogharei A, Zhao J, Deng C, Chai Y. Receptor-regulated and inhibitory Smads are critical in regulating transforming growth factor beta-mediated Meckel's cartilage development. Dev Dyn. 2002;224:69-78.

[26] Wunder A, Tung CH, Muller-Ladner U, Weissleder R, Mahmood U. *In vivo* imaging of protease activity in arthritis: a novel approach for monitoring treatment response. Arthritis Rheum. 2004;50:2459-65.

[27] Lee KS, Kim HJ, Li QL, Chi XZ, Ueta C, Komori T, et al. Runx2 is a common target of transforming growth factor beta1 and bone morphogenetic protein 2, and cooperation between Runx2 and Smad5 induces osteoblast-specific gene expression in the pluripotent mesenchymal precursor cell line C2C12. Mol Cell Biol. 2000;20:8783-92.

[28] Gompels LL, Madden L, Lim NH, Inglis JJ, McConnell E, Vincent TL, et al. *In vivo* fluorescence imaging of E-selectin: quantitative detection of endothelial activation in a mouse model of arthritis. Arthritis Rheum. 2011;63:107-17.

[29] Oh JY, Kim MK, Shin MS, Wee WR, Lee JH. Cytokine secretion by human mesenchymal stem cells cocultured with damaged corneal epithelial cells. Cytokine. 2009;46:100-3.

[30] Liao EY, Liao HJ, Guo LJ, Zhou HD, Wu XP, Dai RC, et al. Membrane-type matrix metalloproteinase-1 (MT1-MMP) is down-regulated in estrogen-deficient rat osteoblast *in vivo*. J Endocrinol Invest. 2004;27:1-5.

[31] Niki Y, Takeuchi T, Nakayama M, Nagasawa H, Kurasawa T, Yamada H, et al. Clinical significance of cartilage biomarkers for monitoring structural joint damage in rheumatoid arthritis patients treated with anti-TNF therapy. PLoS One. 2012;7:e37447.

[32] Amiable N, Tat SK, Lajeunesse D, Duval N, Pelletier JP, Martel-Pelletier J, et al. Proteinase-activated receptor (PAR)-2 activation impacts bone resorptive properties of human osteoarthritic subchondral bone osteoblasts. Bone. 2009;44:1143-50.

[33] Pauling L, Corey RB, Branson HR. The structure of proteins; two hydrogen-bonded helical configurations of the polypeptide chain. Proc Natl Acad Sci U S A. 1951;37(4):205-11.

[34] Campbell RE. Fluorescent-protein-based biosensors: modulation of energy transfer as a design principle. Anal Chem. 2009 1;81:5972-9

[35] Park YJ, Chang LC, Liang JF, Moon C, Chung CP, Yang VC. Nontoxic membrane translocation peptide from protamine, low molecular weight protamine (LMWP), for enhanced intracellular protein delivery: *in vitro* and *in vivo* study. FASEB J. 2005;19:1555-7.

[36] Choi YS, Lee JY, Suh JS, Kwon YM, Lee SJ, Chung JK, et al. The systemic delivery of siRNAs by a cell penetrating peptide, low molecular weight protamine. Biomaterials. 2010;31:1429-43.

[37] Hung CF, Lu KC, Cheng TL, Wu RH, Huang LY, Teng CF, et al. A novel siRNA validation system for functional screening and identification of effective RNAi probes in mammalian cells. Biochem Biophys Res Commun. 2006;346:707-20.

[38] Tung CH, Mueller S, Weissleder R. Novel branching membrane translocational peptide as gene delivery vector. Bioorg Med Chem. 2002;10:3609-14.

[39] Choi YJ, Lee JY, Park JH, Park JB, Suh JS, Choi YS, et al. The identification of a heparin binding domain peptide from bone morphogenetic protein-4 and its role on osteogenesis. Biomaterials. 2010;31:7226-38.

[40] Cao J, Wan S, Tian J, Li S, Deng D, Qian Z, et al. Fast clearing RGD-based near-infrared fluorescent probes for *in vivo* tumor diagnosis. Contrast Media Mol Imaging. 2012;7:390-402.

[41] Tang CH, Yang RS, Liou HC, Fu WM. Enhancement of fibronectin synthesis and fibrillogenesis by BMP-4 in cultured rat osteoblast. J Bone Miner Res.

2003;18:502-11.

[42] van der Horst G, van Bezooijen RL, Deckers MM, Hoogendam J, Visser A, Lowik CW, et al. Differentiation of murine preosteoblastic KS483 cells depends on autocrine bone morphogenetic protein signaling during all phases of osteoblast formation. Bone. 2002;31:661-9.

[43] Edgar CM, Chakravarthy V, Barnes G, Kakar S, Gerstenfeld LC, Einhorn TA. Autogenous regulation of a network of bone morphogenetic proteins (BMPs) mediates the osteogenic differentiation in murine marrow stromal cells. Bone. 2007;40:1389-98.

[44] Sammons J, Ahmed N, El-Sheemy M, Hassan HT. The role of BMP-6, IL-6, and BMP-4 in mesenchymal stem cell-dependent bone development: effects on osteoblastic differentiation induced by parathyroid hormone and vitamin D(3). Stem Cells Dev. 2004;13:273-80.

CHAPTER Ⅳ

Concluding remarks

The literature demonstrates that therapeutic peptides can be developed for the regulation or reactivation of a large variety of important signaling molecules. Furthermore, these peptides can be very specific with regard to their target proteins by binding, cleaving or transporting their target; in some cases, the peptides can also be specific with regard to cell types based on the identification of biomarkers, such as receptor proteins. As increased knowledge and the development of analytical methods have fostered the development of a database of proteins involved in cellular signaling, peptides represent an effectively available regulator for diagnosis and therapy of newly discovered target proteins based on the PPI concept. In this study, two bioactive peptides, LMWP and hBCPP-SBP, were shown to remarkably improve miRNA-induced bio-activation of mineralization and displayed a higher binding affinity to the intracellular target protein compared to osteo-Smad proteins, resulting in the induction of indirect osteogenesis. Moreover, the latter process can reduce the likelihood of “off-target” effects involved in Smurf1 signaling by the non-WW domain due to the very specific interaction. The outcomes of the experiments are encouraging and support the conclusion that bioactive peptides should be further investigated as potential theragnosis molecules with regard to structure modification, use of nanoparticles to enhance visualization or the conjugation of specific tissue-homing domains.

국 문 초 록

줄기세포의 분화제어를 위한 펩타이드 기반 세포 내 표적화 연구

서 진 숙

서울대학교 대학원 치의과학과 치의재생 생명공학 전공

(지 도 교 수 : 박 윤 정)

성체줄기세포 즉, 출생 후 다양한 조직에서 발견되는 다분화성을 가지는 세포는 재생의학 분야의 하나의 요소로 연구되고 있으며 성체줄기세포의 이용성을 높이기 위해서는 세포 자체가 가진 기능성을 극대화시킬 수 있는 조건을 수립함으로 달성될 수 있다. 결손 조직을 복구해야 하는 재생의학의 목적 중 세포이용의 기술적 요소는 미분화된 세포가 재생에 필요한 만큼의 세포 수를 확보하기 위하여 줄기세포 클론을 형성하고 세포의 군집을 이루는 것뿐만 아니라 목적하고자 하는 조직으로의 분화형태를 형성할 수 있는 능력을 갖는 것이다. 성체줄기세포의 분화능의 유도 및 억제와 같은 세포 운명 제어는 생리활성 물질이나 배양환경의 물리적 변화에 의해 가능하다. 특히, 본 논문은 줄기세포의 분화를 제어할 수 있는 생리활성물질의 효율적인 적용에 초점을 맞추고 있다. 세포 배양과정에서 처리하는 생리활성물질은 대표적으로 성장인자나 사이토카인등의 단백질이 있으며 이들은 세포 내 다양한 신호 전달과정에 관여하며 분화적인 특성을 변화시킨다. 이러한 단백질의 생체 내 적용은 고분자적 특성에 따른 한계점이 있으므로 단백질의 기능성 도메인을 화학적으로 합성한 펩타이드 형태를 생리활성물질로 사용할 수 있다. 펩타이드는 합성과 수식이 용이하고 생체 내 특이성이 높으며 면역원성과 독성을 일으키는 가능성이 단백질 분자에 비해 상대적으로 낮다. 이러한 펩타이드는

약물로서의 기능을 보유할 뿐만 아니라 구성되는 아미노산의 서열에 따라 세포투과기능성을 부여할 수 있다. 따라서 세포 또는 조직내로의 낮은 투과율을 가진 단백약물이나 유전자 약물의 전달을 유도하여 약물로서의 기능을 부여하거나 효율적인 기능성을 유도할 수 있다.

세포 내의 전사 후 단계에서 특정 mRNA 서열에 결합하여 단백질로의 전이를 방해하거나 차단하는 microRNA 는 유전자 치료제의 재료로 가능성을 보고하는 연구들이 많으나 이들의 세포 내 이입은 약물로서의 적용시 장애요인으로 제시되고 있다. 본 연구의 첫째 장에서는 석회화를 유도하고 골아세포로의 분화를 촉진할 수 있는 miRNA-29b 를 약물로 선택하고 세포 내 전달체로써 투과 고기능성 펩타이드인 Low molecular weight protamine (LMWP)을 사용하였다. LMWP 와 miRNA-29b 는 비공유결합을 통해 30-50nm 의 지름을 가진 밀도가 높은 입자를 형성하였으며 미분화된 인간 유래 성체줄기세포 내로 고농도의 miRNA 를 이입하였다. 전체적인 실험에서 일반적으로 사용되고 있는 리포좀 형태의 비바이러스성 벡터를 사용하여 miRNA-29b 를 세포내로 이입한 군을 음성 대조군으로 설정하였다. LMWP/miRNA-29b 결합체는 음성대조군에 비해 단시간내에 세포투과가 일어난 것을 알 수 있었으며 리포좀의 처리시간인 5 시간이 지난 후에는 LMWP/miRNA-29 결합체가 음성대조군에 비해 고농도로 세포내에 이입된 것을 관찰할 수 있었다. 뿐만 아니라 LMWP/miRNA-29b 결합체가 이입된 세포는 농도의존적으로 골분화에 특이적인 유전자와 단백질의 발현이 증가되었으며 따라서 골분화의 최종 양상인 칼슘의 세포외 기질 내 침착이 증가되는 것을 확인할 수 있었다. 이러한 결과는 miRNA-29b 가 가진 표적 기능성에 기인한 것으로서 골분화의 negative regulator 로 신호 전달체계에서 작용하는 mRNAs 를 타겟하여 단백질로의 전이를 방해하는 것을 설계된 벡터의 luciferase activity 감소로 검증하였다.

또한 두번째 장의 연구에서는 단백질간의 결합에 관여하는 도메인에 세포투과능을 부여하여 골분화능을 가진 펩타이드 프루브를 제작하였다. 합성한 펩타이드는 골분화 신호전달계의 주요 전사인자인 Smad1/5/8 의 분해를 유도하는 Smurf1 E3 ligase 에 대한 결합 도메인을 포함하고 있으며 동시에 헤파린과 결합하여 세포 이입을 유도할 수 있는 세포투과 기능성 도메인도 포함한다. 본 펩타이드는 Smurf1 과 농도 의존적으로 결합하며 Smurf1-Smad1/5/8 와의 결합친화력보다 수치가 상대적으로 높게 나타남을 확인하였다. 세포 내 투과능도 양성 대조군인 Tat 과 유사하며 세포질 및 핵 내로 이입되어 Smurf1 과 결합함으로써 간접적으로 Smad1/5/8 의 분해를 막아 골세포로의 분화를 유도함을 확인하였다. 생체 내에서 단백질은 다른 단백질과의 결합을 통해 기능을 나타내고 단백질-단백질 결합을 기반으로 한 단백질 상호작용은 세포 내에서 일어나는 신호전달과정의 활성 및 제어의 변화를 초래하여 이 과정의 이상은 질병과 직결되어 있다. 또한 유전자 수준에서의 연구와 정보는 산업화가 불가능하고 단백질 관련 기술과 결합한 분석이 뒷받침 되어야 실용화가 가능하기 때문에 단백질-단백질 결합은 질병의 진단 및 치료연구에 필수적이라고 사료된다. 두번째 장의 연구 역시 단백질간의 상호작용을 기반으로 설계되었기 때문에 질환의 진단 프로브로서의 기능성을 부여하기 위해 펩타이드 양 말단에 형광을 가지는 분자와 발광을 방해하는 소광체를 수식하였다. 이는 거리 의존적인 상호작용에 의한 발광현상 즉, 형광공명 에너지 전이 (Fluorescence resonance energy transfer) 원리를 이용하여 펩타이드가 타겟 단백질인 Smurf1 과 결합할 때 구조적 변형에 의한 에너지 전이율의 감소로 Smurf1 을 인위적으로 과발현시킨 세포 내에서 선택적으로 발광함을 확인하였다. 또한 수식이 가미된 펩타이드 프루브를 Smurf1 이 과다하게 발현되어 있는 류마티스성 관절염 모델 쥐의 피하내로 주입하였을 때, 피부밖으로 감지되는 영상을 관찰하여 질환의 진단 프루브로서의 가능성을 확인하였다.

이와 같은 실험 결과를 통해 유전자 약물의 전달체나 진단 및 세포 기능회복의 생리활성 분자로서 펩타이드를 도입함으로써 줄기세포의 분화제어의 도구로 적용할 수 있다. 특히, 골아세포로의 분화를 위한 생리활성 물질에 세포 투과 기능성을 부여하거나 펩타이드 단독으로 사용되어 조직 재생 기능의 증가를 기대할 수 있다.

주요어 : 세포투과성 펩타이드, 표적분자 결합능 도메인, 약물전달시스템, 진단 프루브, 마이크로 RNA(MicroRNA), 골조직재생

학 번 : 2006-23511